UNIVERSITY *of the*
WESTERN CAPE

A comparison of black-oil versus compositional simulation methods for evaluating a rich gas-condensate reservoir

---

A mini dissertation in Petroleum Geoscience (Reservoir Engineering)

Completed by

Mr. Victor Edward DELICADO°

Email: **°3518573@myuwc.ac.za**

Submitted in partial fulfilment of the requirements for the degree of Masters in Science (MSc) of the Faculty of Sciences, University of the Western Cape, South Africa

Supervisor: Mr. John Egan (PetroSA)
Co-supervisor: Dr. Mimonitu Opuwari (UWC)

DECEMBER 2016

Declaration

I hereby declare that this thesis titled "**A comparison of black-oil versus compositional simulation methods for evaluating a rich gas-condensate reservoir**" represents my own work which has been done in partial fulfilment of the Masters in Science degree in Petroleum Geoscience of the Faculty of Science, Earth Sciences Department, University of the Western Cape, South Africa. I declare that it has not been previously included in any other thesis submitted to this or any other institution for a degree, diploma or other qualification. I also assert that all sources used during the completion of this study have been included and acknowledged by means of complete references.

Victor Edward Delicado ***December 2016***

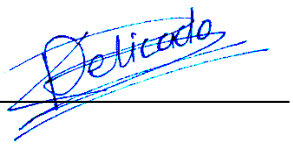

Signature

Foreword

First and foremost I would like to thank Mr. Sofyan Salem and Mr. Sbusiso Mkhize for their astounding technical support and knowledge; without whose help it would not have been possible to complete this project successfully. I would also like to thank PetroSA for providing me with the opportunity and necessary data for the project. To my supervisor, Mr. John Egan and co-supervisor, Dr. Mimonitu Opuwari, special thanks for your support, experience and input in order for me to be able to complete and hand in this MSc thesis.

This project is dedicated to my mother, Franciska Bothma; grandmother, Mechaela Scott van Wyk as well as the rest of my family and friends without whose continued support, prayers and sound words of encouragement all the work done would not have been possible.

Finally, I would like to thank my saviour, Lord Jesus Christ, for always being my light and rock, bringing me comfort during tough times throughout this Masters project.

Abstract

Over time, researchers have endeavoured to use conventional black-oil (BO) models to model volatile-oil and gas-condensate reservoirs as accurately as possible, with variable levels of success. The black-oil approach allows for the implementation of a simpler and less expensive computational algorithm than that associated with a compositional model. The first-mentioned can result in substantial time-saving in full field studies. This project evaluates the use of modified black-oil (MBO) as well as compositional (equation of state-EOS) approaches to determine the expected recovery and performance of a rich gas-condensate reservoir. After initialization, the models reflected very similar in-place hydrocarbon volumes, with a deviation percentage of less than 5 % between the two modelling approaches.

The study shows that, regarding all natural depletion cases, both gas and oil production rates, and subsequent cumulative volumes, portray close similarity when comparing the MBO and compositional simulation models. In addition, Bottom Hole Flowing Pressures (BHFP) and Well Head Pressures (WHP) also showed to be very similar. However, differences in water production in the MBO and compositional models appear to be an area of concern. The results show that MBO models predict the production of about 10 times more water compared to the equivalent compositional model. Possible reasons for this discrepancy have been identified, chief among which is the type of relative permeability model used, as well as how each model (MBO vs compositional) calculates the K_r. Further research on the water production discrepancies is proposed to ascertain the true causes of these problems. Interestingly, the water production discrepancies mentioned do not seem to influence the hydrocarbon production rate nor recovery. Finally, runtime comparisons given showed that the MBO models tended to be 1/6 of the runtime of the compositional modelling methods, proving the time saving capabilities of these types of models. It is thus evident that the MBO modelling approach can be used for all simulations concerned with natural depletion studies.

The gas cycling scenarios of this study afforded some interesting results. The results, for both above and below the dewpoint cycling, showed that recovery volumes exhibited some promising matches between the two modelling approaches for oil and gas production rates. The MBO model produced more oil than the compositional model, not less as was seen in the natural depletion study, which would suggest that the MBO model might be overestimating recovery volumes. The study emphasized that if the pressure difference between reservoir pressure and dewpoint pressure is small, or if it is higher than dewpoint pressure, the reliability of the MBO modelling approach's recovery results is sufficient and this method could be used for gas cycling scenarios. It is only when reservoir pressure falls far below dewpoint pressure that more research is required in order to have full confidence in MBO recovery results. Remarkably, compositional model running times were only two times slower than the equivalent MBO model. This implies that the compositional model can be used for gas cycling irrespective of the MBO model, since it reflects more accurate results for the complex component exchange behaviour of the rich gas-condensate fluid. However, as indicated by this study, this would not have any major additional time constraint problems as had first been feared and seen in the natural depletion studies.

Table of Contents

List of Figures

List of Tables

List of Abbreviations

Artificial Neural Network	ANN
Black-oil	BO
Bottom Hole Flowing Pressure	BHFP
Bottom Hole Pressure	BHP
Binary Interaction Coefficients	BIC
Constant Composition Expansion	CCE
Central Processing Unit	CPU
Constant Volume Depletion	CVD
Drill Stem Test	DST
Equation of State	EOS
Flow Zone Indicator	FZI
Gamma Ray	GR
Gas Initially in Place	GIIP
Gas-oil Contact	GOC
Gas-oil Ratio	GOR
Gas-water Contact	GWC
Infrared	IR
Initial Fluids in Place	IFIP
Interfacial Tension	IFT
Modified Black-oil	MBO
Molecular Weight	MW
Net to Gross	NTG
Oil in Place	OIP
Oil-gas Ratio/condensate-gas ratio	OGR/CGR
Oil-water Contact	OWC
Pressure-Volume-Temperature	PVT
Production Logging Tool	PLT
Productivity Index	PI
Repeat Formation Tester	RFT
Resistivity of the rock	RT
Separator	SEP
Spontaneous Potential	SP
Tubing Head Pressure	THP
True Vertical Depth Sub Sea	TVDSS
Ultraviolet	UV
Velocity-dependent Relative Permeability	VDRP

Vertical Flow Performance	VFP
Water in Place	WIP
Well Head Pressure	WHP

Nomenclature

Compressibility	z
Critical gas saturation	S_{wcr}
Critical water saturation	S_{gcr}
Density (Rhob)	ρ
Dewpoint	Dp
Formation volume factor for gas	Bg
Formation volume factor for oil	Bo
Gas	g
Gas saturation	S_g
Irreducible water saturation	S_{iw}
Molar density of gas at standard conditions	ρ_{gst}
Molar density of oil at standard conditions	ρ_{ost}
Molar solution gas-oil ratio	r_o/r_s
Molar vapourised oil-gas ratio	r_g/r_v
Mole fraction of pseudo components in gas	y_g/y_o
Mole fraction of pseudo components in oil	x_g/x_o
Neutron	NPHI
Oil	o
Oil saturation	S_o
Omega	Ω
Permeability	k
Porosity	ϕ
Pressure	P
Relative permeability	K_r
Relative permeability gas	K_{rg}
Relative permeability gas to water	K_{rgw}
Relative permeability hydrocarbon to water	K_{rhw}
Relative permeability oil	K_{ro}
Relative permeability oil to gas	K_{rog}
Relative permeability oil to water	K_{row}
Relative permeability water	K_{rw}
Solution Gas-oil Ratio	R_o/R_s
Temperature	T
Time step	t=

Vapourised Oil-gas Ratio/condensate-gas ratio	R_g/R_v
Viscosity	μ
Volume of clay	Vcl
Water saturation	S_w

UNIVERSITY of the WESTERN CAPE

A comparison of black-oil versus compositional simulation methods for evaluating a rich gas-condensate reservoir

1 Chapter One: Introduction

1.1 Background Information

The study area of this project is located offshore South Africa, within the larger Outeniqua Basin; more specifically within the Bredasdorp Sub-Basin (**Figure 1.1**).

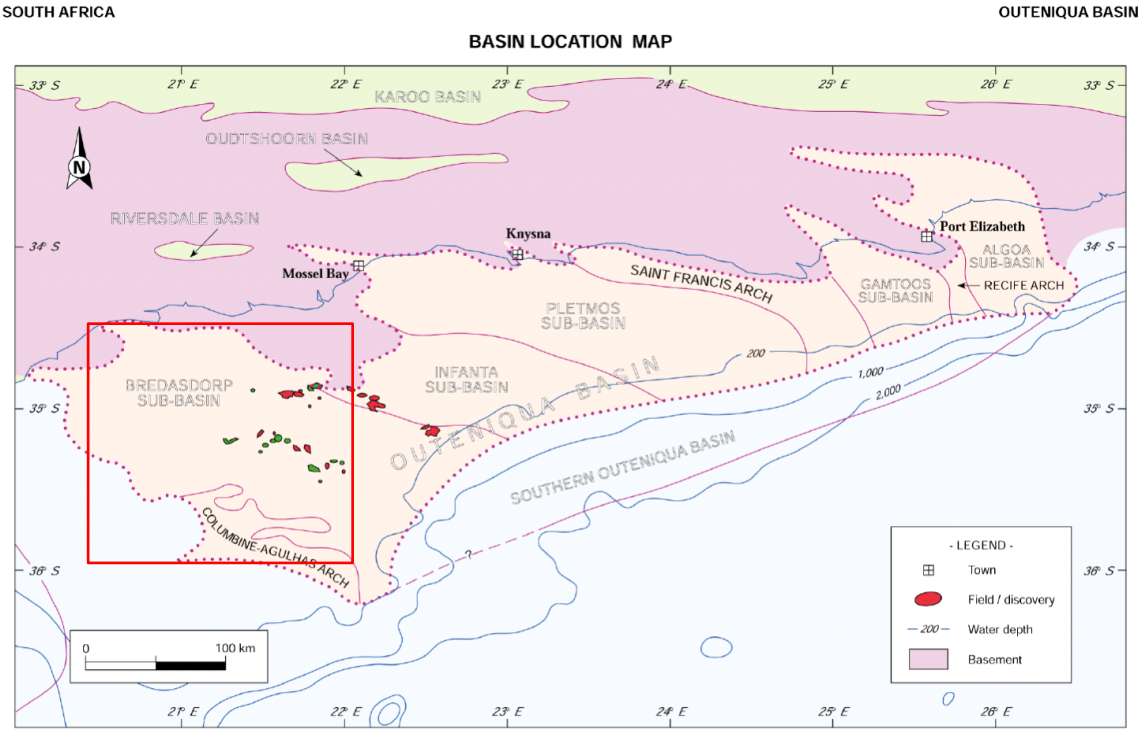

Figure 1.1: General Basinal Overview of the study area, offshore South Africa (IHS Energy, 2010)

As indicated in **Figure 1.1**, the Outeniqua basin is an offshore basin, covering most of the ocean mass on the south coast of South Africa. The basin extends to onshore regions in a few places, however, mainly near Port Elizabeth. The greater basin consists of a number of northwest-southeast trending en-echelon sub-basins and interbasinal highs. Among these sub-basins are the Bredasdorp, Infanta, Pletmos, Gamtoos and Algoa sub-basins. A northwest-southeast shallow water fault trend to the south separates the Outeniqua basin from the smaller Southern Outeniqua basin (IHS Energy, 2010).

The sandstone reservoir harbours a rich gas-condensate fluid at a depth of ~8500 ft TVDSS. The fluid has a gas-condensate ratio of ~180bbl/MMscf. This project endeavoured to evaluate whether a modified black-oil (MBO) approach will be able to simulate gas-condensate reservoirs efficiently and accurately (within 10% accuracy) within the specific field (the Outeniqua basin) where this research was done, as compared to the results of prior research done with a compositional model. This would result in substantial time-saving in full field studies and field volume recovery predictions as well as supply answers to difficult problems in a cost-effective manner.

1.2 Problem Statement

Reservoir engineers, similar to other researchers in the North Sea region, have found it difficult to model gas-condensate reservoirs as accurately with conventional black-oil models as could be modelled with compositional models (Izgec; 2003:3). The use of fully compositional models is therefore important for accurate representation and simulation of gas and the associated recovery efficiency of the condensate fluids. These methods are costly and time-consuming, however.

In order to find an explanation for this phenomenon, the following key questions would guide the study:

- Does a modified black-oil model have the capacity to model gas-condensate reservoirs accurately, or does it simply give an approximation?
- Is it necessary to use costly and time-consuming fully compositional models for accurate representation and simulation of gas and the associated recovery efficiency of the condensate fluids?
- Is it possible to evaluate whether the MBO approach will be able to simulate gas-condensate reservoirs efficiently and accurately within the specific field (the Outeniqua basin) where this research is being done, as compared to the results of the compositional model?

1.3 Objectives

The main objective of the study was to determine if the MBO simulation model could be used as the basis for modelling a rich gas-condensate reservoir under natural depletion as well as gas cycling development scenarios. The study evaluated whether the use of the MBO approach delivers different recovery and performance rates for a rich gas-condensate reservoir than the compositional (equation of state - EOS) approach. The two models were compared in terms of the reliability of the computationally efficient black-oil approach under natural depletion as well as gas cycling development scenarios.

> Note that correct pseudoization or lumping of components is of the utmost importance if the reduced-component EOS model is to reflect, as closely as possible, the true full component system. Since the lumping process had already been done prior to the undertaking of this current research, this set of data was used in the compositional model for this study.

1.4 Scope of the Study

The study endeavoured to validate the findings of Fevang *et al*. (2000:2); which showed that the black-oil approach used in the North Sea region could replicate compositional model results for all depletion cases as long as the black-oil PVT data were generated properly. The study was to show that the MBO PVT formulation gave similar results when compared to the fully compositional EOS PVT approach for natural depletion above and below dewpoint. In other words these methods would be applied and the findings replicated for the offshore Outeniqua basin where our study is located.

Furthermore, such results would also agree with the findings of Coats (1985:1822) that the black-oil model could replicate the results of compositional simulation cases for gas cycling above the dewpoint, but would not give accurate results for cases reflecting gas cycling which is occurring below the dewpoint.

2 Chapter Two: Literature Review

2.1 Understanding the Reservoir Fluid

As mentioned in chapter one, the sandstone reservoir used in this study harbours a rich gas-condensate fluid. To develop the field and production performance optimally, and simultaneously model the fluid correctly with the available software, a maximum understanding of the field and the fluid with its behaviour needs to be achieved.

According to Fan *et al. (*2005:14) and Lal (2003:1), the term *gas-condensate* refers to a fluid which exists as a single-phase when it is at original reservoir conditions (temperature and pressure). This fluid comprises mostly of methane (C_1) as well as some other short-chain hydrocarbon strands. There will, however, also be "heavy ends" present in such a fluid; in other words, hydrocarbon chains of the longer variety. When certain reservoir conditions arise, such as a change in temperature and pressure, the mentioned fluid will tend to separate into two phases, namely a gas and a liquid. This phenomenon reformulates the fluid into a so-called *retrograde condensate* (Lal; 2003:1), since these types of gas-condensate fluids behave conversely to what is expected of fluids comprising of pure components. Thus, as Izgec (2003:27) noted, when the reservoir pressure declines (finally passing through the dewpoint), liquid starts to form as determined by the phase envelope. The total volume of the liquid phase would increase as the pressure drops until the system reaches a point in the retrograde condensate behaviour where, as pressure continues to decline, the liquid re-vaporizes, as is shown in **Figure 2.1**.

Shi (2009:2) as well as Fan *et al.* (2005:15) reiterates that once the reservoir starts to produce, the *temperature* associated with the reservoir formation does not change; instead, the pressure would have to change (pressure declines when fluid is taken out). It has been noted that pressure declines the most within the area closest to the well, since only the fluid near to the producing well is mobilized and drained at a notable rate (There needs to be a notable pressure difference between the open hole and the reservoir rock for flow to occur). Thus, with production pressure continues to decline, and after a period it reaches a certain pressure point (unique to each reservoir), called the saturation pressure or dewpoint. When this point is reached, liquids rich in "heavy ends" drop out of the solution, rendering the gas phase depleted of these components. As pressure continues to decrease, this liquid volume increases up to a certain maximum amount, and thereafter decreases again (retrograde behaviour). This behaviour is explained in the pressure-volume-temperature (PVT) diagram, **Figure 2.1**, as well as in the liquid dropout graph (**Figure 2.2c**).

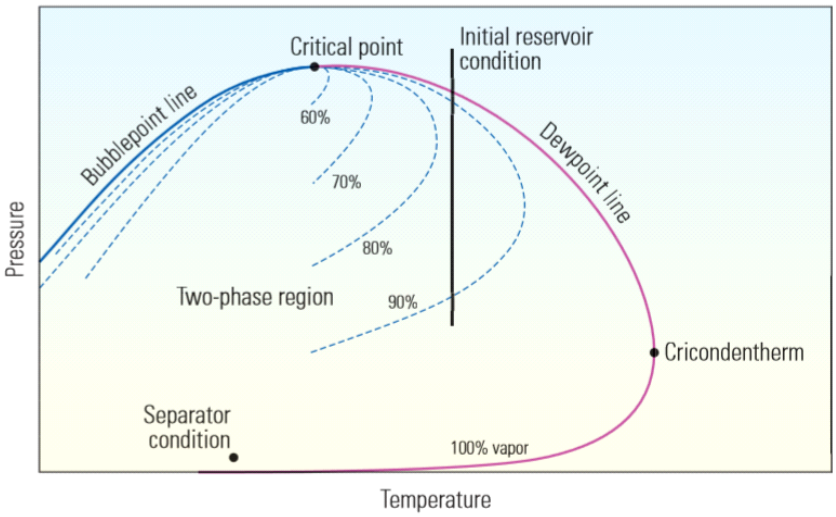

Figure 2.1: Phase diagram of a gas-condensate system (Fan et al.; 2005:15)

Fan *et al.* (2005:16) further state that the amount of liquid phase to drop out of the solution does not only depend on the pressure and temperature, but also on the composition of the reservoir fluid. For instance, a dry gas, by definition, does not possess the heavy components necessary for generating liquids in the reservoir, even under circumstances of near-well drawdown. According to Fan *et al.* (2005:16), two classes of gas condensates can be defined: a *lean gas condensate* and a *rich gas condensate.* The first-mentioned

defines fluid systems where a small volume of liquid is generated, usually less than 100 bbl per million ft^3 (< 561 m^3 per million m^3), where the latter defines fluid systems that generate 150 bbl per million ft^3 (> 842 m^3 per million m^3) or more. However, Fan *et al.* (2005:16) caution that these figures should only be taken as indicators of a range, since there are no set/established boundaries. **Figures 2.2[a-d]** afford visual representations with more information on these two classes.

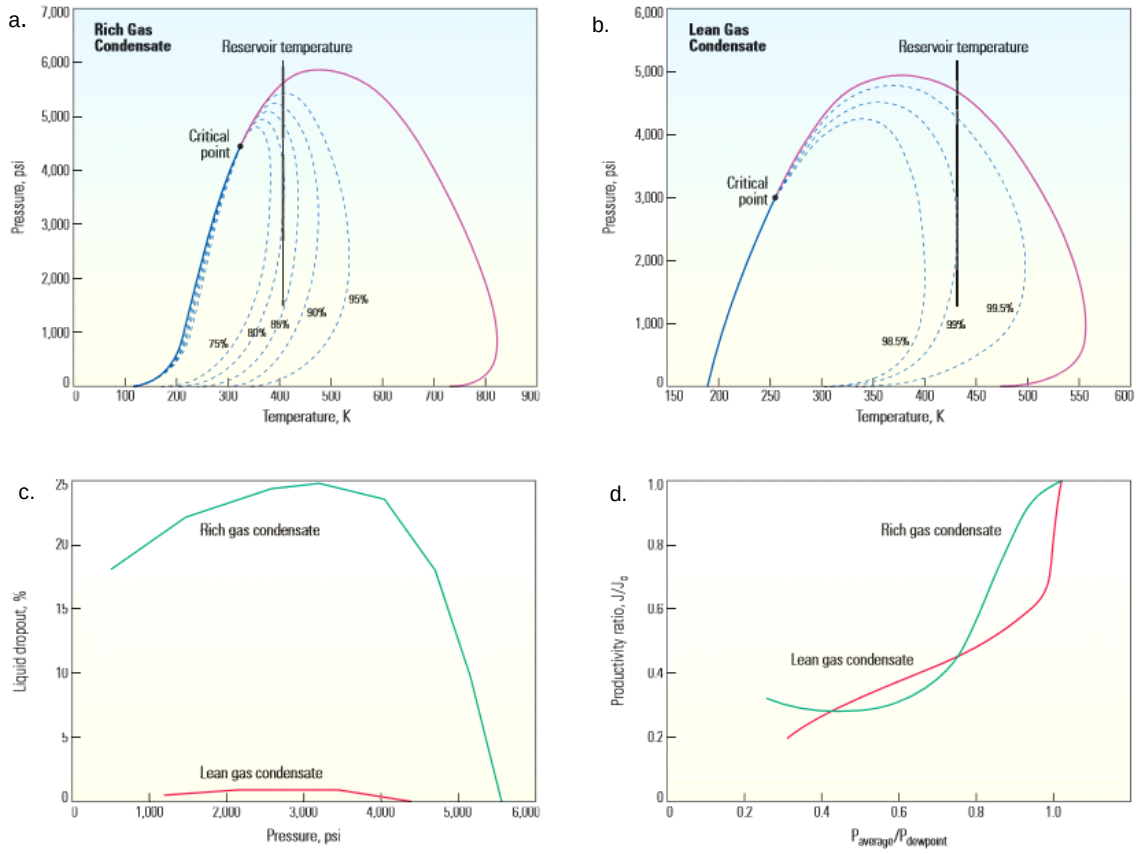

Figure 2.2: Examples of rich and lean gas-condensate behaviour, liquid dropout % and productivity ratios (Fan et al.; 2005:17)

Now that the concept of a gas-condensate and its retrograde behaviour is explained, **Figure 2.3** (a conceptual schematic drawn by Fan *et al.*) will help us to understand how these hydrocarbon fluids flow through gas-condensate fields.

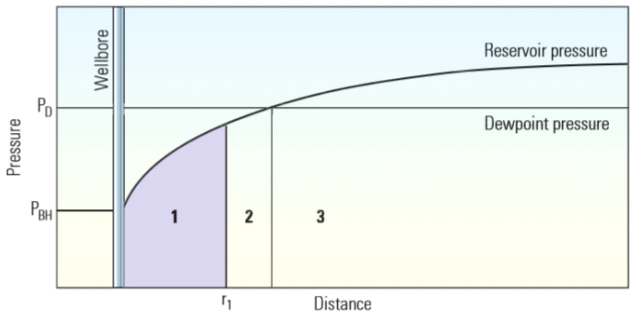

Figure 2.3: Different regions for fluid flow within a producing field (Fan *et al.*; 2005:19)

Shi (2009:13-15) mentions that any producing field can be divided into three reservoir regions, which might not necessarily be present within the field all the time. Regions one and two would exist when bottom hole pressure (BHP) is below the dewpoint of the fluid. Region three would only exist when reservoir pressure is above the dewpoint (this region includes most of the reservoir and would form far away from a well if the well is producing). As the pressure in this region is above the dewpoint, the only hydrocarbon phase present and flowing would be gas. The interior boundary between this region and region two would be where the

reservoir pressure is equal to the dewpoint pressure of the original fluid (gas). According to Fan *et al.* (2005:18) this boundary would also not be stationary, but would move outward as production occurs and pressure drops.

Region two would be described as the condensate build-up region (**Figure 2.3**). This is where liquid drops out of the original gas phase, but the liquid saturation remains low enough so that the liquid is immobile (there is still relative permeability towards gas flow, and thus single-phase gas flow is still present). The amount of liquid to drop out of the gas is entirely dependent on the fluid's phase characteristics, as indicated by its PVT diagram (**Figure 2.1**). The inner boundary of region two is usually determined by the residual oil saturation within the region. To elucidate: this is where enough liquid is present for relative permeability to allow both gas and liquid to flow (critical liquid saturation point) (Shi, 2009:14-15).

As this liquid drops out of solution within a gas reservoir (even for rich gas-condensate reservoirs with substantial liquid dropout), the small droplets are immovable due to capillary forces acting on the fluids. In other words, these droplets are trapped in the small pores or pore throats. The mobility of this liquid is thus dependent on the ratio of relative permeability to viscosity. This ratio remains very insignificant away from the wellbore (Fan *et al.*; 2005:18). This implies that if the pressure drops below the dewpoint in the reservoir, and condensate liquid starts to drop out, the liquid would be lost to production. This phenomenon can be avoided somewhat if the reservoir depletion plan includes gas cycling (Fan *et al.*; 2005:18).

Close to a producing well (Region one), according to Lal (2003:12), the circumstances are much different. According to **Figure 2.3**, this region allows both gas and condensate phases to flow (Lal; 2003:11). When the BHP drops below the dewpoint, liquid drops out. For a moment a transient period exists until enough liquid accumulates to render its mobility noteworthy. Subsequently, gas and liquid compete for flow paths in line with the relative-permeability relationship of the formation (see **Figure 2.4**). The ensuing drop in reservoir pressure below the dewpoint leads to two main results. Firstly, it reduces the gas and condensate production due to "blockage"; and secondly it also implies that the produced gas has less valuable heavy ends as mentioned above because of dropout throughout the reservoir (Fan *et al.*; 2005:18).

According to Fan *et al.* (2005:1), Barker (2005:2), Lal (2003:16) and Petrowiki (2015) this "blockage" encountered during production of a gas-condensate reservoir, is called condensate blockage or condensate banking. Condensate banking usually occurs when a well is produced under a natural depletion production plan. A gas-condensate reservoir can literally "choke" on its most valuable components; the condensate liquid builds up near the well because of pressure drawdown below the mentioned dewpoint, ultimately restricting gas flow because of relative permeability. This "choking" effect can have detrimental consequences on productivity of a well by sometimes a factor of two or more (Fan *et al.*; 2005:1).

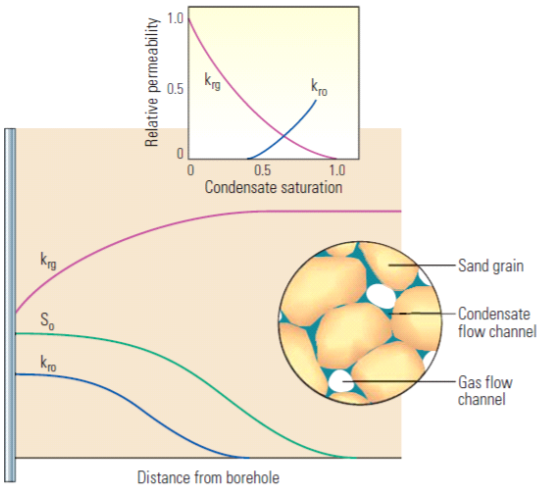

Figure 2.4: Explanation of relative permeability and condensate blockage (Fan *et al.*; 2005:18)

According to Petrowiki (2015), formation damage in gas-condensate reservoirs can be caused by a build-up of fluids (condensate) around the wellbore. Barker (2005:2) reports that the term condensate banking is a well-known phenomenon in gas-condensate reservoirs. He mentions that it ensues because the bottom-hole pressure falls below the dewpoint pressure when a well produces for a period of time. The consequence is that condensate drops out in the reservoir around the well, which quickly accumulates as each cubic metre of

fresh gas produced deposits further condensate. This happens because the pressure near the well is lower than the pressure further away from the well (pressure difference). This accumulated condensate volume near the well reduces gas saturation within this region, and thus gas relative permeability. This has detrimental consequences for the productivity of the well. **Figure 2.5** gives a visual representation of how condensate drops out near a well due to the abovementioned phenomenon.

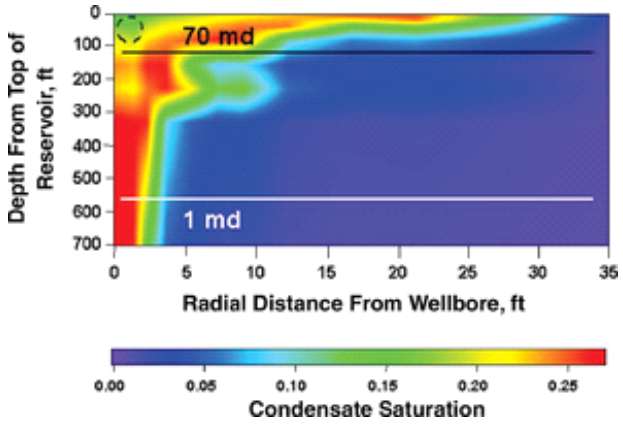

Figure 2.5: An illustration of condensate dropout in the near-wellbore region. Build-up of liquid hydrocarbons in this region can cause large reductions in gas relative permeability (Petrowiki; 2015)

Petrowiki (2015) also supplies the following figure from a real-life case study done in Indonesia (**Figure 2.6**). In this study (a well in the Arun gas field), a significant reduction in well productivity is observed because the average reservoir pressure declines below the dewpoint. The mechanism of formation damage, namely condensate build-up, is related primarily to changes in fluid saturation in the near-wellbore region which results in decreases in gas relative permeability.

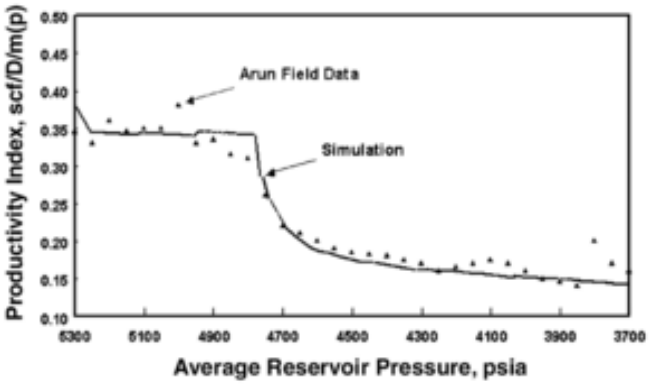

Figure 2.6: Reduction in well productivity caused by condensate build-up, Arun field, Indonesia (Petrowiki; 2015)

This occurrence of condensate build-up (i.e. the condensate bank) and its associated consequences on well productivity, according to Lal (2003:1), have been well studied in literature. Researchers have indicated productivity losses by a factor of 2 to 4 because of this liquid build-up when looking at the productivity index (PI). Barker (2005:2) mentions that even though the occurrence of condensate banking is widely recognized, there is currently no accord within the industry as to when it occurs and whether or not it will have an effect on well productivity. Barker (2005:3) gives several possible reasons for this:

- Identifying its presence from well test data is considered more difficult than anticipated due to the fact that it may be masked by wellbore storage effects. Reasons for this could be because of the data quality, or due to velocity-dependent relative permeability (VDRP) effects complicating the analysis.
- Other effects, such as well damage or even reaching the end of production life of the well, could also cause a decline in productivity with time.
- Some gas-condensate reservoirs could be close to their dewpoint pressure even before they are drilled and produced. This implies that there may be no reduction of productivity because the initial

productivity is already influenced by condensate deposition right from the start of production (Barker; 2005:3).

There is however ways of reducing condensate build-up when it is identified. According to Petrowiki (2015) the most direct method of reducing condensate build-up is by reducing the drawdown so that the BHP remains above the dewpoint. Where this is not a desirable solution, the impact of condensate accumulation can be reduced by increasing the inflow area and achieving linear flow rather than radial flow into the wellbore. This minimizes the impact of the reduced gas permeability in the near-wellbore region. Both of these benefits can be achieved by hydraulic fracturing.

Hydraulic fracture stimulation is one of the, if not the most common methods used to remedy condensate build-up problems. When this fracture is created, a significant decrease in the drawdown needed to produce the well is created. Another bonus is that liquid hydrocarbon build-up on the faces of the fracture won't affect well productivity as much as in radial flow around the wellbore (Petrowiki, 2015).

Finally, in recent times, companies started turning to the use of solvents and surfactants (such as methanol) to stimulate gas-condensate wells where hydraulic fracturing is not the preferred option. Its use results in the removal of the condensate and water banks around a wellbore, ultimately allowing unimpeded gas flow through the near-wellbore region (Petrowiki; 2015).

2.2 The Black-oil (BO) and Compositional Simulation Approaches

The foundation for understanding how fluid composition affects the behaviour of the reservoir fluids, as well as how fluid moves through the different regions within the reservoir has been laid. In the following section the use of different simulation approaches to describe or represent real-life reservoir regions with their individual fluid compositions and movement will be explained.

According to Haukas *et al*. (2004:1), the purpose of a reservoir simulation is to create a computer generated replica of a reservoir, so as to predict the future flow of hydrocarbon liquids from an anticipated hydrocarbon reservoir. Reservoir simulators can only be deemed effective if they solve a set of differential equations, such as for a reservoir fluid comprising of Nc amount of chemical components (C_1 to C_4, H_2O, etc.), which necessitates Nc flow equations to be solved. Currently industry utilizes two types of simulation packages, namely black-oil simulators (BO) and compositional (equation of state – EOS) simulators. In terms of the black-oil simulation approach, the hydrocarbon fluids within the reservoir can be fully described by two components, firstly a pseudo-oil component and secondly a pseudo-gas component. Wang (2007:2) concurs with this statement, and mentions that, although the crude oil and gas in a reservoir may contain many hydrocarbon components, a black-oil model divides these components into two classes based on specific characteristics; all possible components are characterized by two classes: one class reflects "stock-tank oil" while the other reflects "separator gas". According to Izgec (2003:1-2) the oil component can't be dissolved in the gas phase with a conventional BO approach, which is the main constraint that prevents consistent simulation results for volatile oil and gas condensate reservoirs. Due to the complex thermodynamic behaviour which gas-condensate reservoirs exhibit (as has been explicated previously), simple pressure-dependent functional relations cannot fully describe the processes within such reservoirs. This is because of the constant fluid compositional change when such reservoir is produced either through pressure depletion, or by gas cycling above and below dewpoint pressures.

Izgec (2003:2) mentions research indicating that one alternative to the standard black-oil approach that shows promise is to treat the reservoir fluid as a gas-condensate, consisting of a gas component and vaporized oil. The basic supposition for this pseudo two-component hydrocarbon system is that the dry reservoir gas holds hydrocarbon liquid solely as a function of pressure. This assumption is cardinal to the characterization of the condensate gas as a two-component system, and based on one factor: When the pressure is reduced isothermally from the dewpoint, liquid condenses from a condensate gas by retrograde condensation. This retrograde liquid is vaporized by dry gas. Each pseudo-component is then viewed to be a multi-component hydrocarbon fluid in its own right. A water-phase (if present), forms a third component but is usually considered immiscible in the oil and gas phases and exists as a single liquid phase.

In addition, Mahmudi *et al.* (2013:323), mention that gas can be dissolved in the oil phase when looking at a standard black-oil model. This model usually treats the PVT properties of hydrocarbon phases as a single

function of pressure and temperature. This implies that hydrocarbon (oil and gas) properties, among which density, viscosity and specific volume, are calculated by means of experimental correlations at every pressure and temperature step or progression. The dissolved gas existing within the oil phase is calculated by means of empirical correlations. However, compositional effects on pressure and temperature are neglected.

Mahmudi *et al.* (2013:325) and Izgec (2003:13) conclude to say that quite a few modifications to the standard black-oil model have been proposed by a wide array of researchers to extend its range of applications to accommodate variable bubblepoint situations. These recommendations and alterations led to the use of the term "modified or extended black-oil" models (a four-component system comprising of: oil, dissolved gas, gas and vaporised oil).

The main difference between a standard BO model and a modified Black-oil model (MBO) lies in how the oil in the gas phase is treated. The MBO approach assumes first and foremost that, under reservoir conditions, the stock-tank oil component can exist in both oil and gas phases. In addition, it also assumes that the oil content of the gas phase can be defined as a sole function of pressure called vaporized oil-gas ratio, R_g (presented as r_v by Izgec (2003:29)). This function is similar to the solution gas-oil ratio, R_o (presented as r_s by Izgec (2003:29)), used to describe the amount of gas-in-solution in the oil phase. When looking to the fluid in the MBO description, separator gas (suffix g) and stock-tank oil (suffix o) are the pseudo-components used. Notably, either component may be present in the hydrocarbon gas and oil phases. The mole fraction of the pseudo-components in the gas, y_g and y_o, and oil phases, x_g and x_o, is constrained by:

$$Y_o + Y_g = 1 \quad (1)$$

$$x_o + x_g = 1 \quad (2)$$

These may be evaluated from the molar gas-oil ratio and molar oil-gas ratio as:

$$y_o = \frac{1}{1+r_o} \; and \; y_g = \frac{r_o}{1+r_o} \quad (3)$$

$$x_o = \frac{1}{1+r_g} \; and \; x_g = \frac{r_g}{1+r_g} \quad (4)$$

The molar gas-oil ratio, r_o and molar (vaporized) oil-gas ratio, r_g (both dimensionless in nature), can be determined from the standard black-oil parameters, R_g and R_o, through using:

$$r_o = R_o \frac{\rho_{gst}}{\rho_{ost}} \; and \; r_g = R_g \frac{\rho_{ost}}{\rho_{gst}} \quad (5)$$

where ρ_{ost} and ρ_{gst} are the oil and gas molar densities at standard conditions. The following figure gives an indication of how the non-iterative MBO flash calculation procedure would work:

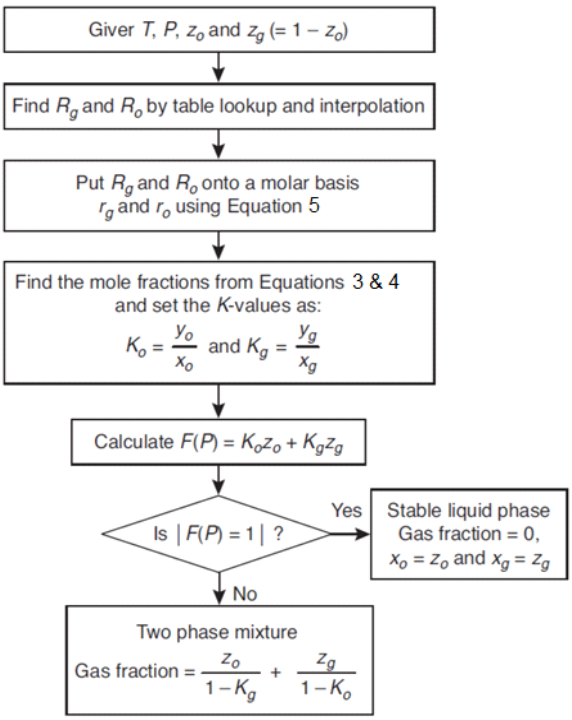

Figure 2.7: An example of the non-iterative MBO flash calculation procedure (Mahmudi *et al.*; 2013:325)

According to Izgec (2003:29) conventional black-oil models use three pressure-dependent functions: formation volume factor for oil (Bo), formation volume factor for gas (Bg) and R_s. The primary limitation of the mentioned functions is that they do not account for the liquid that condenses from the vapour phase. Izgec (2003:30) concurs with the findings of Mahmudi *et al.* (2013:325) who state that modified black-oil models should include an additional pressure dependent function, r_v. This parameter, as mentioned previously, reflects the amount of oil carried in vapour phase (which is a function of pressure below the dewpoint). The modified black-oil representation is based on fixed densities of surface gas and oil, similar to black-oil models.

The variation versus depth of both the solution gas-oil ratio (GOR) and the vaporised oil-gas ratio (OGR), according to Izgec (2003:30), gives rise to compositional disparity in the MBO model. Fluid composition is represented by the mentioned black-oil PVT properties, and should thus be used when initializing the reservoir model. Regardless of an initialization of composition with depth, where solution GOR and OGR are taken directly from the compositional EOS model, it is common knowledge that the saturation pressure versus depth will not be represented properly in the black-oil model, since a single PVT table is used for the MBO model whereas fluid at each depth interval has its own set of PVT tables.

Izgec (2003:3) argues that, despite the shortcomings, the extended black-oil (MBO) simulation models give the researcher or engineer the opportunity of using a simple and less expensive model. The major question that arises, however, is whether the MBO models can represent the compositional phenomena adequately during natural depletion or gas cycling of gas-condensate reservoirs.

As early as 1985, Coats (1985:1822) had already conducted a study in which he ran a few simulations of a gas condensate reservoir using radial-well placements. The study showed that the black-oil PVT formulation gave similar results when compared to the fully compositional EOS PVT formulation for natural depletion above and below dewpoint. Furthermore, he discovered that under certain conditions, the MBO model could replicate the results of compositional simulation cases for cycling above the dewpoint as well. The only major problem scenario he encountered was with gas-cycling below the dewpoint. This two-component simulation rendered quite inaccurate results when cross-referenced with the EOS PVT simulation. The black-oil approach was thus found to be inept for modelling the large compositional gradients of the more complex scenario.

Results of research replicated by Fevang *et al*. (2000:8) supported some of the conclusions drawn by Coats (1985:1822). However, when the scenario included a reservoir with a very rich gas-condensate and

increasing permeability downwards, substantial differences arose in predicted oil recovery calculated by compositional versus MBO models. They finally concluded that a MBO simulator may only be effective in circumstances where the effect of gravity is negligible. They also added that for gas-injection studies a MBO model may only be adequate for lean to medium-rich gas-condensate reservoirs undergoing cycling above dewpoint. Additionally, Fevang *et al*. (2000:8) issue a word of caution when looking to the findings of Coats (1985:1822) as his EOS characterization uses seven components with one C_{7+} fraction. With a more detailed C_{7+} split, oil viscosity differences between black-oil and compositional formulations often yield noticeable differences in well deliverability.

El-Banbi *et al.* (2000:14), however, disagrees with Fevang *et al.* since they found that the MBO approach could be used regardless of the complexity of the fluid. In a full field simulation study for a rich gas-condensate reservoir, the performance of an MBO model was compared with that of a compositional model in the presence of water influx. They also conducted a field-wide history match study with temperatures above and below the dewpoint. Their results reflected an accurate match of average reservoir pressure and water production rates between the two approaches. However, gas-oil ratio and condensate saturation plots were not provided. Initial condensate production rates did not represent a clear match for 500 days. The supposition that modified black-oil models form an intermediate model between the black-oil and the compositional approaches seems plausible.

An advantage of the compositional approach is that a random amount of hydrocarbon components can be built into the model, which would describe the reservoir fluid more precisely. The addition of many components results in impractically lengthy simulation run times, however, which is one of the main pitfalls of this formulation (Haukas *et al*.; 2004:1). Compositional simulations have other advantages as well, among which the fact that "they can account for effects of:

- Phase behaviour;
- Multi-contact miscibility;
- Immiscible or near-miscible displacement;
- Composition-dependent phase properties, such as viscosity and density on miscible sweep-out; and
- Interfacial tension (IFT) especially the effect on residual oil saturation" (Schlumberger; 2014).

EOS models are undoubtedly mathematically much more complex than BO PVT models, resulting in the longer run-times associated with these models. One other important distinction between a BO and a compositional simulator, according to Gundersen (2013:13), is the method which the simulation approach uses to select compositional gradients. A compositional gradient in a BO model is defined by the solution GOR (R_o) versus depth variation for an oil zone and the vaporised OGR (R_g) versus depth variation for a gas zone. The black-oil mass balance equations for oil and gas flow are given as:

$$\nabla \cdot \left[\left(\frac{r_o k_{rg}}{\mu_o B_g} + \frac{k_{ro}}{\mu_o B_o}\nabla\rho\right)\right] = \frac{\varphi}{k}\frac{\vartheta}{\vartheta t}\left(\frac{r_o S_g}{B_g} + \frac{S_o}{B_o}\right) \qquad (6)$$

and

$$\nabla \cdot \left[\left(\frac{R_o k_{ro}}{\mu_o B_o} + \frac{k_{rg}}{\mu_g B_g}\nabla\rho\right)\right] = \frac{\varphi}{k}\frac{\vartheta}{\vartheta t}\left(\frac{R_o S_o}{B_o} + \frac{S_g}{B_g}\right) \qquad (7)$$

respectively, where $S_o + S_g + S_{iw} = 1$, R_o = gas dissolved in the oil-phase and R_g = oil vaporised in the gas phase.

In a compositional model, fluid parameters like density ρ and viscosity μ are dependent on the fluid composition (similar to pressure) and can be expressed as:

$$\rho_o = \rho_o(\rho_o, x_1, \ldots, x_{nc}) \qquad (8)$$

$$\rho_g = \rho_g(\rho_g, y_1, \ldots, y_{nc}) \qquad (9)$$

where x_{nc} and y_{nc} represent multiple components of liquid and vapour respectively (Gundersen, 2013:14).

A computationally less intensive compositional reservoir model uses an EOS with a reduced number of components, which accommodates the central processing unit (CPU) and memory limitations in the compositional simulator more effectively (Gundersen, 2013:13). Pseudoization, or lumping, is a term used to describe the process of reducing compositional components. The procedure for characterizing a fluid in PVT

simulations often divides the fluid into between 13 and 30 pseudo-components, which can be described either as a pure component, such as methane, or as a group of components. The number of components in an EOS characterization depends not only on computational restraints, but also on the desired level of accuracy from the EOS (Gundersen, 2013:13). In order for the pseudoization to have the best possible outcome, a stepwise pseudoization procedure, rather than a random reduction of components, is highly recommended. This implies a procedure where several pseudoized characterizations are developed sequentially (e.g. 15, 12, 10, 7, and 5 pseudo-components). According to Whitson *et al*. (1999:20), the goal with each pseudoization is to maintain PVT predictions as close to the original full characterization as possible. This stepwise approach enables the researcher to determine the smallest amount of pseudo-components that can be used in the model; but which still reflects similarity to the original full characterization (Whitson *et al*., 1999:20).

Once the correct input data have been determined, the EOS calculations can be performed without difficulty. The minimum data required cover: molar composition, molecular weight, and specific gravity of the heaviest components. Once these minimum criteria have been met, any phase and volumetric properties can be calculated by means of the EOS characterization. More simply stated, bubblepoint/dewpoint at specified temperature, P-T diagrams, densities, Z-factors, separator GOR and surface gravity can be determined (Gundersen; 2013:15). This pseudoization procedure permits the engineer or researcher to determine which components are best grouped together, as well as at what point during the procedure the quality of EOS predictions deteriorates beyond the point which is acceptable for engineering calculations (Fevang *et al*.; 2000:2).

In the next paragraph a description follows on how the advantages of a compositional model outweigh those of a black-oil model in certain cases.

Gundersen (2013:13) found that during the drawdown of a gas-condensate reservoir, the fluid composition in the wellstream will not change significantly when reservoir pressure is above the dewpoint pressure of the reservoir fluid. The reason for this being that when looking at a PVT diagram for this illustration, the fluid stays within the one-phased gas zone, outside the two-phased envelope from reservoir to separator conditions. A change in fluid composition of the wellstream would occur once the reservoir pressure decreases below the dewpoint, due to retrograde condensate drop-out in the reservoir (fluid composition moving into the two-phased envelope). For this situation, a BO simulation model may be insufficient to give accurate results, because the component exchange between the oil and gas phase becomes more complex than what the BO model can handle (e.g. when gas is injected into an oil reservoir, since condensates are extracted through gas cycling). This is where a compositional reservoir simulator would be of more use because it would be able to model the component exchange between gas and liquid phase more accurately. Whitson *et al.* (1999:19) reaffirm Coats' statement that gas-condensate reservoirs need to be modelled with the compositional EOS modelling approach.

As mentioned earlier, Coats found that gas cycling below the dewpoint is the only situation where BO modelling may be inadequate. His results indicate that the BO model works well for depletion, single-well modelling, and gas cycling cases above the dewpoint. Fevang *et al*. (2000:2) reported similar findings for gas cycling in medium rich gas-condensate reservoirs above the dewpoint.

In conclusion, a number of factors influence the decision of choosing the best modelling approach, amongst which, the type of gas present in the reservoir, whether the reservoir pressure is above or below the dewpoint, and the time-frame of the project. *This, in effect, delineated the aim of this project as part of the study, namely: to determine the threshold of accuracy of the black-oil model before the use of the more complex compositional modelling approach is necessitated.*

According to Fevang *et al*. (2000:8) a BO model is always adequate for simulating depletion performance of petroleum reservoirs given that the solution GOR and solution OGR are initialized properly, and secondly the PVT data are generated properly. In addition, compositional simulation models are generally recommended for gas injection studies because a BO model can only be used in:

- oil reservoirs when there is minimal vaporization; and
- lean to medium-rich gas-condensate reservoirs undergoing cycling above the dewpoint for gas-condensate fluids.

Initial fluids in place (IFIP) can be calculated accurately for pseudoized-EOS and BO models by initializing with the correct compositional gradient. In a compositional model, compositional gradient should be calculated from the original EOS model – i.e. the EOS model prior to pseudoization. In a MBO model, the solution GORs and OGRs versus depth should be used. BO PVT data should be generated from a properly-selected fluid with sufficiently-high saturation pressure.

Finally, considering the information gleaned from the literature research, evaluated together with the data available some conclusions are evident. During simulation of the field, since the sandstone reservoir used in this study harbours a rich gas-condensate fluid, aspects mentioned such as the retrograde behaviour of the fluid, the different flow regions of a gas-condensate reservoir as well as condensate banking effects would all have major influence on how each model calculates recovery volumes. Care should thus be taken during simulation in order to correctly describe and account for these occurrences. From the information gathered and research done regarding the different modelling approaches that can be used during reservoir simulation, the MBO modelling approach (as an alternative to the conventional BO model) would be evaluated and compared to the field compositional model.

3 Chapter Three: Geological Overview

3.1 Basin Evolution

Explicated in IHS Energy (2010), the initial breakup of Gondwana during the Middle to Late Jurassic period triggered the development of the Northwest-southeast trending half-grabens within the Outeniqua basin. This massive break-up event culminated in the separation of South America from Africa, after which further rifting took place during the Valanginian period. Tectonic activity continued, especially in the eastern sub-basins, until the Aptian period and for as long as transcurrent movement continued between the Falkland Plateau and the southern margin of Africa along the Agulhas-Falkland Fracture Zone. IHS Energy (2010) describes the succession that infilled the syn-rift grabens as mostly continental clastic sediments and red beds, becoming lagoonal to shallow marine in nature. Hereafter a drifting phase commenced, which is clearly marked by a Late Valanginian unconformity. In contrast to the other sub-basins, the drift phase within the western sub-basins was accompanied by thermal subsidence, which formed a deep marine basin in which circulation was often restricted, thus causing periods of anoxia. According to IHS Energy (2010), periods of relatively low sea level caused turbidite fan systems to be built out into the deeper parts of the Bredasdorp sub-basin. Extension into the eastern sub-basins continued as a result of the mentioned drifting event, which caused substantial differences in stratigraphy between west and east. "Basin-wide unconformities mark intervals of rift-flank uplift and erosion, at some of which deep canyons were cut into the underlying sequences and were infilled with clastic sediments (IHS Energy, 2010)".

The Falkland Plateau finally separated during the Aptian period, resulting in thermal subsidence affecting the whole basin. The thermal subsidence culminated in shelf sediment deposition, which gradually prograded southwards across the basin (IHS Energy, 2010). During the Early Tertiary period, uplift of southern Africa caused erosion along the northern edge of the basins, synchronous with subsidence further south, causing general tilting of the basin. **Figure 3.1** shows a seismic cross-section and schematic interpretation of the Bredasdorp sub-basin.

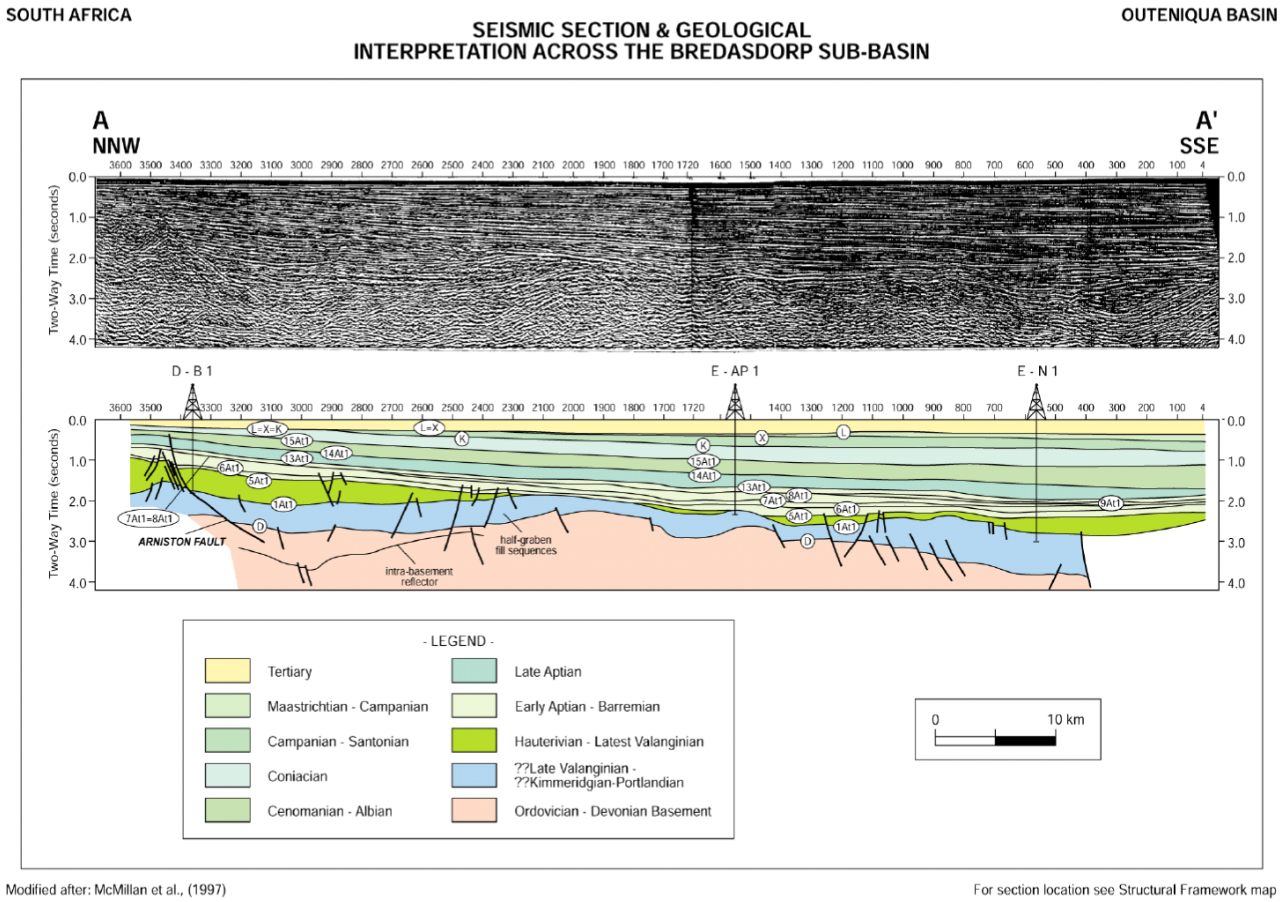

Figure 3.1: Seismic Section and Geological interpretation across the Bredasdorp Sub-Basin (IHS Energy, 2010)

3.2 Reservoir Geology

The geology of the reservoirs in the northern Bredasdrop sub-basin is described in IHS Energy (2010), as consisting mainly of shallow marine sandstones of Valanginian age, which underlay the rift-drift unconformity. These sandstones are typically well sorted, with significant secondary porosity. The other major reservoirs are deep-water mass flow sandstones in channels and fans within the mudstone-dominated sequences that overlie the rift-drift unconformity (IHS Energy, 2010).

4 Chapter Four: Research Methodology

4.1 Introduction

Reservoir simulation is a versatile tool for reservoir engineering. Full field simulation models and history matching the field performance help to finalize the critical management decisions such as number and location of wells to be drilled, pressure maintenance schemes and the design of the facilities. The choice of model for evaluating a rich gas-condensate reservoir is dependent on the type of gas, on whether the reservoir pressure is above or below the dewpoint, and on the time-frame of the project.

We state as hypothesis that while it has the characteristics of being more time consuming and expensive, the compositional model shows greater accuracy in terms of both natural depletion and gas cycling development scenarios. Regarding the modelling of rich gas-condensate reservoirs under natural depletion development scenarios, it will be acceptable if the faster and less expensive MBO model delivers results within a variance of 10% of the compositional model results.

4.2 Methodology

The first step with regard to any project of this nature is to model the reservoir fluid. This has been done by utilizing the software PVTi. As mentioned previously, it is impractical to conduct full-field and large-sector model simulations using a full-component EOS model (due to CPU and memory limitations). Instead a "pseudoized" or reduced-component EOS model should be developed. The EOS has to be tuned properly, incorporating some of the steps in the procedure proposed by Whitson *et al.* (1999:20), albeit it with a few alterations.

- Step 1: Input the components; namely C_1 to C_{12+}, N_2 and CO_2 as well as their mole percentages.
- Step 2: Reduce the number of components by lumping the heavy components together as a C_{7+} pseudoized group; keeping all other components as single carbon components, as well as N_2 and CO_2.
- Step 3: Input laboratory experiments, namely constant volume depletion (CVD), constant compositional expansion (CCE), Flash and Separator experiments.
- Step 4: Match with Peng-Robinson EOS, where the bulk of the adjustments are made on the C_{7+} lumped group. Parameters such as, Binary Interaction Coefficients (BIC's), MW, Pc, Tc and omega (Ω) are altered in order for matching to occur.
- Step 5: After all these steps have been completed, all of the results must be saved and exported as either compositional- or BO-eclipse data files (Whitson *et al.*; 1999:20).

The PVTi (Fluid modelling) workflow can be summed up using the following figure.

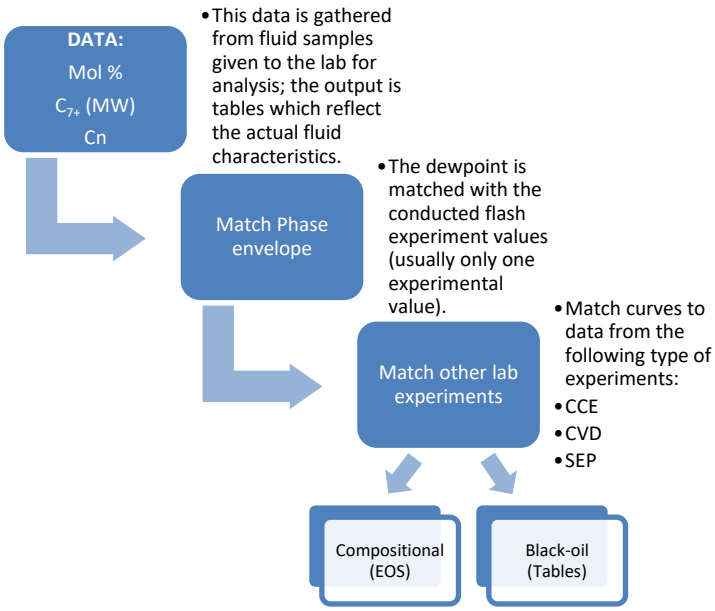

Figure 4.1: Fluid modelling workflow

After the above mentioned process has been quality controlled and reassessed, the fluid model is built. The results of the altered procedure by Whitson *et al.* (1999:20) can then be used in the simulation data file. The "fluid properties" (taken from the created fluid model) are then added into the static model properties (grid) in order to generate the dynamic model (simulation model).

The simulation model is constructed using the following data:

- Grid (consisting of attributes such as porosity (ϕ), permeability (k), Net to Gross (NTG), water saturation (Sw) et cetera.)
- Relative permeabilities
- PVT - EOS
  - Black-oil
- Well definition
- Well production schedule
- Well injection schedule

This model is then initialized. Note that proper initialization of both MBO- and compositional-models is of paramount importance. This implies proper treatment of:

1. Fluid contacts and phase definitions;
2. PVT models; and
3. Compositional (solution-GOR) gradients (Fevang *et al*.; 2000:3).

This initialization is done in order to estimate IFIP for both modified black-oil and compositional models which are consistent (in other words, having the same IFIP volume amounts). The petrel software also features an individual volume calculation option which uses fluid contacts, NTG, porosity, water-, gas-, oil-saturation, Bo, Bg and R_g values in order to calculate oil and gas volumes for the created 3D model. This method together with previous mentioned MBO and compositional model initializations will be tabled in order to verify and confirm the validity of the initialization.

Furthermore, before running any real simulation strategies, an equilibration run is recommended to ensure that critical parameters such as pressure, gas initially in place (GIIP), oil in place (OIP)- and water in place (WIP)-values remain constant over the run and do not migrate in the absence of injection and production. This would confirm that the model is set up correctly and is stable (implying no movement of fluids occurs).

The final step in the methodology is to run these models under natural depletion as well as gas-cycling development scenarios and then evaluate and compare the reliability of the modified black-oil simulation results with that of the compositional model results. In terms of gas-cycling, two types of scenarios will be analysed, namely above the dewpoint, and below the dewpoint.

The figure below summarizes the set objectives for the project workflow.

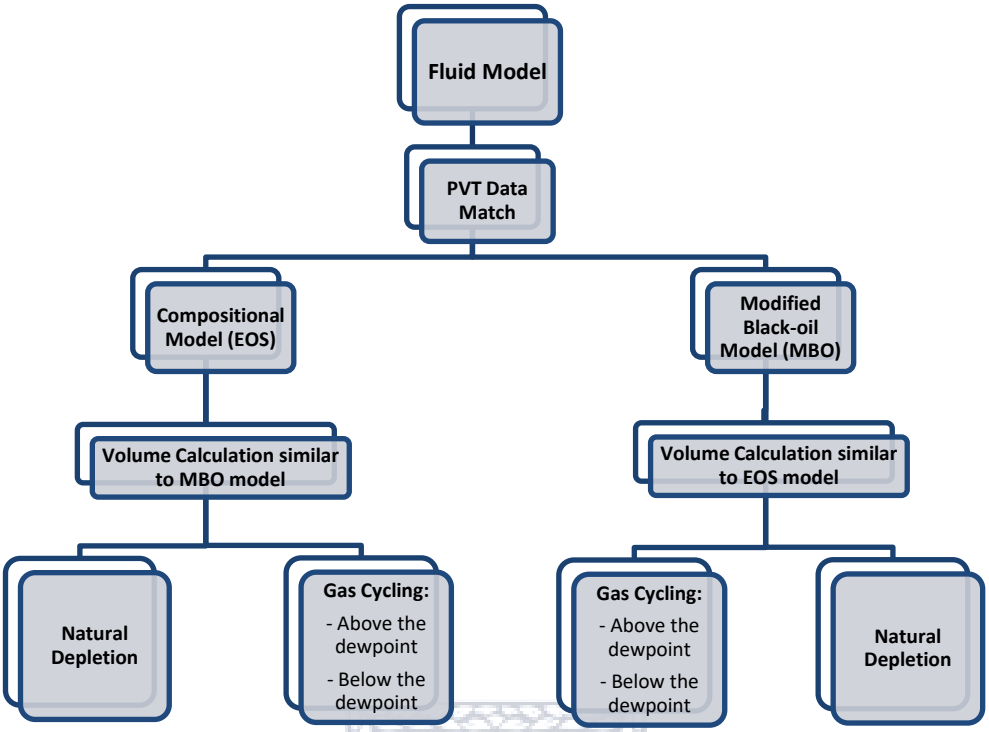

Figure 4.2: Summarized methodology workflow for the project

5 Chapter Five: Results and Discussion

5.1 Reservoir Characterization and Experimental Fluid Description

The fluid selected for our study area is a rich gas-condensate sampled off the coast of South Africa in the Bredasdorp-basinal area. **Table 5.1** represents the Appraisal Well (AW1) well test input and results summary (depth measured in TVD SS).

Table 5.1: Test summary and fluid/reservoir analysis parameters

Test Description	
Tested interval (ftTVDSS)	8526.9 – 8592.5
Net thickness (ft)	65.6
Perforation interval (ftTVDSS)	8522.6 – 8586
Fluid/Reservoir Parameters	
Areal extent of reservoir (mi^2)	~1.16
Reservoir temperature (°F)	242
Initial reservoir static pressure (psia) at 8591 ftTVDSS	3803
Dewpoint pressure (psia)	3805
Well bore radius (ft)	0.354
Porosity (%)	15.9
Water saturation (%)	21
Reservoir top depth (ft)	8486.58
Gas-water contact depth (ft)	8591.54
Initial Maximum thickness of hydrocarbon-zone (ft)	105
Gas formation volume factor – Bg (rb/Mscf)	0.9262
Condensate-Gas Ratio – R_g (stb/Mscf)	0.1625

Separator samples (which include liquid and gas samples) were submitted to a PVT laboratory in France for analysis. These had been collected from the subject well during a routine Drill Stem Test (DST). After recombination of liquid and gas samples a compositional analysis of hydrocarbon components including of C_{12+} was done. In addition, constant mass/composition expansion (CCE) and constant volume depletion (CVD) tests were used to characterize the fluid. Sampling conditions are presented in **Table 5.2**.

Table 5.2: Sampling conditions

Choke Size (in)	32/64”
Flowing Bottom Hole Pressure (psia)	3 640
Well Head Pressure (psia)	2 043
Well Head Temperature (°F)	120
Separator Pressure (psia)	164
Separator Temperature (°F)	80
Fluid Fpv factor	1.02
Separator gas relative density	0.810
Separator gas flow rate (MMscf/day)	8.3
Separator liquid flow rate (Stb/day)	1 387.53
GOR at separator conditions (Scf/Stb)	5 956.29

**All fluid data taken from the PVT laboratory study report done by Schlumberger in 1990.*

A separator test was also conducted; this test is important because it gives the engineer clarity regarding the oil-gas ratio (R_g) of the particular reservoir and fluid system at various separator conditions. Separator conditions used throughout this study reflect two-stages, the second stage being at standard conditions. These conditions are listed in **Table 5.3**.

Table 5.3: Separator conditions

Stage Index	Temperature (°F)	Pressure (psia)
1	80	320
2	60	14.7

The separator liquid was physically recombined with corresponding separator gas, using the field GOR (in SCF/STB) which was corrected for shrinkage. A summary of the recombination experiment is presented in **Table 5.4**.

Table 5.4: Recombination results

Field separator GOR (Scf/Bbl)	5494
Corrected GOR – used (Scf/Bbl)	5549
Stock tank oil density – std (g/cm^3)	0.755
Stock tank liquid gravity (API)	56
Stock tank shrinkage factor (Sbbl/Bbl)	0.892
Separator gas relative density (air=1)	0.79

Table 5.5 presents the compositional description of the recombined fluid entering the well.

Table 5.5: Extended compositional description of the recombined reservoir fluid

Component	Symbol	Mol %
Carbon Dioxide	CO_2	3.31
Nitrogen	N_2	0.63
Methane	C_1	62.83
Ethane	C_2	9.59
Propane	C_3	6.86
Isobutane	iC_4	1.17
N-Butane	nC_4	3.11
Isopentane	iC_5	1.10
N-Pentane	nC_5	1.50
Hexanes	C_6	1.71
Heptanes	C_7	2.31
Octanes	C_8	2.21
Nonanes	C_9	1.24
Decanes	C_{10}	0.83
Undecanes	C_{11}	0.49
C_{12+}	C_{12+}	1.13

Table 5.6 and **Table 5.7** present the results obtained from the constant mass expansion study of the reservoir fluid at reservoir temperature. The reservoir fluid was subjected to pressure depletion from 5000 to 1300 psia.

Table 5.6: Constant Mass Expansion results

Pressure		Relative	Compressibility factor		Z	Ret. Liq. D.
psia	MPa	volume	1/psia	1/MPa		% vol. Pd
5000	34.47	0.8910			1.034	
4745	32.72	0.9084	74.80E-6	10.849E-3	1.000	
4500	31.03	0.9281	86.91E-6	12.606E-3	0.969	
4242	29.25	0.9516	95.55E-6	13.858E-3	0.937	
4000	27.58	0.9773	108.71E-6	15.768E-3	0.907	
Pd= 3805	26.23	1.0000	116.36E-6	16.877E-3	0.883	
3800	26.20	1.0006	123.48E-6	17.910E-3		0.002
3798	26.19	1.0008	106.61E-6	15.463E-3		0.182
3786	26.10	1.0028	162.35E-6	23.547E-3		0.687
3762	25.94	1.0065	151.95E-6	22.038E-3		1.734
3713	25.60	1.0142	155.25E-6	22.516E-3		3.593
3621	24.97	1.0297	164.28E-6	23.827E-3		6.797
3418	23.57	1.0699	185.00E-6	26.831E-3		11.900
3094	21.33	1.1517	219.18E-6	31.789E-3		16.369
2675	18.44	1.3000	272.28E-6	39.492E-3		18.459
2154	14.85	1.5956	355.59E-6	51.574E-3		20.343
1648	11.36	2.0894	467.05E-6	67.740E-3		19.566
1300	8.96	2.6824	635.28E-6	92.139E-3		18.519

Table 5.7: Main results - Constant Mass study at 242°F

Dewpoint pressure – Pd (psia)	3805
Compressibility factor (1/psia)	$123.480E^{-6}$
From (psia):	3805
To (psia):	3800
Gas Z-factor	0.883

The results from the Constant Volume Depletion experiment are shown in **Table 5.8**. CVD of the reservoir fluid was carried out at reservoir temperature from dewpoint pressure down to 354 psia. Retrograde liquid deposit, Cumulative Produced Fluid and gas compressibility factor at each pressure step were also measured.

Table 5.8: Depletion study results (z)

Pressure		Retrograde liquid deposit	Cumulative produced fluid	Z
psia	MPa	% of fluid vol. at Pd	mole % of init. fluid	
3805	26.23	0.000	0.00	0.883
3800	26.20	0.073	0.22	0.873
3794	26.16	0.468	0.46	0.874
3769	25.99	1.198	0.87	0.893
3718	25.63	2.984	1.72	0.889
3619	24.95	6.241	3.43	0.868
3438	23.70	10.466	6.83	0.855
3194	22.02	13.522	11.90	0.834
2820	19.44	15.638	20.56	0.817
2438	16.81	16.139	30.34	0.824
1950	13.44	15.746	43.48	0.845
1355	9.34	13.889	59.55	0.881
738	5.09	12.822	75.75	0.925
354	2.44	11.590	85.40	0.961

**All fluid data taken from the PVT laboratory study report done by Schlumberger in 1990.*

Finally, a molar composition graph is given in **Appendix A, Figure 7.1**, which plots the molar composition of the recombined fluid. The "fingerprint" of the liquid obtained from the direct flash of the separator liquid is also presented in **Figure 7.2, Appendix A**.

5.2 Tuning the EOS

The compositional treatment is based on the Peng-Robinson equation of state, which is widely used as characterization method for gas-condensate fluids. We reduced the number of components by lumping all components greater than C_6 into a pseudoized C_{7+} group, and thus **Table 5.9** reflects this final "regressed" fluid together with a host of other component properties. The first few columns represent fixed parameters for component type, molecular weight and mol % owing to real data gathered from the laboratory experiments (data which can't be altered). Other columns in the Table reflect set literature values gathered through chemical study of each pure component.

Table 5.9: Final values for Fluid Composition and Component Properties

Name	Molecular Weight	ZI (%)	Weight Fraction (%)	P_{crit} (Bar)	V_{crit} viscosity (m^3/kg-mole)	Z_{crit} viscosity	Vol shift	Acentric factor	Parachor (dyne/cm)	Omega A	Omega B
N_2	28,01	0,63	0,53	33,94	0,09	0,29	-0,19	0,04	41,00	0,46	0,08
CO_2	44,01	3,31	4,40	73,87	0,09	0,27	0,03	0,23	78,00	0,46	0,08
C_1	16,04	62,81	30,44	46,04	0,10	0,28	-0,17	0,01	77,00	0,46	0,08
C_2	30,07	9,59	8,71	48,84	0,15	0,28	-0,13	0,10	108,00	0,46	0,08
C3	44,10	6,86	9,14	42,46	0,20	0,28	-0,09	0,15	150,30	0,46	0,08
iC_4	58,12	1,17	2,05	36,48	0,26	0,28	0,13	0,18	181,50	0,46	0,08
nC_4	58,12	3,11	5,46	37,97	0,25	0,27	0,05	0,20	189,90	0,46	0,08
iC_5	72,15	1,10	2,40	33,89	0,31	0,27	-0,01	0,23	225,00	0,46	0,08
nC_5	72,15	1,50	3,27	33,70	0,31	0,27	-0,01	0,25	231,50	0,46	0,08
C_6	84,00	1,71	4,34	30,10	0,35	0,25	-0,02	0,30	271,00	0,46	0,08
C_{7+}	130,60	8,21	29,26	28,98	0,48	0,27	-0,44	0,39	384,49	0,35	0,06

In order to fit the phase envelope to the corresponding flash experiment values, the above mentioned literature values must be altered (using regression). The bulk of the adjustments are made on the C_{7+} lumped group. Parameters such as, BIC's, MW, Pc, Tc and Ω are altered to ensure matching. These literature values were thus altered and through multiple efforts the phase envelope was matched to the flash experiment data.

A visual representation of the phase envelope is given in **Figure 5.1**.

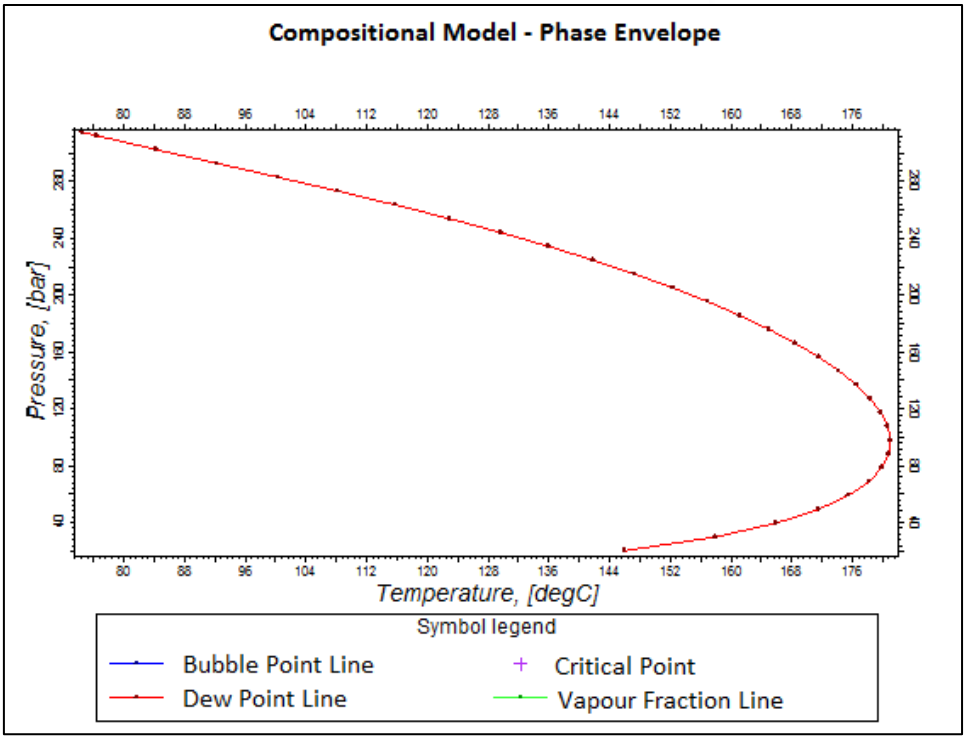

Figure 5.1: Fluid Phase Envelope

After the regression process was done, a good match between experimental and simulated data for CCE, CVD and Separator experiments was obtained (as is represented through **Figure 7.3** to **7.9, Appendix B**). The fluid model could thus be incorporated into the simulation model together with the static parameters in order to generate the dynamic model.

5.3 The Simulation Model and Static Properties

The reservoir model has Cartesian (Corner point) co-ordinates with a typical grid block size of 164 x 164 x 1.64 ft. The gas-water contact (GWC) is found at 8591.54 ft with an initial static pressure of 3803 psia. The total number of grid cells (nI*nJ*nK) generated are 230 x 108 x 100 which reflect a total of 2 484 000 cells. The field, however, possesses NW-SE trending sealing fault which implies that the area of interest (active cells) consists of about 714 852 cells (Referring to **Figure 5.2**, the area of interest would be the yellow segment of the model).

An exploration well (AW1) is located in block 107,62,1 (I,J,K) of the reservoir model, and it was drilled on an anti-form (four-way) closure. An illustration of the reservoir model with the different segments can be seen in **Figure 5.2**.

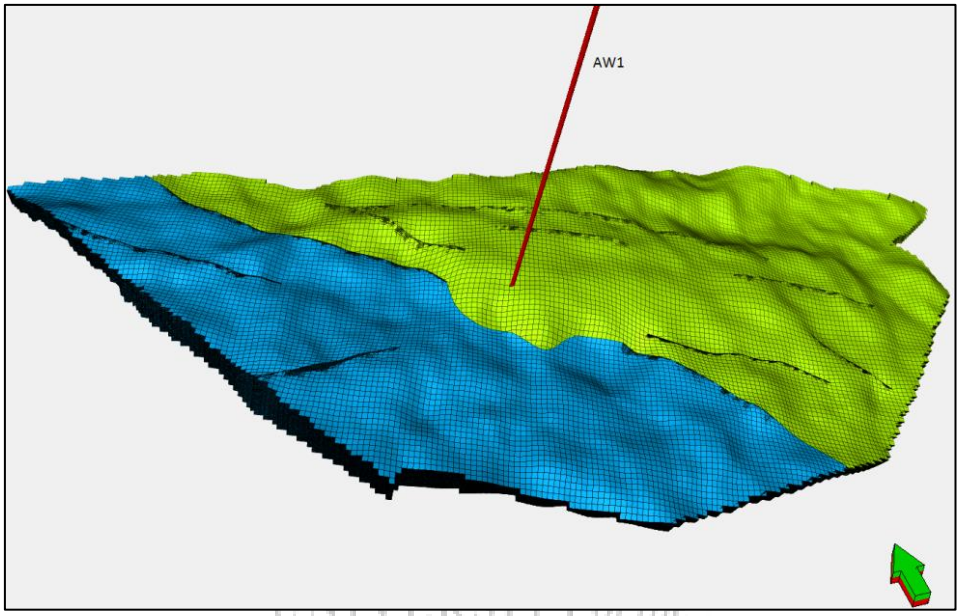

Figure 5.2: Full reservoir model

Some information regarding how the static model was built must also be provided. A few key building blocks must be incorporated in order to correctly describe the static and dynamic model workflow. The impact of these key elements on GIIP as well as the quantification of subsurface uncertainties and associated risks for the project must then be evaluated. The static model workflow and its associated "key steps" are summarized below.

Firstly, the structural grid was built. This fine grid (grid size: 164ft x 164ft) of the structural framework was created to incorporate the different faults seen on the seismic. Further aspects considered reflect horizon modelling and correlation, grid size and orientation, contacts and finally the layering scheme.

Thereafter the "tank container" was assessed. This static model container was constructed taking into account the regional geological understanding of the area. Channel complexes were identified and defined by using several seismic attributes as inputs together with volume of clay, Vcl (sand content) as the training data set. Neural network estimation of sand facies was then carried out. The specific set of seismic attributes necessary to obtain a sand facies were captured (probability cube), which enabled the building of the tank model (using Truncated Gaussian Simulation) to distribute tank sand and tank shale facies.

Electro-facies modelling was then carried out. This is necessary in order to refine facies distribution inside the tank sand facies. An artificial neural network (ANN) classification was performed on the following available log set: Caliper, Gamma Ray (GR), Neutron (NPHI), Permeability (K), Density (Rhob), Resistivity of rock (RT), Spontaneous Potential (SP) and Flow Zone Indicator (FZI). According to the static model analysis and core data comparison, four electro-facies groups are reflected within the cells of the model, namely:

1. Group 1: Shale encountered inside the reservoir (grey)
2. Group 2: Concretions, cemented tight streaks in the logs (green)
3. Group 3: Sand having very good reservoir properties (orange) and
4. Group 4: Sand having good reservoir properties (yellow).

Figure 5.3 presents the entire model with all electro-facies shown.

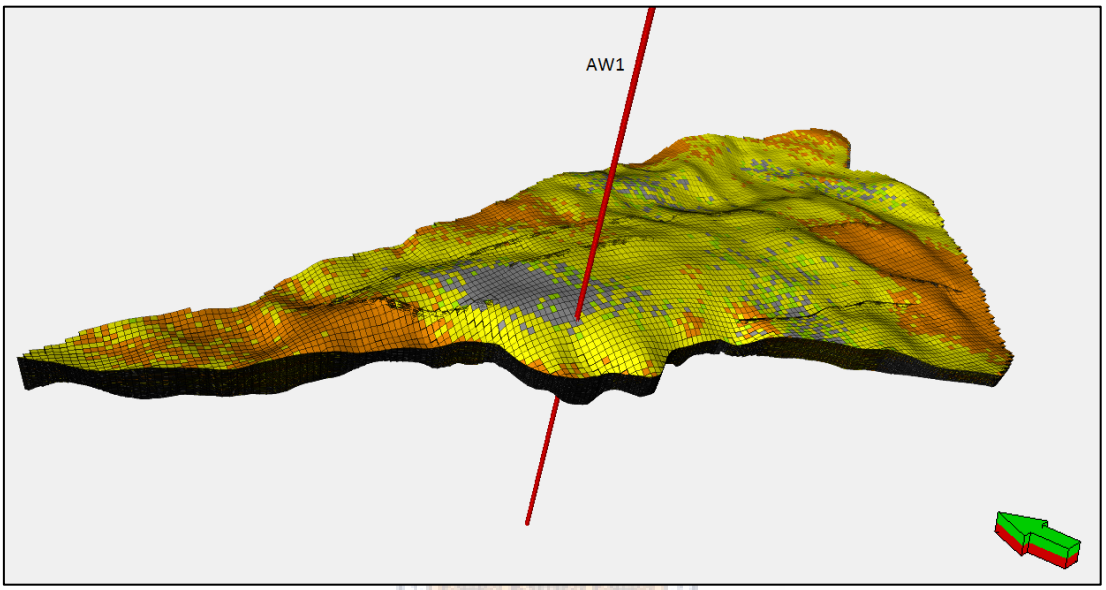

Figure 5.3: Electro-facies properties for the reservoir model

Table 5.10 reflects the distribution of the electro-facies groups by AW1.

Table 5.10: Distribution percentage of electro-facies according to AW1

	AW1
Group 1	11.6%
Group 2	2.1%
Group 3	31.6%
Group 4	54.7%

The different electro-facies groups were then separated to enhance cell visualization reflecting Group 1 and 2 (**Figure 5.4**) and Group 3 and 4 (**Figure 5.5**).

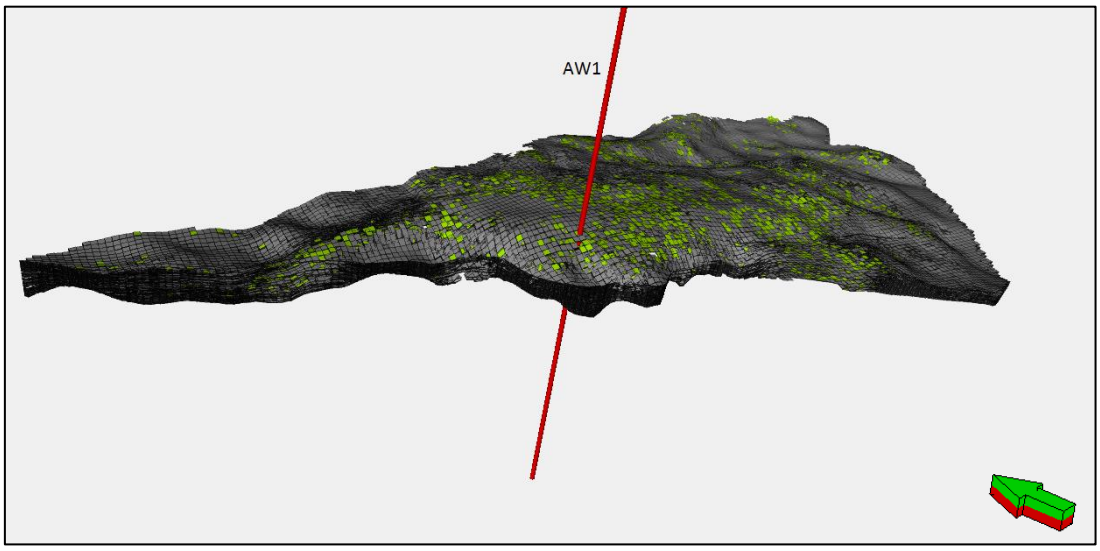

Figure 5.4: Filtered model showing only shales (green and grey cells)

This was done so that a visual distinction could be made between which areas in the model are characterised as “poor” and “good” reservoir respectively, as well as where reservoir properties will reflect the best quality. Note that the bottom parts of the reservoir consist of Group 1 and 2 facies, while the upper parts have better reservoir quality (Group 3 and 4).

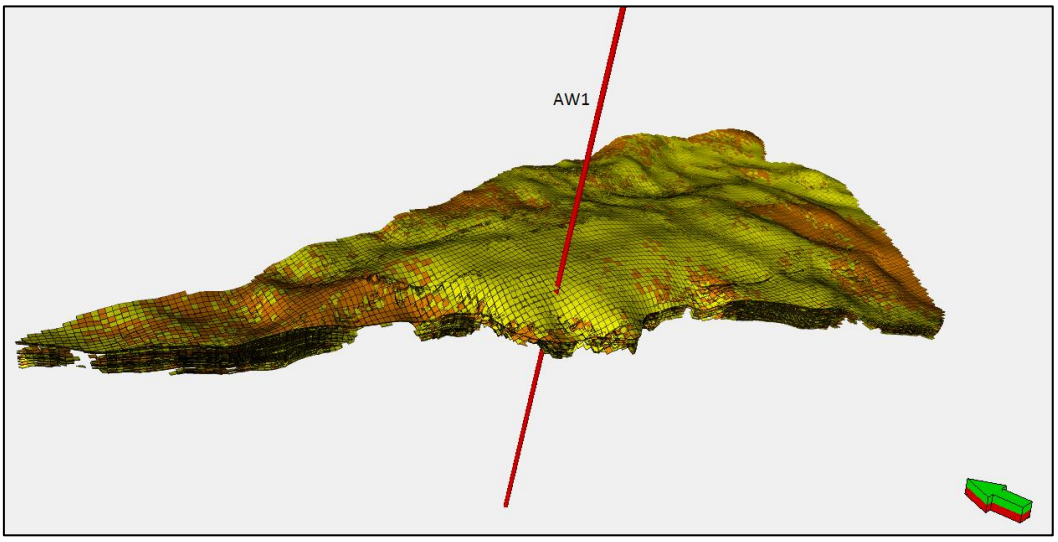

Figure 5.5: Filtered model showing sandstones (yellow and orange cells)

An important part of the project comprises petrophysical reservoir properties modelling. This incorporates porosity modelling, where Sequential Gaussian Simulation with no co-kriging was adopted for building the porosity model. Thereafter, permeability was addressed; again Sequential Gaussian Simulation was used per electro-facies group, with co-located co-kriging on porosity which was adopted for building the permeability model. This method allows for using a permeability value range for a single porosity value, and it preserves the vertical variation of permeability as observed on the log. Lastly water saturation was modelled by using the standard equation for calculation in the form of the Pc and J function derived from petrophysical work, where:

$$J = 0.005845 * \text{height above contact} * \text{sqrt}(\text{perm}/\text{poro}) \quad (10)$$

$$SW = 0.15604 * J^{(-0.39845)} \quad (11)$$

Since no wells with production data were present, history matching was only conducted on data from a five-day drill stem test (DST) conducted after AW1 had been drilled. This history matching process was done in order to calibrate the permeability for the model to the DST data, since there was a discrepancy between the permeability calculated by the geologists used in the static model and the actual permeability values measured during the testing of AW1 (a permeability multiplier of 1.25 was used).

Table 5.11 presents the average rock properties used in the model. It reflects average porosity (ϕ) for the above mentioned sandstone reservoir, as well as average permeability (k) values in the x, y and z directions for this reservoir. The kv/kh ratio was chosen as 0.1 throughout the study area. The rock relative permeability curves for gas-water and oil-water can also be seen in **Figure 7.10, Appendix C**.

Table 5.11: Average Static properties for the sandstone reservoir

Reservoir Avg porosity (%)	15.9
Reservoir Avg permeability$_x$ (md)	21.7
Reservoir Avg permeability$_y$ (md)	21.7
Reservoir Avg permeability$_z$ (md)	2.17

The final step in the static modelling workflow is associated with uncertainty analysis (the study used a nested stochastic approach) and volumetric calculation. Simply stated, one incorporates an uncertainty analysis on all parameters within the static model setup. Multiple realisations (different scenarios) with different combinations of these parameters are run in order to estimate volumetrics. Finally the P10/P50/P90

volumetrics (**Table 5.12**) are determined and a tornado plot is drawn up in order to capture the relative importance of each parameter on GIIP.

The plot showed that the three main parameters which influenced GIIP volumes were the variation in the structural top depth and contact depth and the variation of the relative proportion of the different electro-facies.

Table 5.12: GIIP associated with the 900 stochastic geological model scenarios performed

P10/50/90 Volumetric Range	
Case	**GIIP (MMMscf)**
P90	43.59
P50	59.61
P10	83.38
Base case	56.18

It is important to keep in mind that these volumetric ranges may differ from the simulation GIIP volumes due to PVT differences.

5.4 Model Initialization and Equilibration

Initialization refers to defining the initial conditions of the simulation (Schlumberger; 2015:20), which entails defining pressures and phase saturation at the start date of the simulation. These initial conditions are defined by specifying the gas-oil contact (GOC), oil-water contact (OWC) or gas-water contact (GWC) depths, as well as the pressure at a known depth. ECLIPSE then uses this information together with grid properties and PVT definition to calculate the initial hydrostatic pressure gradients in each zone of the reservoir, and allocate the initial saturation of each phase in every grid cell before production and injection (Schlumberger; 2015:21). The initial reservoir conditions can be defined in one of four ways, namely:

- Method number one assumes the reservoir is in hydrostatic equilibrium (Basic hydrostatic equilibration).

The final three methods are all forms of non-equilibrium initialization:

- The initial conditions can be read from a RESTART file generated by an earlier run (Restarts).
- The initial conditions can be set explicitly (Enumeration).
- The initial conditions can be calculated by a combination of equilibration and enumeration (Mixed hydrostatic equilibration).

Assuming that the reservoir was in hydrostatic equilibrium, the method of basic hydrostatic equilibration was used in this study to define initial conditions.

When a reservoir consists of a single phase fluid, only fluid density is needed in order to determine the vertical pressure gradient. With the reservoir pressure at a given datum depth available, fluid density can be calculated (at that depth) and thus the reservoir pressure can be determined by moving up (and down) the reservoir in small steps, recalculating the density at each step.

When, however, there are more than one phase present, the algorithm becomes significantly more complex. The contact depths where the two phases meet, together with the capillary pressure at these depths, must be provided. Sufficient information is needed to ensure that the densities of all phases present can be calculated. Starting at the datum depth, the hydrostatic pressure for the “datum phase” can be calculated by moving up and down the reservoir. Pressures in the other phases can then be determined at the contact depths, and thereafter the hydrostatic pressures can be determined throughout the reservoir. Only once the phase pressures are known, can the phase saturations be determined at each depth, ensuring that the hydrostatic pressure variation is balanced by the capillary pressure between the phases.

Note that regarding these multi-phase situations, the algorithm assumes that water is heavier than oil which is heavier than gas. Might this condition not hold, the algorithm will fail to produce representative results, which could indicate exceptional heavy oil or improper characterization of the fluid.

This hydrostatic equilibration method provides output in the form of tables consisting of pressure- and saturation-values as a function of depth. One is also able to perform the equilibration on a finer grid than that used for simulation, in which case the resulting saturations are integrated over the cell volumes at the end of the equilibration to provide a starting point for the simulation. Using a finer grid for equilibration will have the advantage of yielding a more accurate fluid-in-place result, but may have the disadvantage of some fluid movement upon starting the simulation.

For calculating the initial conditions within each equilibration region, two stages must be performed. Stage one implies that an internal table of phase pressures (Pw, Po, Pg), and composition (or R_o and R_g for black-oil) against depth must be set up. Thereafter, stage two interpolates this table and uses the saturation functions to obtain the fluid conditions in each grid block in the region.

Unpacking stage one, one sees that these depth points for the internal tables are spaced equally throughout the region. The number of depth points is set using the EQLDIMS keyword in the RUNSPEC section. If one requires finer definition, this value should be increased. This is done, for example, in problems where the oil zone occupies only a small fraction of the overall reservoir thickness.

The pressure gradient for each phase between each pair of depth points in the table are then calculated iteratively using a density consistent with the average pressure within the depth step. If the datum depth lies in the oil zone, the oil pressure values are calculated first, stepping from the datum depth up to the top and down to the bottom of the equilibration region. Thereafter, the water pressure on the oil-water contact can be attained, and the water pressure values are calculated. The gas pressure values are also calculated in a similar manner starting from the gas-oil contact.

Regarding the second stage of the equilibration calculation, local fluid conditions in each grid block in the equilibration region are determined. The internal table is then interpolated throughout the entire reservoir model to obtain the values of phase pressures and composition. Water saturation is determined by inverse look-up of the water capillary pressure table (entered with keyword SWFN or SWOF) for the grid block, such that

$$Pcow\ (Sw) = Po - Pw \qquad (12)$$

If Po - Pw is found to exceed the highest capillary pressure value in the SWFN/SWOF table (corresponding to the lowest saturation value Sw_{min}), the water saturation is set equal to Sw_{min}. In turn, if Po - Pw is less than the lowest capillary pressure in the table (corresponding to the highest saturation value Sw_{max}), the water saturation is set equal to Sw_{max} and the oil pressure is adjusted to follow the water pressure gradient.

The gas saturation is similarly determined by inverse look-up of the gas capillary pressure table (keyword SGFN, SGOF or SLGOF) for the grid block, such that

$$Pcog\ (Sg) = Pg - Po \qquad (13)$$

If Pg - Po is less than the lowest capillary pressure value in the table (corresponding to the lowest gas saturation value Sg_{min}), the gas saturation is set equal to Sg_{min}. If Pg - Po exceeds the highest capillary pressure in the table (corresponding to the highest gas saturation value Sg_{max}), the gas saturation is set equal to Sg_{max} and the oil pressure is adjusted to follow the gas pressure gradient.

To summarize, equilibration involves the process of defining the initial saturation of each phase and initial hydrostatic pressure gradients everywhere in the model based on contact depths in association with a pressure value at a known depth. This information is normally gathered from well testing, well logs, repeat formation tester (RFT) and production logging tool (PLT) measurements. ECLIPSE assumes that the pressure and saturation are in equilibrium. The aim of equilibration is thus to set up a static initial configuration in which the phases present are in equilibrium and in which the inter-block flows are zero. Successful equilibration can be verified by running the simulation without wells to check that no flows occur. This method of initialization is appropriate when initializing a simulation before production and injection; but not after production or injection has begun (Schlumberger; 2015:23).

We performed an initialization run for both black-oil and compositional models with the producer well shut in (non-existent). The original hydrocarbon volume and reservoir pressure stay constant with time, which means that the material balance is correct and no mass and pressure losses are present. Another important aspect to be accounted for in order to correctly and accurately estimate the IFIP of both models, concerns how the model calculates fluid saturation in and around the grid blocks near the GWC. When using the

EQUIL keyword, the ninth item within this keyword is denoted by the integer N. This value specifies how the model calculates the fluid saturation for each cell close to the GWC. An integer value of N<0 causes the simulator to take an average of the conditions at 2N+1 equally-spaced sub-blocks within each grid block. The blocks are treated as being horizontal. With N=0, the simulator sets the fluid saturation in each grid block according to the conditions at the centre of the block. Finally, an N>0 is equivalent to the N<0 option, but the grid blocks are treated as being tilted. This is illustrated by the following figure taken from the Eclipse Help Reference Manual.

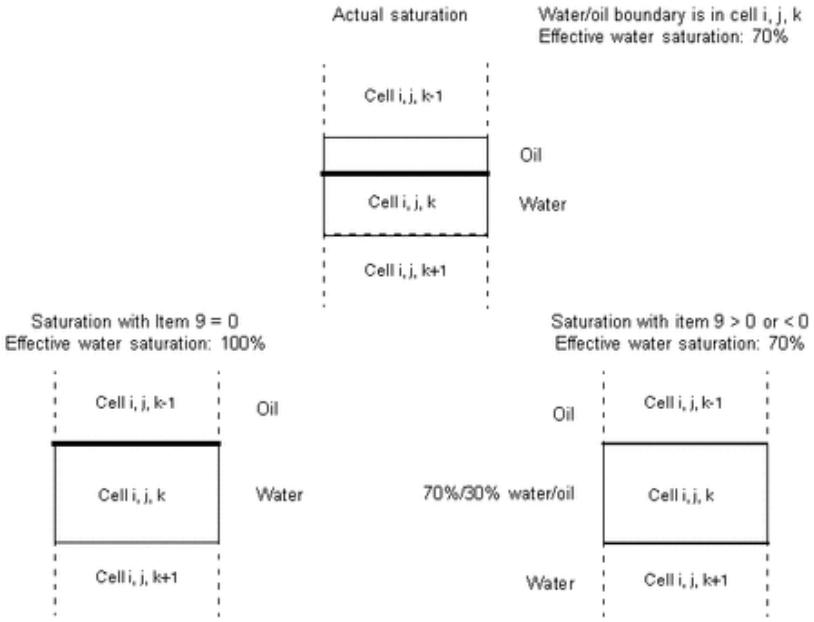

Figure 5.6: Effect of item 9 on saturation definition (Eclipse Help Reference Manual)

Because the grid blocks of our model are tilted blocks, an integer value of N>0 (20 to be specific) was chosen. For reference, a run with N=0 was also done to show the difference in IFIP between the two equilibration scenarios (**Table 5.13**).

Table 5.13: Initial fluid in place volumes for both models, using an integer value of 0 and 20

Modified Black-Oil Model			
	Oil (MMstb)	**Gas (MMMscf)**	**Water (MMMstb)**
1_BO_Initialization_run_equil_0	9.5	58.5	480.5
1_BO_Initialization_run_equil_20	9.7	59.9	479.2
Compositional Model			
	Oil (MMstb)	**Gas (MMMscf)**	**Water (MMMstb)**
1_Comp_Initialization_run_equil_0_lbccoeff	10.1	58.6	483.4
1_Comp_Initialization_run_equil_20_lbccoeff	10.2	59.7	482.5

Petrel also gives the engineer the added option of calculating initial volumes by using a simple volume calculation equation (as described in the methodology section). This was also done in order to further strengthen and assess the initialization's findings. **Table 5.14** presents the findings of the IFIP for both initialization runs together with a volume calculation answer for the 3D model. It also provides an indication of the deviation percentage associated between the different methods in order to assess the accuracy between both initialization runs as well as the volume calculation option of Petrel. A deviation percentage less than 5% is considered to be within an acceptable range.

Table 5.14: Volumetric comparisons and percentage deviation

	Oil (MMstb)	Gas (MMMscf)	Water (MMMstb)
BO_Initialization	9.7	59.9	479.2
Comp_initialization	10.2	59.7	482.5
Volcalc_case	9.8	58.5	N/D
% Deviation			
	Oil	**Gas**	**Water**
BO vs Comp	4.9	-0.4	0.7
Volcalc vs Comp	4.4	1.9	N/D
BO vs Volcalc	0.5	-2.4	N/D

As is mentioned in the methodology, equilibration tests were carried out on both the MBO and compositional models. These equilibration tests allow the dynamic model to time-step for 1 year with no production or injection to check if there is significant fluid movement.

Figure 5.7 illustrates the results of these equilibration runs (dashed lines reflect the compositional model whilst solid lines reflect the MBO model); note that for GIIP, OIP and WIP the parameters remain constant for both the MBO and compositional model. Regarding the field pressure curves, the change is considered negligible. These findings confirm that the models are initialized and calibrated properly and that the natural depletion and gas cycling development scenarios could be run.

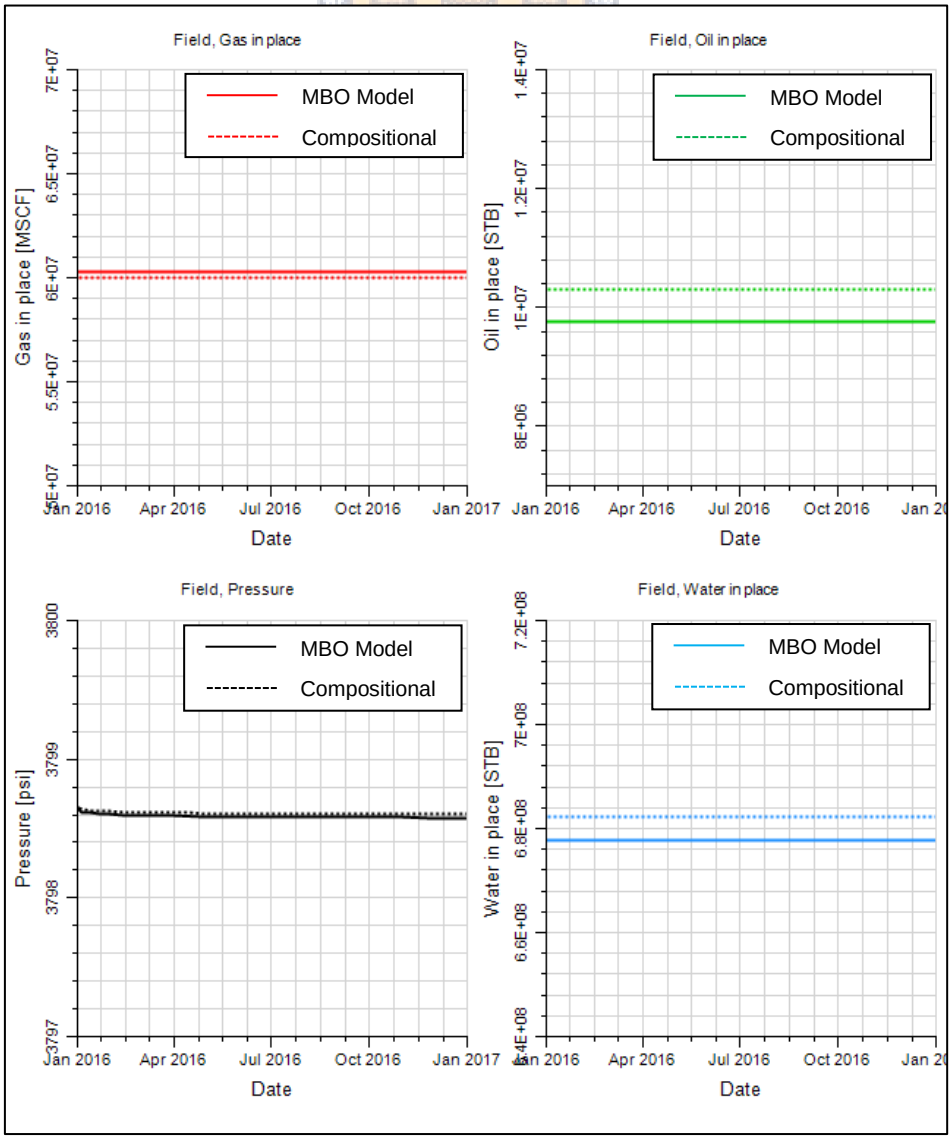

Figure 5.7: MBO and Compositional model equilibration checks comparison

5.5 Development Scenarios

Since AW1 is the only well that has been drilled within the study area thus far (no production wells have been drilled to date), development scenarios had to be run on newly engineered simulation wells. Regarding this study, one producing well, Horizontal Well 1 (HW1) and one gas injection well, Gas Injector 1 (GI1) was proposed, engineered and used during all simulation runs.

Horizontal Well, HW1, has a total length of 18 020.44 ft, drilled to a total depth of 8513.78 ft. The start of the horizontal section is located in block 103 59 1 (I,J,K) and its length within the reservoir is approximately 5249.34 ft terminating in block 135 59 1. The horizontal part of the well houses a perforation section approximately 3280.84 ft in length (as is shown by **Figure 5.8b**). The tubing size used during all simulations reflects 4.5 inch tubing with a well skin factor of 10.

Gas Injector, GI1, is a vertical well located in grid block 135 57 1. The perforation interval has a total length of 32.81 ft and is located at vertical depth interval 8500.66 ft to 8533.47 ft. The total depth of the well is 8584.15 ft.

The following figure reflects all parameters mentioned above, as well as the proposed wells' proximity to AW1. It also reflects the GWC emphasizing a 77.76 ft distance to the horizontal section of the production well.

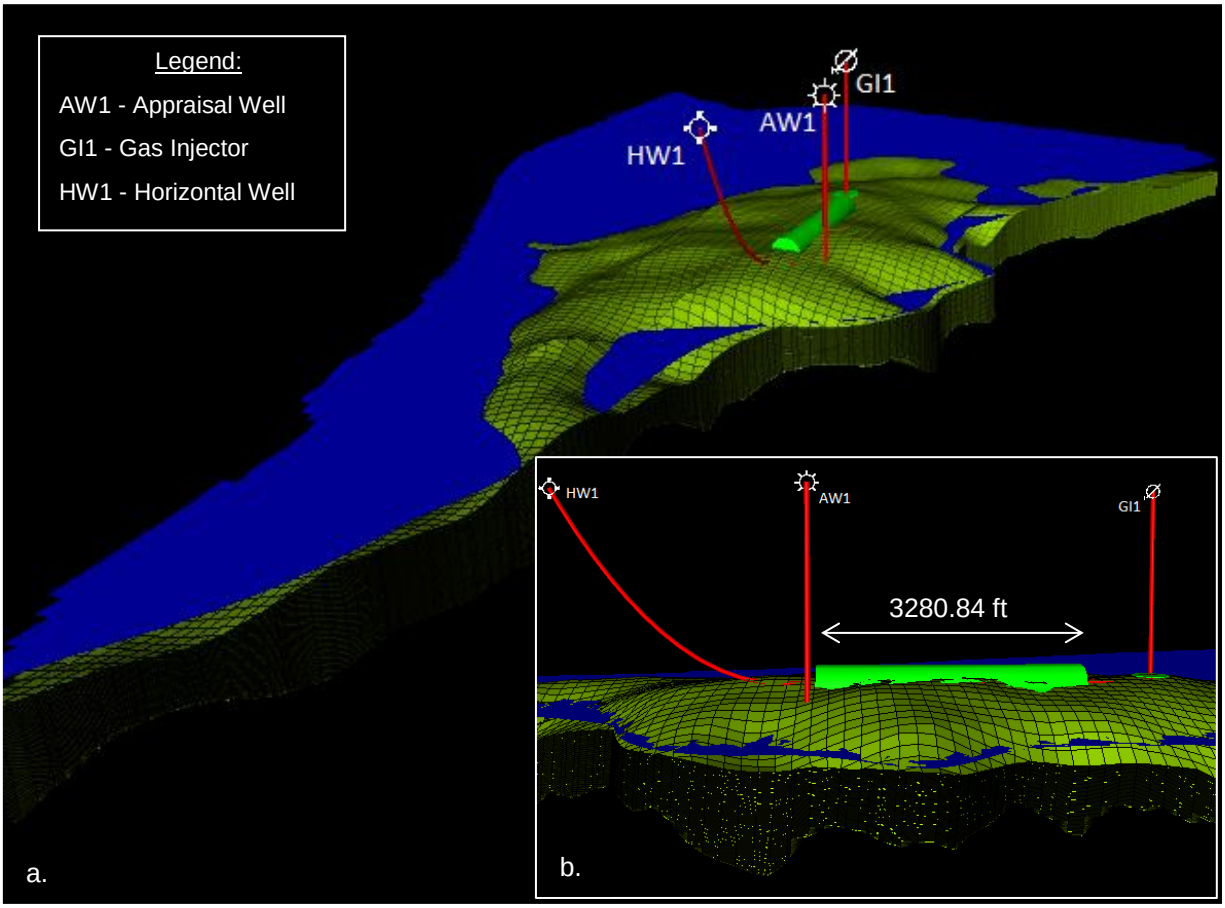

Figure 5.8: (a) Reservoir, GWC, production and injection well locations together with (b) perforation intervals

All simulations were run on the same desktop computer running Petrel 2015, with specifications as follows:

- Type and model: Dell Precision T5600 series
- Processor: Intel®Xeon® CPU E5-2630 0 @ 2.30 GHz 2.30 GHz (2 processors)
- RAM: 64.0 GB
- System type: 64-bit operating system.

The parallel option was used during all simulation runs which allows for the simulation of a single data set to be distributed across a number of processors. For all simulations a total number of 8 processors per simulation case could be used as specified by the user in the data file.

5.5.1 Natural Depletion Development Scenarios

We decided that regarding the natural depletion development scenarios, a base case development scenario would firstly be created. This base case development scenario was run on both the MBO as well as compositional model in order to verify that there is a good match between the two models during simulation without any external rules (for instance introducing limits to oil production rates, tubing head pressure (THP) or water production). The only rules which were imposed on the development scenario was a gas rate production control maximum of 50 000 MSCF/day, as well as a BHP min limit of 580 psia (other aspects such as THP and gas production minimum cut-offs are not addressed here, but consequent cases will follow addressing such issues). It is important to reiterate that the idea of these base case results is not to reflect an accurate real life development strategy, but rather to confirm that under "simple" circumstances the results for both models do in fact portray similarity.

On completion of the base case simulation runs, comparison graphs for a number of well responses were created in order to evaluate the feasibility of whether these different modelling methods might behave in a similar manner when looking at natural depletion development scenarios, as was claimed by several authors (Fevang *et al*. (2000:2), Coats (1985:1822) and El-Banbi *et al.* (2000:14)). **Figure 5.9** depicts gas- and oil-production rates for a simulation period of ten years.

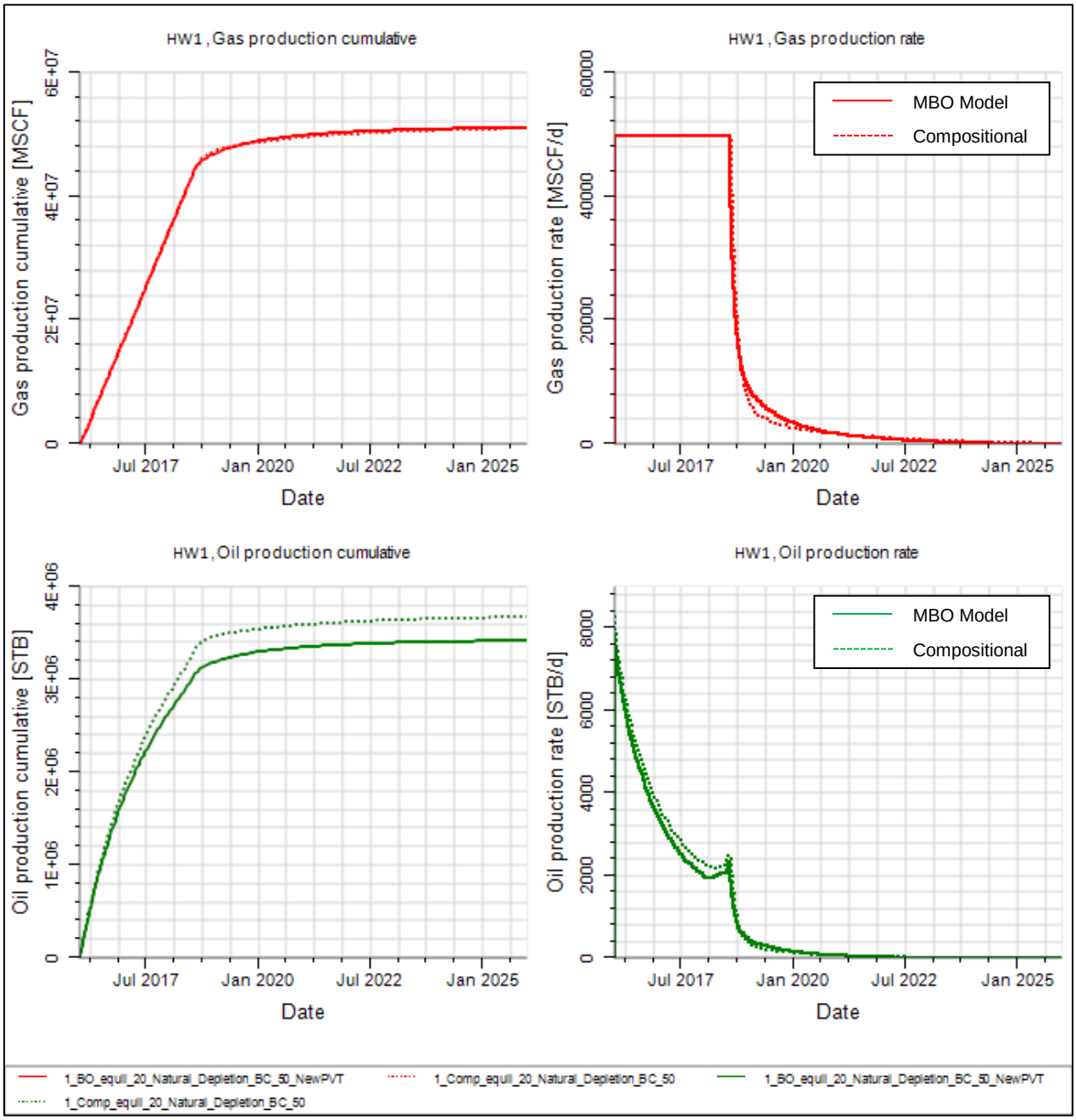

Figure 5.9: Natural depletion base case oil and gas comparisons

A comparison between water-production rates, cumulative water volumes, BHP as well as tubing head pressure (THP) is also presented in **Figure 5.10**.

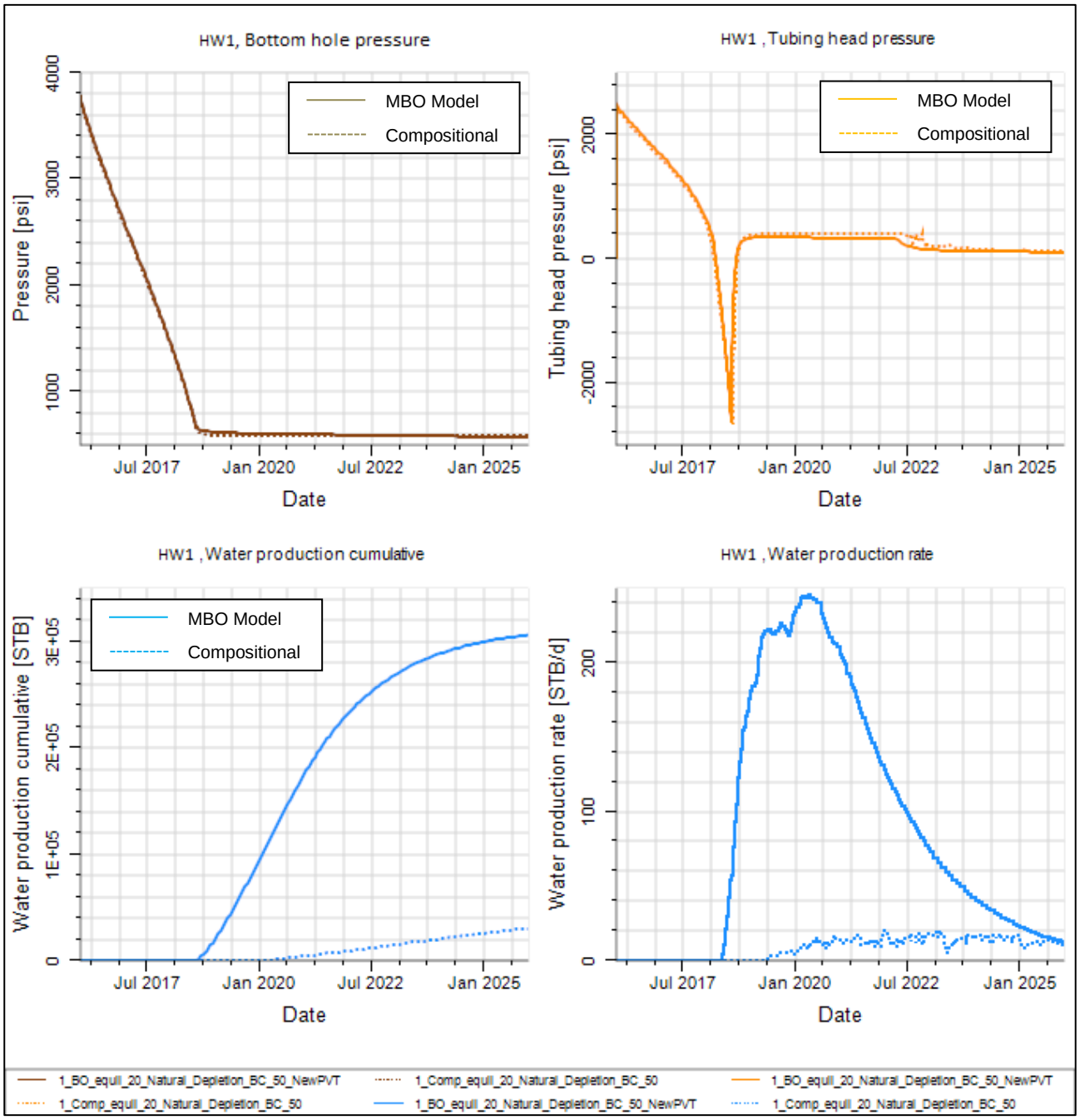

Figure 5.10: Natural depletion base case pressure and water comparisons

It is clear from Figures **5.9** and **5.10** that the two models show close similarity for all parameters, except water-production rates. The extent of the difference in water production rate is a major concern. In order to clarify this discrepancy, the way simulation models calculate relative permeability within each cell during production, needs to be investigated.

Three-phase relative permeability is generated from two-phase relative permeability curves of the oil-water system and the gas-oil system. The two-phased curves represent the end curves when either the gas saturation or water saturation equals zero. Various relative permeability models can be employed to calculate these values; e.g the Stone I model, the Stone II model (a modification of Stone I), and the Barker model (see Eclipse Technical Description, relative permeability models (2015)).

The Stone I probability model estimates three-phase permeability data from laboratory measured two-phase data. It uses the channel flow theory in porous media to obtain a simple result for determining the relative permeability to oil in the presence of water and gas flow. The model implies that water-relative permeability

and water-oil capillary pressure in three-phase systems are functions of water saturation alone, irrespective of the relative saturations of oil and gas. Similarly, the gas-phase relative permeability and gas-oil capillary pressure are the same functions for gas saturation in the three-phase system as in the two-phase gas-oil system. This model is widely used in the industry as the benchmark for oil simulation. It is appropriate for water-wet systems, and is not suited for intermediate wet systems.

In Stone II the formula for calculating the permeability factor k_r *is* modified. It is a better predictor than Stone I in high-oil saturation regions. It is more appropriate for water-wet systems and is not suited for intermediate wet systems.

Barker's three-phase model is based on saturation-weighted interpolation between the two-phase relative permeability values. It is well suited for intermediate wet or oil-wet systems. It is incidentally also the permeability model used as a default for all simulation models.

These relative permeability models allow a transition from immiscible relative permeability curves at low capillary number to miscible relative permeability curves at high capillary number. Initially, saturation end points of the different curves are interpolated. In order to make sure that the interpolation process honours the original end points, both the immiscible and the miscible curves are scaled. Thereafter, as a function of the current grid cell's saturation, relative permeability values are looked up on both curves, giving rise to the final relative permeability which is taken as an interpolation between these two values. Both the water relative permeability (k_{rw}) and the oil-to-water relative permeability (k_{row}) are calculated this way. In the three-phase case, k_{row} is then used with a three-phase relative permeability model to calculate the oil relative permeability (k_{ro}) (see Eclipse Technical Description, relative permeability models (2015)).

Looking at the MBO model, the default three-phase oil relative permeability model as well as both the k_{row} and the oil relative permeability to gas (K_{rog}) are interpolated in the manner described above before being combined to form the three-phase oil relative permeability.

In contrast, the compositional cases reflect an extra step in calculating k_{ro}. The k_{row} value is determined as above from the miscible and immiscible values. It is then combined with the gas-to-water relative permeability (k_{rgw}) to determine a hydrocarbon-to-water relative permeability (k_{rhw}). The k_{rhw} is then used in one of the three-phase relative permeability models to calculate k_{ro}.

Thus, the type of relative permeability model used, as well as how each model (MBO vs compositional) calculates the k_r will greatly influence the predictions for amount of oil, gas and water produced. These should be investigated in view of the discrepancies in our model results regarding water production. This, however, falls beyond the scope of the present study.

To further strengthen some of the similarities attributed to the simulation results of the base case scenario, **Table 5.15** gives clarity on the total amount of oil, water and gas produced during this 10 year simulation interval. It also depicts simulation run time for each model in order to show how much faster the MBO model run is in comparison (from here on CPU times will also be normalized with respect to the fastest run in order to show the comparison relative to this run). Note that even with the base case (case without any 'fine tuning' done on the development scenario), the MBO approach shows to be 6.2 times faster than the compositional simulation method.

Table 5.15: Natural depletion base case cumulative production and simulation run time

	Oil (MMstb)	Gas (MMMscf)	Water (MMstb)	Running Time (s)	Normalized CPU Time
MBO_BC	3.4	51.4	0.31	3622.52	1
Comp_BC	3.7	51.3	0.03	22374.42	6.2

With this data providing the base of our natural depletion study, we could start to modify or "fine tune" the base case scenario because, as was mentioned, this case was simply a theoretical development scenario in order to assess the similarity in results between the two models. There are thus some issues within the development scenario that need to be altered in order for accurate simulation and production estimates. Firstly, regarding the tubing head pressure (THP), values lower than 0 (as is shown in **Figure 5.10**) are considered impossible. A limiting THP of 319 psia was introduced in order to make sure that the THP does not drop below this pressure; otherwise the well would stop production.

Looking at **Figure 5.10**, there is a major discrepancy in the MBO water volumes produced when compared to the compositional simulation case. In addition to the relative permeability model issues mentioned as a potential source of the water production discrepancies, another reason for this difference could be due to the fact that after initialization, as depicted in **Table 5.14**, the MBO model has approximately 500 000 bbls less oil-volume (in place) when compared to the initialized compositional model. Thus during simulation, water breakthrough would occur sooner in comparison to the compositional model because of this volume deficiency.

To try and limit water production and also extend the production life of the well (HW1), a sensitivity analysis on the gas rate was introduced. A gas production economic minimum limit of 1000 Mscf/day was also introduced in order to facilitate comparability between MBO and compositional models, especially at late field-life stages. The models in our study also use vertical flow performance (VFP) tables in order to calculate THP from BHP in order to control the well on THP. The extra limits mentioned for BHP and THP are thus added for extra precaution.

Calculations involving THP are done with these VFP tables, which are supplied as input data. These tables relate the BHP of a well to the THP at various sets of flowing conditions. There are two types of VFP tables, namely:

- injector tables, which describe the vertical flow performance of injection wells, and
- producer tables, which describe the vertical flow performance of production wells.

A separate interactive program VFPi is available to calculate VFP tables, using a choice of multiphase flow correlations to calculate the pressure losses within the tubing string. The vertical flow performance table of a well contains a set of tubing performance curves at different flowing conditions. The curves are calculated based on specified ranges of flow rates, pressures, water fractions and gas fractions. In order to create a vertical flow performance table, one of the pressures (either THP or BHP) needs to be selected and the other pressure is solved covering all the possible combinations of the specified parameters.

In summary, the three cases which were run on both MBO and compositional models, covering all mentioned parameter alterations, as well as the 3 different gas rates in order to estimate the optimum gas production rate for this study, are shown below.

- **Case 1** - Gas Rate: 50 000 Mscf/day, THP limit: 319.1 psia, BHP limit: 580.2 psia, and a gas production economic minimum limit of 1000 Mscf/day for a simulation period of 10 years (*green colored curves*).
- **Case 2** - Gas Rate: 40 000 Mscf/day, THP limit: 319.1 psia, BHP limit: 580.2 psia, and a gas production economic minimum limit of 1000 Mscf/day for a simulation period of 10 years (*blue colored curves*).
- **Case 3** - Gas Rate: 30 000 Mscf/day, THP limit: 319.1 psia, BHP limit: 580.2 psia, and a gas production economic minimum limit of 1000 Mscf/day for a simulation period of 10 years (*red colored curves*).

The following table reflects the findings of the simulation runs showing field production volumes for oil, gas and water of all three cases utilizing the MBO and compositional model. CPU running time is also given in order to assess the time-saving effectiveness of the MBO model.

Table 5.16: Cumulative production volumes and CPU running time

Model Production Cumulative - Natural Depletion					
	Oil (MMstb)	**Gas (MMMscf)**	**Water (MMstb)**	**Running Time (s)**	**Normalised CPU Time**
MBO_50	3.39	50.81	0.23	3617.56	1.00
Comp_50	3.65	51.67	0.02	23664.86	6.54
MBO_40	3.41	49.83	0.23	3611.53	1.01
Comp_40	3.67	51.69	0.02	23430.68	6.48
MBO_30	3.44	51.87	0.22	3747.13	1.04
Comp_30	3.71	51.75	0.02	22079.99	6.10

Table 5.16 shows that both models give roughly similar cumulative production volumes (per comparative case) when it comes to oil and gas production. The only real difference between the models is reflected by the cumulative water production volumes. **Table 5.16** also shows that the MBO model demonstrates to be roughly 6 times faster than its equivalent compositional model counterpart for all three scenario runs without greatly affecting prediction accuracy (CPU running time curves for all natural depletion simulation runs are given in **Figure 7.11**, **Appendix D**).

Table 5.17 lists the percentage difference between the MBO and compositional models for both oil and gas cumulative volumes for the three different cases (note that a positive deviation reflects a larger compositional volume and a negative deviation reflects larger MBO volumes).

Table 5.17: Deviation percentage between the different cases for both MBO and compositional models

% Deviation		
	Oil	**Gas**
MBO_50 vs Comp_50	7.12	-0.28
MBO_40 vs Comp_40	7.08	-0.28
MBO_30 vs Comp_30	7.28	-0.24

Furthermore, **Figure 5.11** below gives the water production profiles for all the natural depletion cases.

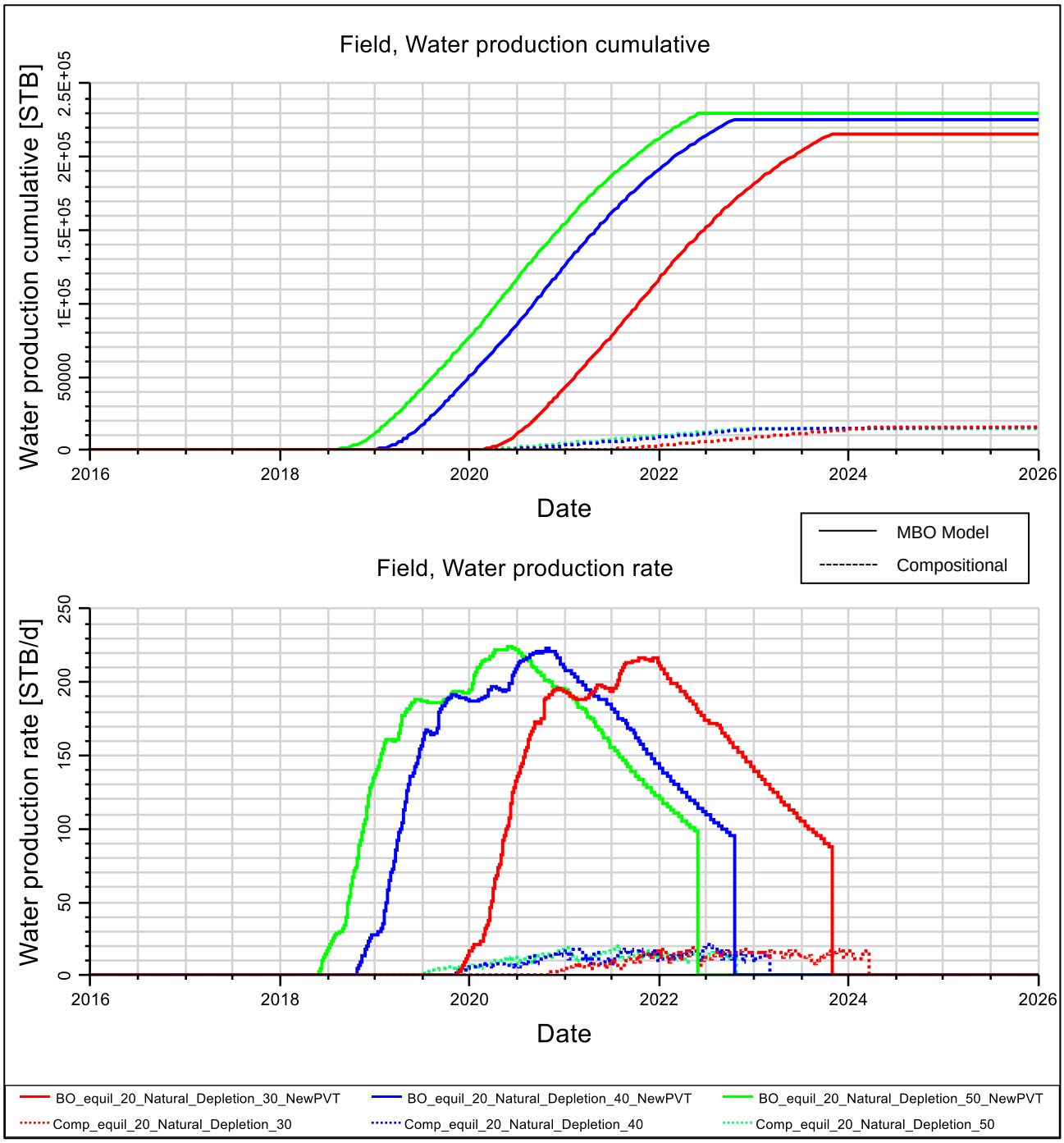

Figure 5.11: Water production rates and cumulative volumes

As was mentioned during the base case explanation, this water production difference could largely be attributed to the way in which each modelling approach assesses relative permeability within each cell in the model (i.e., how it calculates the proportion of oil, gas and water within the cell). Furthermore, after water begins to break through (water encroachment), the reservoir will become more prone to water movement, limiting gas movement and subsequently oil production (water would cone up towards the well, trapping hydrocarbon within the reservoir). This might also be a reason for the high water production in the MBO models, because as soon as water breaks through, preferential flow to water would have a greater effect on water production, trapping hydrocarbon within the reservoir as is mentioned.

Interestingly, water production of the compositional model showed to be about a 10^{th} of the MBO model's water production volumes. This might also suggest an error in either the MBO or compositional model's way of accounting for K_{rw} (again related to the relative permeability model). One could also assess whether μ_{gas}, μ_{oil} and μ_{water} are the same in both the MBO and compositional models. Further study regarding this matter is thus also strongly suggested as the scope of this study does not cover an in depth study of these issues.

After the simulations had been run, production graphs were also created in order to estimate the optimum production gas rate (a rate on which the following section's gas cycling development scenarios would be run). **Figure 5.12** supplies information on the three different scenarios for both models, reflecting how the different gas production rates would affect the overall cumulative gas production volumes.

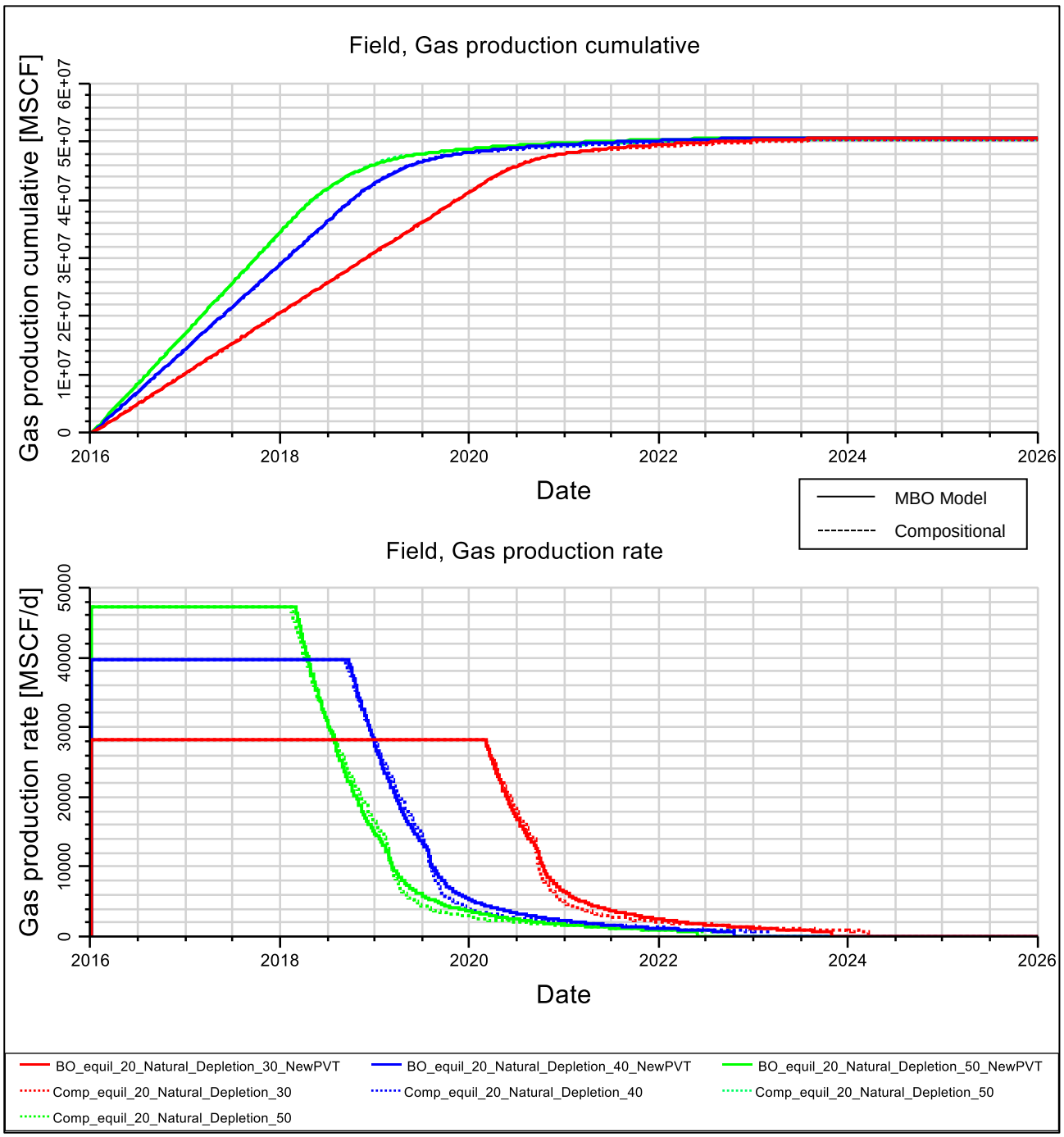

Figure 5.12: Cumulative gas production volume and gas production rate curves for both modelling methods

From **Figure 5.12** it is notable that even with the alteration in gas rate (green curves for case 1, blue curves for case 2 and red curves for case 3 – a description of the different parameters used in each case is given on p. 33); we still observe a good fit between both MBO and the EOS approaches for all three development scenarios (**Figure 5.12**).

The cases also reflect similar cumulative gas production volumes (also see **Table 5.16**). Thus, even with the alteration in gas production rate, the sensitivity analysis simply postpones water breakthrough and production and extends the well's production life. This implies that according to the relative permeability curve (**Figure 7.10**), the reservoir fluid would stay in the oil area of the graph for a longer period before

moving to the critical water saturation area (S_{wcr}). There seems to be no significant volume advantage by producing at lower rates.

In all three cases, both models initially show similar constant gas production rates with plateau durations of approximately 2.2 years for case 1, 2.7 years for case 2 and 4.2 years for case 3. Interestingly, we see a steep drop in gas production (at about 3 years for case 1, 3.5 years for case 2 and 4.7 years for case 3). This is solely due to water production.

A closer look at case 1 reveals that the MBO model shows that after about 6.5 years hydrocarbon production for HW1 ceases because of the fact that the gas production economic minimum limit specified was reached (well shut on the 01/06/2022). The compositional model, on the other hand, continues to produce for about 5 months until it reaches the economic limit. From an economic standpoint, the question must be if the extra amount of gas (and subsequently oil) produced from the compositional case during this period is economical, because this phenomenon definitely affects accuracy between the MBO and compositional model. There is evidence to suggest that if better and more 'real life' economic constraints are used (actual limits due to production procedures; for instance introducing an actual minimum gas rate which would reflect the lowest possible gas production rate at which the well would still be economical), closer simulation results between the two modelling approaches would be acquired. This would affect final cumulative produced volumes in a positive manner, minimizing the percentage deviation between the two modelling approaches and increasing accuracy.

Regarding case 2 simulations, again there is a discrepancy in production life of HW1 of approx. 5 months (**Figure 5.11**). In the MBO model, the well is shut on 16/10/2022, whereas in the compositional model it is shut on the 08/03/2023 due to the minimum gas production limit. Economically, cases 1 and 2 might be more feasible because of higher production rates. However, as the scope of this project does not cover these economic aspects within the study, it was decided that the chance of error associated with cases 1 and 2 was of too great magnitude and they were not considered as viable development scenarios in this regard (because of the 5 months difference in when the wells are shut).

Case 3, however, shows a better comparison for production lifespans between the two models. The well is shut on 01/11/2023 for the MBO, and on 18/03/2024 for the compositional model; a difference of only 4 months. This was favourable in the context of our study since the % deviation between the oil and gas production volumes between the two models for case 3 was shown to be about 7.28 % for oil and 0.24 % for gas (**Table 5.17**). This meant that an honest and accurate comparison could be made between the two modelling approaches in order to assess the feasibility of using the MBO model instead of the compositional model in field development situations without any concerns regarding model accuracy. Due to these results it was decided that a gas production rate of 30 000 MSCF/day (**Case 3**) is considered to be the best suited development scenario for this study and subsequent gas cycling development scenarios.

Figure 5.13 presents the oil production rates for all three cases. As was mentioned, the oil production curves display very similar attributes, be it that the compositional models produce oil at slightly higher rates when compared to the MBO counterparts. This might be because the compositional model handles the component exchange between the gas and liquid phase more accurately (as this exchange is not just entirely dependent on GOR and pressure, but on the composition of the fluid as well) or simply due to the fact that there is more oil in place within the compositional model after initialization.

The THP curves for all simulations are also given in **Appendix D**, **Figure 7.14** in order to show that the THP limits were adhered to as well as to show a good match between the two models. As seen on **Figure 7.14**, for the interval on the graph where the THP declines, one has a stable gas production rate (see **Figure 5.12**). The lowest point on the THP graph is where the limits on the mentioned VFP table are reached, and thus the gas rate starts to decline. After this period, one can see that the THP of the well goes up again; this is due to the fact that water encroached to such an extent that water is produced from HW1, ultimately increasing the THP (because of a heavier fluid in the tubing).

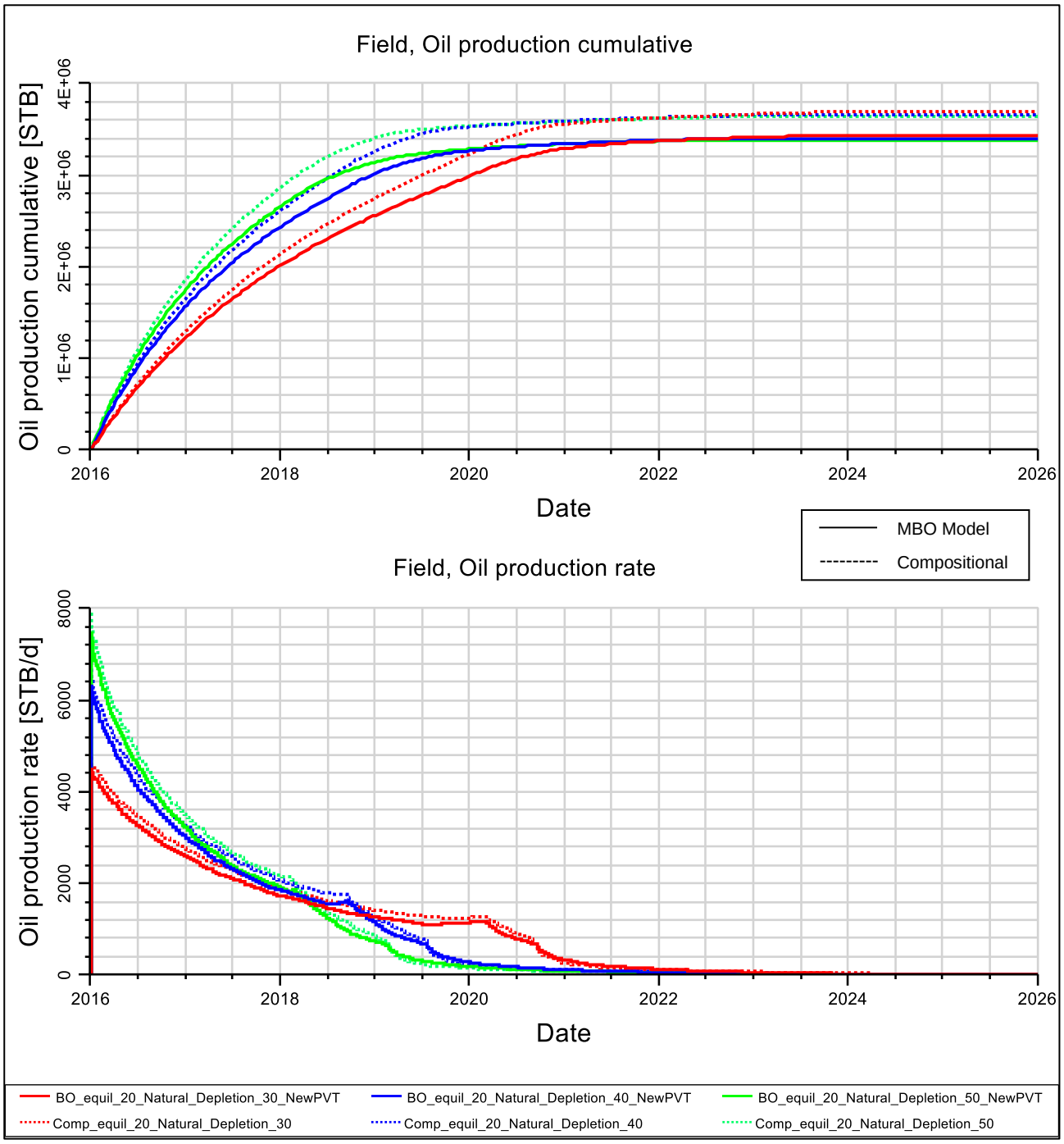

Figure 5.13: Cumulative oil production volume and oil production rate curves for both modelling methods

Another facet which could not be neglected regarding the natural depletion scenarios concerned the effect which condensate banking had on reservoir production performance and produced hydrocarbon volumes. **Figures 5.14** through **5.20** give an indication of the extent of condensate banking on the 30 MSCF/day development scenario (**Case 3**), and how this phenomenon influences both MBO and compositional models.

As can be seen from **Figure 5.14**, at the onset of the simulation run (t=0), both MBO and compositional models reflect similar saturation for each cell in the reservoir model (no condensate (oil) is present, cells only reflect gas saturation within the hydrocarbon zone above the GWC). The main figure also has small inset figures which show a cross section through HW1 to give an indication of the gas saturation vertically throughout the hydrocarbon zone.

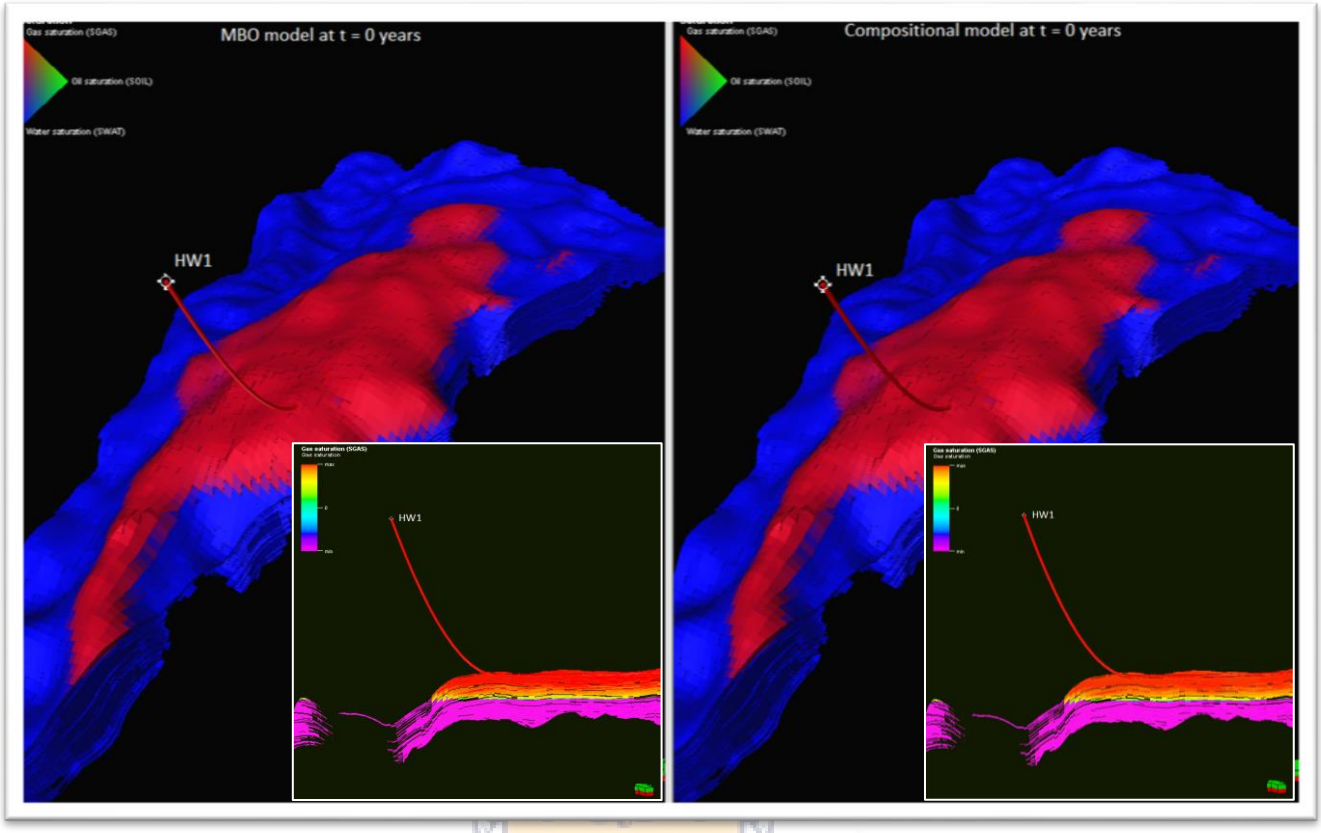

Figure 5.14: Fluid saturation of the reservoir model at t = 0 years

As the reservoir is depleted, heavier components condense out of the gas phase (resulting in a leaner gas phase over time) and oil saturation begins to increase. The same pattern can be observed from the oil saturation figures (**Figure 5.15** and **5.17**) as well as by the producing solution gas-oil- and vapour oil-gas-ratios presented in **Appendix D**, **Figure 7.12** and **7.13**. For the MBO model, changes in saturation pressure with depth cannot be represented properly. The liquid content of the reservoir gas is a function of pressure, and thus the compositional effects are ignored. Because of this, liquid drop-out is observed as soon as the saturation pressure is reached. Re-vaporization effects are moderately ineffective in the case of the MBO model. These effects are determined by the oil-gas ratio plot (**Figure 7.13**) generated by the EOS, which allows gas to pick-up oil until it reaches the value determined by the PVT table.

Figure 5.15 gives a visual representation of the oil saturation throughout the reservoir half way through the ten year simulation period (t=5 years). From the simulation results we found that condensate dropout occurs earlier in the MBO case as changes in reservoir pressure become more drastic. However, looking at **Figure 5.15**, it is evident that oil saturation is much more prominent in the case of the compositional model halfway through the simulation run. As will be shown in **Figure 5.17**, because of the way the compositional model treats liquid saturation (allowing for compositional exchange, etc.) the model has the ability to re-vaporize oil with flowing reservoir gas much more effectively, ultimately producing more oil as a consequence. The MBO model, however, simply builds up a greater condensate bank over time (thus minimal oil is re-vaporized).

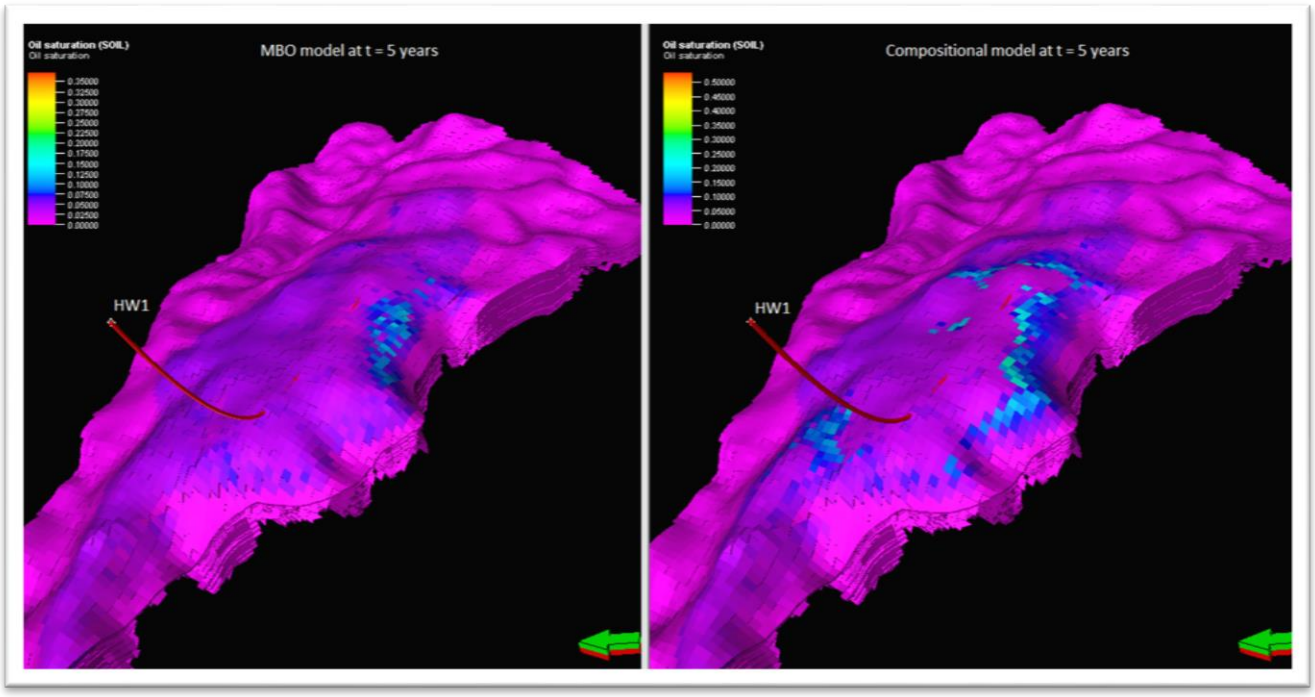

Figure 5.15: Oil saturation of the reservoir model at t = 5 years

Figure 5.16 gives an indication of the gas saturation (Sgas) throughout the reservoir, showing a cross sectional view through HW1. Note that the gas saturation is much less in the MBO case in comparison to the compositional model. This is due to the fact that the compositional model handles phase exchange behaviour in a more realistic manner when compared to the MBO model (because in general the MBO over-estimates gas production volumes).

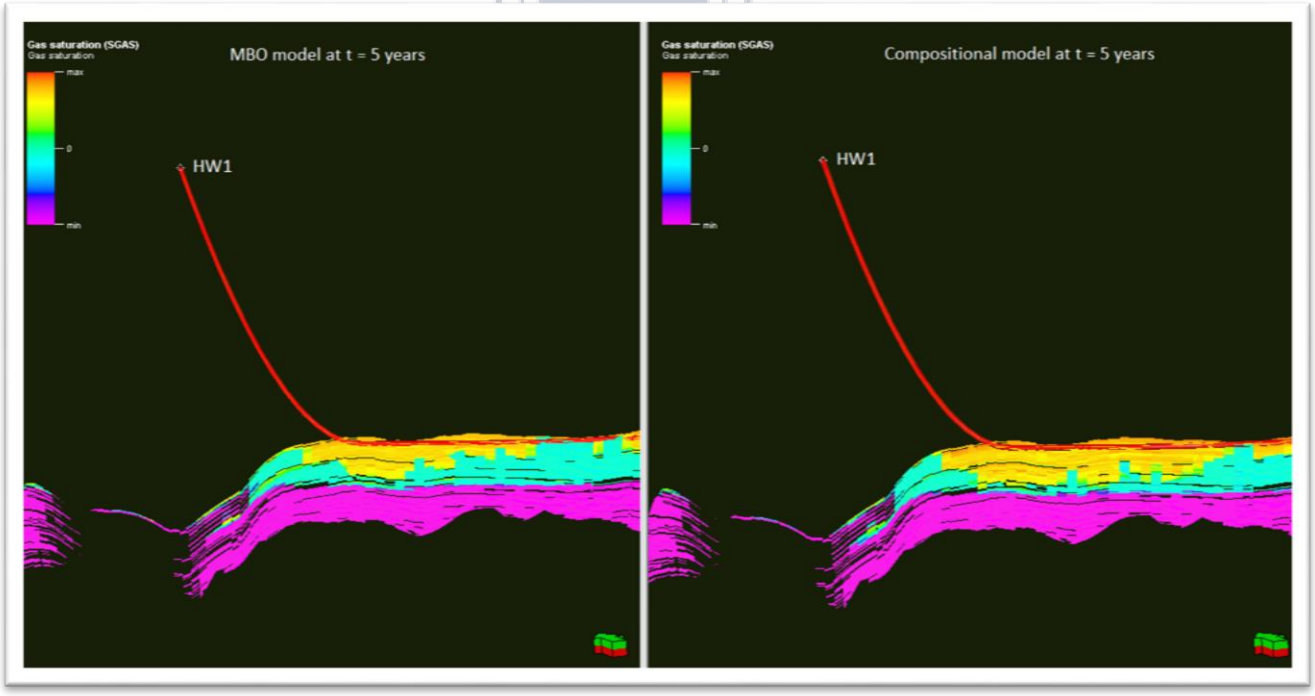

Figure 5.16: Gas saturation of the reservoir model at t = 5 years

Figure 5.17 shows final oil saturation after the ten year simulation interval (t=10 years). Now that most of the reservoir gas has been produced, as can be seen in **Figure 5.18** (no more gas flowing from the reservoir to the well, thus no re-vapourization effect), one can see that the compositional model (to the right) also shows a significant condensate bank developed. For the MBO model (to the left) the figure shows higher oil saturation values (brighter blue colours) confirming that the model builds the condensate bank as simulation

time progresses. Thus, higher amounts of oil are left in the reservoir resulting in higher production of gas-oil ratios because less oil is produced (**Figure 5.16** and **7.12**). On the contrary, lower producing gas-oil ratios (**Appendix D**, **Figure 7.12**) are seen in the compositional model simulation since most of the oil in the reservoir was re-vaporized and carried by the gas phase. This ultimately confirms, as is seen from **Table 5.16,** the fact that the MBO models are giving lower oil production rates and volumes compared to the compositional model.

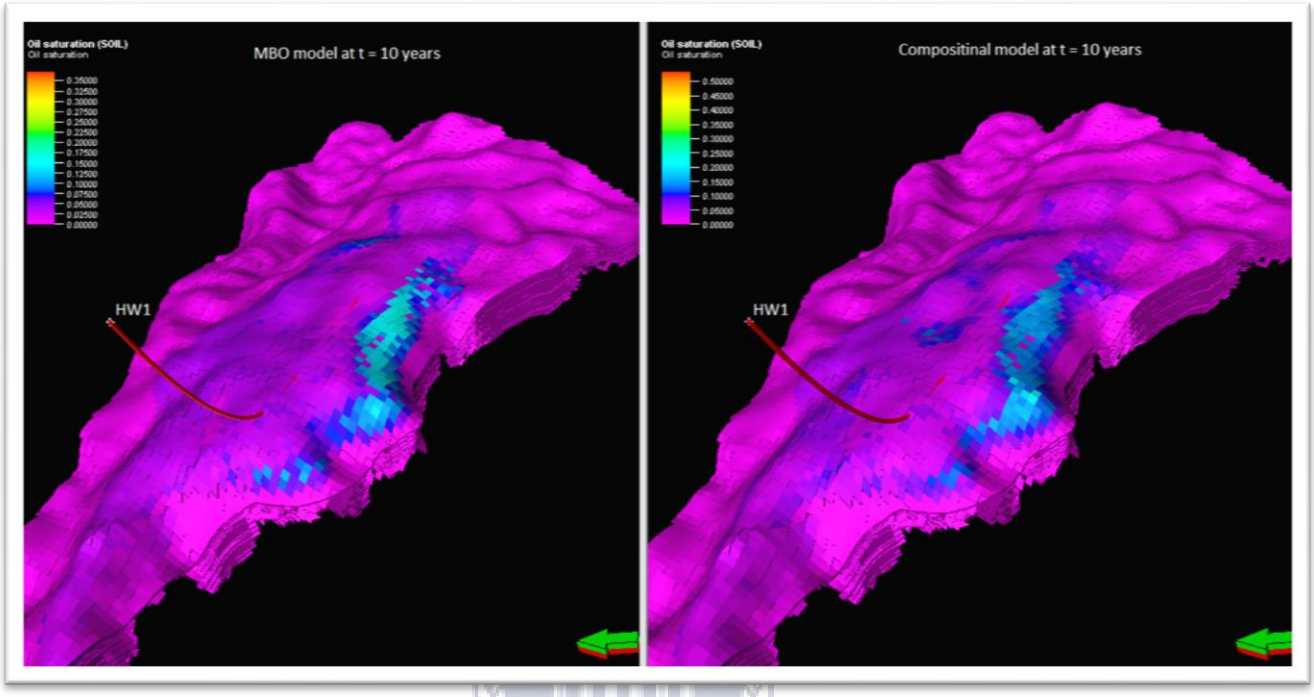

Figure 5.17: Oil saturation of the reservoir model at t = 10 years

Figure 5.18 gives final gas saturation (Sgas) throughout the reservoir at the end of the 10 year simulation interval.

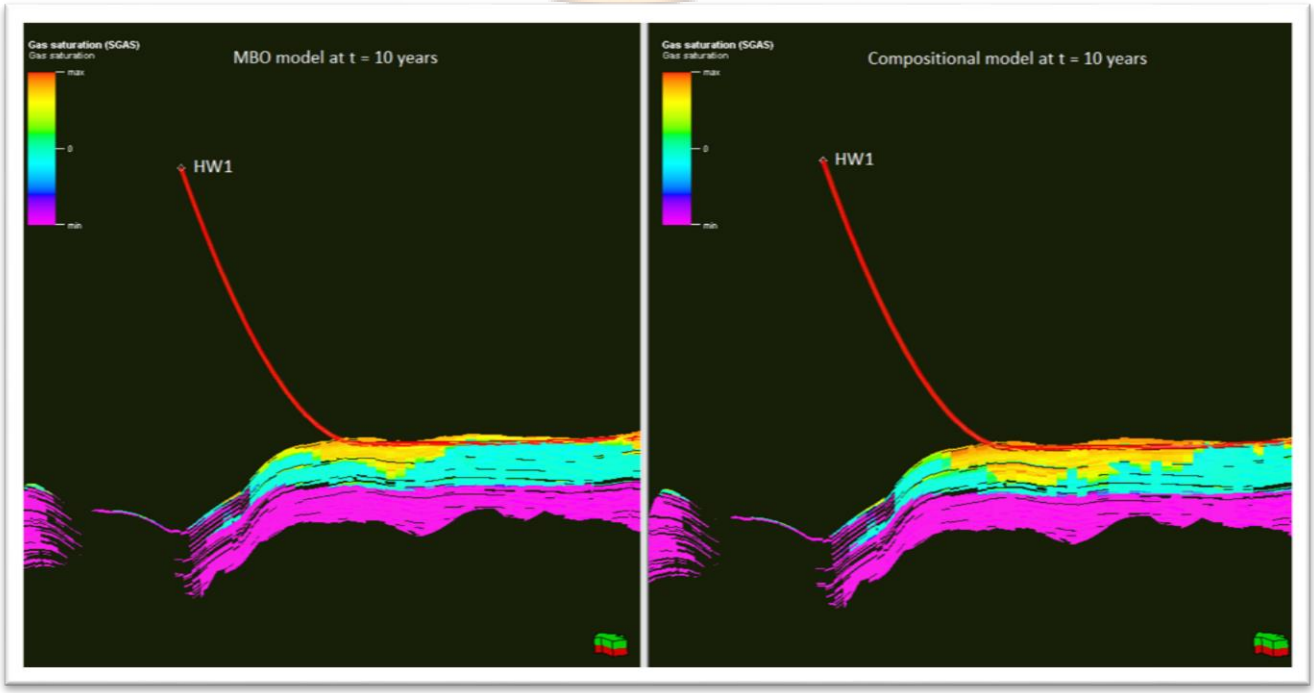

Figure 5.18: Gas saturation of the reservoir model at t = 10 years

Looking at **Figure 5.19** and **5.20**, one can see that gravitational segregation is also evident. This implies that a gas condensate would get richer as the depth increases (due to increasing C_{7+} mole fraction as well as dewpoint pressure). The following figure shows a reservoir property intersect (J67 cells) through the well.

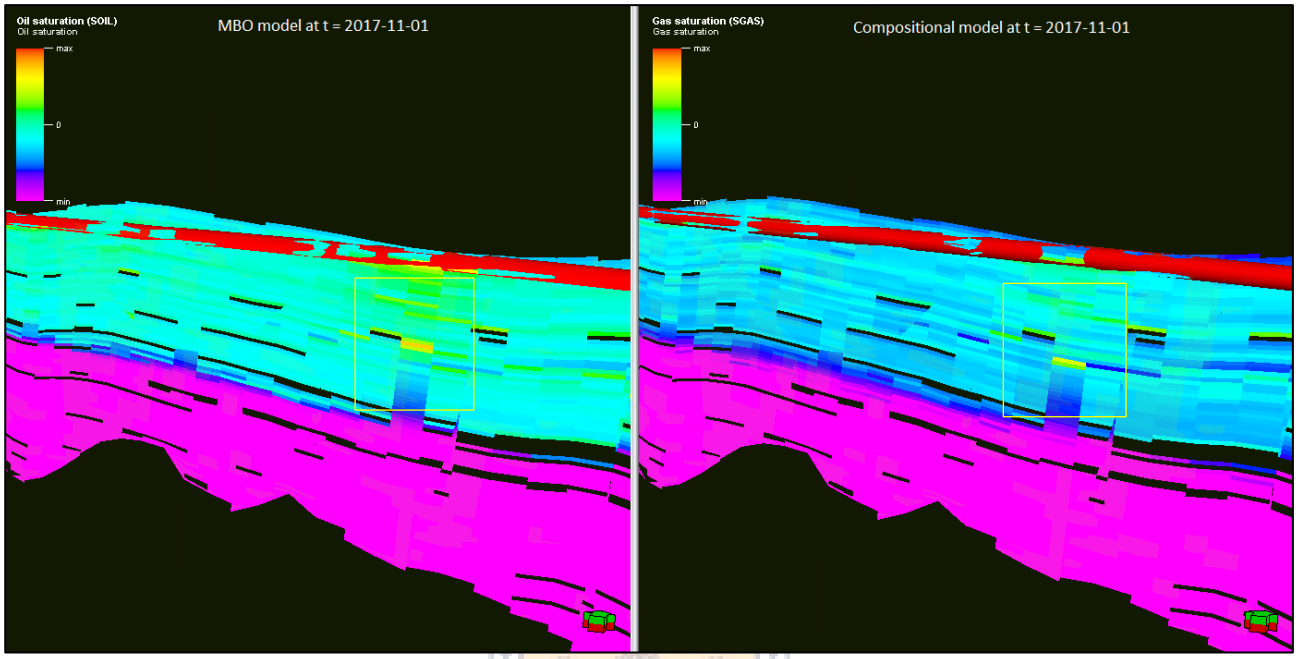

Figure 5.19: Cross sectional view through the reservoir showing condensate formation one year eleven months into the simulation

Oil saturation is first observed within the bottom layers for both models and as the simulation develops, it progresses upwards (As is shown by the red-yellow blocks moving upwards with simulation time, emphasized by the yellow boxes). Due to the inability of the MBO model to represent the changes in dewpoint pressure versus depth properly, it gives earlier and bigger amounts oil saturation in the bottom layers compared to the compositional model.

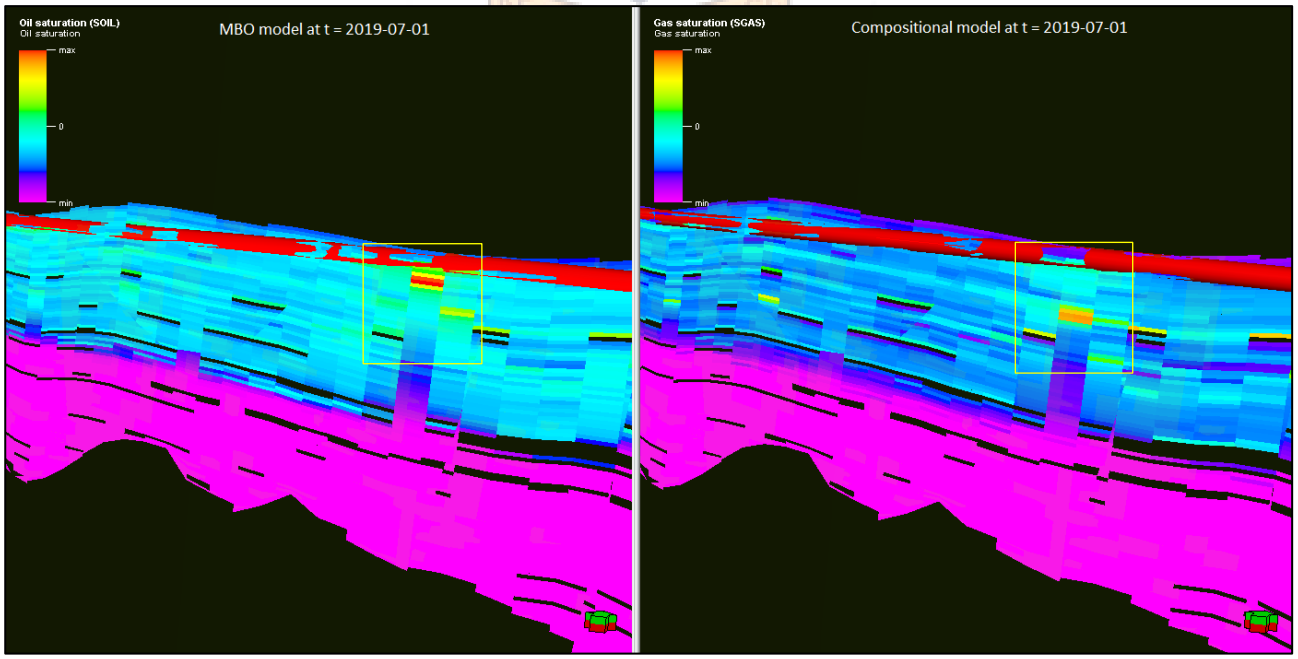

Figure 5.20: Cross sectional view through the reservoir showing condensate formation three years seven months into the simulation

Thus, in conclusion, the difference between the two models is created by the higher oil production rate in the compositional model relative to the early condensate drop-out in the MBO model. Also, as the reservoir gas gets depleted from heavy ends, re-vaporization effects in the compositional model contribute to higher recoveries. In contrast, the MBO model has limited capacity to re-vaporize the condensate forming from the

reservoir gas, particularly at lower pressures due to smaller values of oil-gas ratio (**Figure 7.13**, **Appendix D**). In the simulator oil-gas ratio tables obtained from the EOS model would determine this re-vaporization effect.

The results show that both gas and oil production rates, and subsequent cumulative volumes, portray close similarity when comparing the MBO and compositional simulation models. We see that the compositional models produces slightly higher oil volumes compared to those of the MBO models; however, this could be due to the fact that from the in-place calculations the compositional model showed to have higher STOIIP volumes during initialisation (approximately 500 000 bbls more oil in place). In addition, Bottom Hole Flowing Pressures (BHFP) and Well Head Pressures (WHP) also showed to be very similar. Finally, runtime comparisons given showed that the MBO models tended to be 1/6 of the runtime of the compositional modelling methods, proving the time saving capabilities of these types of models.

One area of concern would definitely be the considerably higher water production rates seen in the MBO models versus the compositional simulation results. A possible explanation for this was given in this study, but it was felt that a more in depth analysis would be of importance and value moving forward on this field. Interestingly, the water production discrepancies mentioned do not seem to influence the hydrocarbon production rate nor recovery. Research points proposed for the study encompass:

1. An in depth study on the type of relative permeability model used, as well as how each model (MBO vs compositional) calculates the K_r. This is of utmost importance because it has the greatest influence on the amount of oil, gas and water produced and thus on the discrepancies seen in our model results regarding water production. Comparing the different results of the mentioned K_r models for both the MBO and compositional model would give a greater indication of which models would be best suited to be used in tandem (thus running all simulation models with each relative permeability model).
2. Because of the fact that the water production of the compositional model is about a 10^{th} of the MBO model's water production volumes, it is suggested that further study regarding this matter is also done.
3. A sensitivity analysis on the S_{wcr} and S_{gcr} values selected at the setup stages of the project can be considered in order to estimate how these endpoint-values influence water production for the respective modelling approaches.

From the preliminary analysis done on both MBO and compositional models for natural depletion development scenarios, it is clear that, the MBO model is able to simulate natural depletion scenarios for the field with notable accuracy (within 10% accuracy difference) when compared to the compositional model, with the added advantage of huge time saving.

5.5.2 Gas Cycling Development Scenarios

Regarding the gas cycling development scenarios associated with this study, the fact that the initial reservoir pressure was close to/ slightly below the dewpoint pressure of the reservoir fluid, proved to be somewhat problematic. In our case, the reservoir pressure (currently at 3803 psia) of the study area was already below the dewpoint pressure (calculated at 3805 psia) of the reservoir fluid even before the start of development and production. Although very small, this difference implies that some condensate could have begun to drop out of the gas phase (even before production), which would hamper gas flow. This problematic phenomenon would thus only increase in magnitude with time, hampering gas flow as production begins and progresses. This would create condensate banks throughout the reservoir (as was discussed in the literature review as well as shown by the natural depletion development section).

The first approach attempted in our study was to keep the reservoir pressure as high as possible by injecting gas in order to try and increase the BHP of the injection well. Thus, by introducing a bottom hole target pressure (6000 psia) for GI1, one could see if this gas injection influences the rest of the reservoir to such an extent that the pressure is kept above 3805 psia in the vicinity of the well (thus reflecting an above the dewpoint cycling scenario). Another scenario was also run whereby gas was injected with a BHP target of 3800 psia, reflecting current reservoir pressure and thus attempting to simulate gas cycling below the dewpoint (because, as will be evident, even though the target BHP is set at 3800 for GI1, actual reservoir pressure would be way below that of the dewpoint pressure). To reiterate then, both the MBO and compositional modelling approaches were run with:

1. One scenario reflecting all production parameters mentioned during the natural depletion simulation run (Case 3 - p.36) together with gas injection with GI1 reflecting a BHP target pressure of 6000 psia, and
2. Another scenario reflecting all production parameters mentioned during the natural depletion simulation run (Case 3 - p.36) together with gas injection with GI1 reflecting a BHP target pressure of 3800 psia.

For all gas cycling cases, development scenarios were created with a rule set to reflect voidage replacement injection. This controls the gas injection rate in order to replace the total production voidage. Additionally, it was also decided that the composition of injection gas for all gas injection scenarios will reflect dry gas properties, namely 50% C_1, 30% C_2 and 20% C_3 components.

On initial inspection of the results, **Table 5.18** gives an indication of the volumes of oil, gas, injection gas and water recovered as simulated for both above and below the dewpoint cycling scenarios. Simulation run time is also shown.

Table 5.18: Cumulative production volumes – Gas Injection

Model Production Cumulative - Gas Injection							
		Oil (MMstb)	Gas (MMMscf)	Inj. Gas (MMMscf)	Water (MMstb)	Running Time (s)	Normalised CPU Time
Below P_{res}	MBO_3800_voidrep	4.21	104.11	101.37	0	4544.72	1
	Comp_3800_voidrep	3.88	104.11	96.83	0	8980.90	1.98
Above P_{res}	MBO_6000_voidrep	4.30	104.11	106.43	0	7435.72	1
	Comp_6000_voidrep	3.92	104.11	102.80	0	9888.67	1.33

The results presented in **Table 5.18** show that injecting gas indeed enhances greater yields for oil production when compared to the volumes produced for the natural depletion development scenarios presented in **Table 5.16** (although these gains are not at all what was expected). Interestingly, when looking at the oil recovery volumes, the MBO model produces more oil than the compositional model when looking at gas cycling and not less, as was predicted by the natural depletion results. These results would suggest that the MBO model might be overestimating recovery volumes during the gas cycling scenarios because it is not as apt in simulating the complexity of the component exchange when cycling of gas occurs. The results from **Table 5.18** also show that top-up gas from neighbouring fields would also be necessary for the scenario reflecting gas injection with a BHP target of 6000 psia (roughly in the range of 2.5 MMMscf extra in volume) since the MBO model shows to be injecting more gas than is produced. **Table 5.19** gives further analysis of

these volume gains contributed to the cycling of gas. Gas cycling is done in order to keep reservoir pressure up as well as re-vaporise any oil within the reservoir.

Table 5.19: Production volume comparison between natural depletion and gas cycling development scenarios

Comparison between Natural Depletion and Gas Cycling Cases			
Volume differences:	**Oil (MMstb)**	**Gas (MMMscf)**	**Water (MMstb)**
MBO_3800 psia (GC) vs MBO model (ND)	0.77	53.24	-0.22
Comp_3800 psia (GC) vs Comp model (ND)	0.17	53.36	-0.02
MBO_6000 psia (GC) vs MBO model (ND)	0.86	53.24	-0.22
Comp_6000 psia (GC) vs Comp model (ND)	0.21	53.36	-0.02

The table shows that regarding the 3800 psia gas injection cases, gas injection accounts for a 0.77 MMSTB and 0.17 MMSTB production volume gain for the MBO and compositional models respectively. That is a 22.4 % oil gain in the case of the MBO and roughly a 4.6 % gain in the compositional model. Looking at the 6000 psia injection cases, again we encounter a gain, roughly 0.86 MMSTB for the MBO gas injection case (a 25 % oil gain) and about 0.21 MMSTB for the comparative compositional case (which is a 5.7 % oil gain). Another interesting aspect is that, as expected, when gas is cycled, reservoir pressure is kept up, as is shown by **Figure 5.21** below, consequently completely inhibiting any water production (as is also evident from **Table 5.18** and **Table 5.19**).

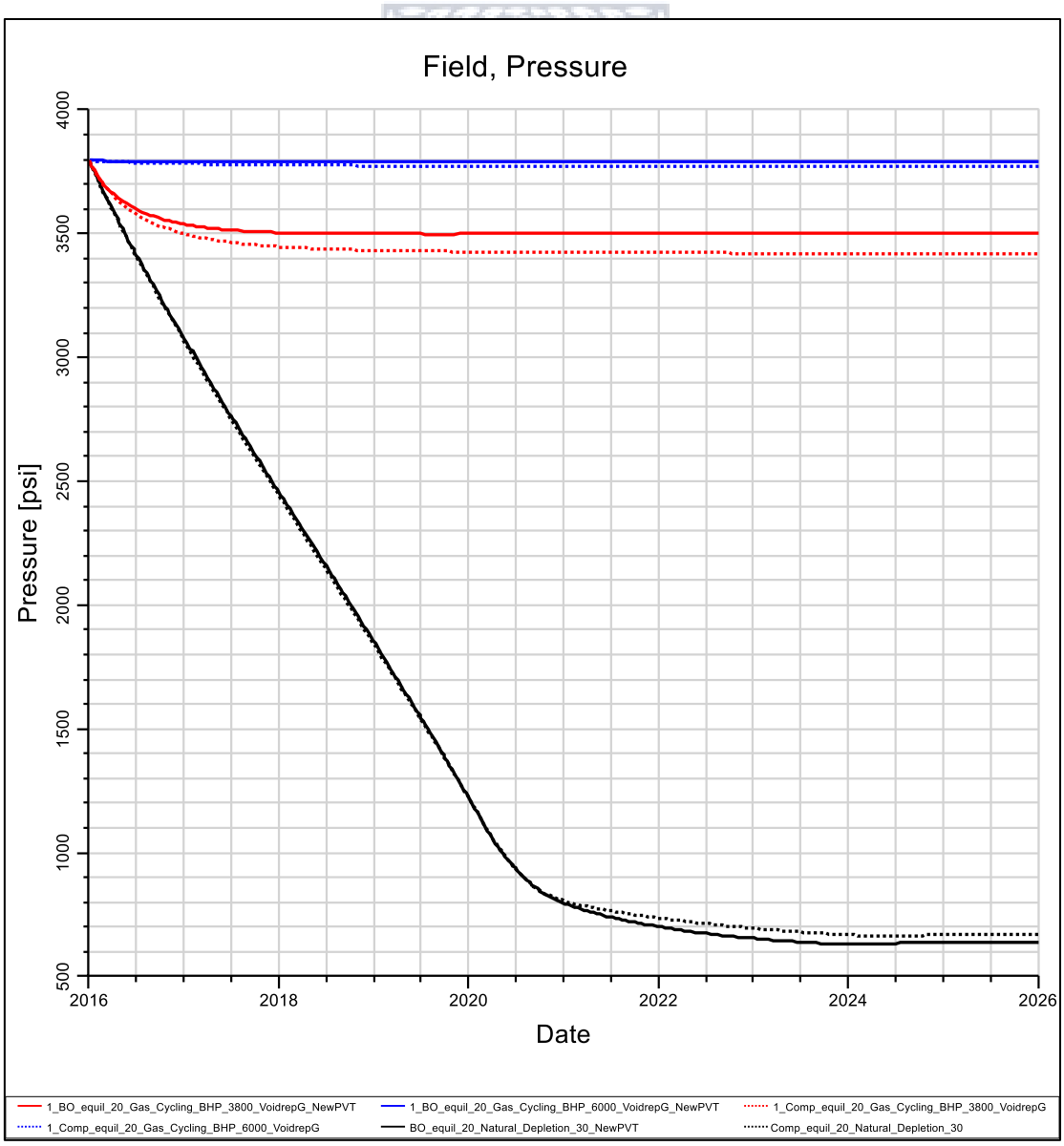

Figure 5.21: Comparative pressure curves for natural depletion, above the Dp and below the Dp scenarios

Finally, simulation running times are roughly about 1.5 - 2 times longer for the MBO gas cycling simulations compared to the equivalent natural depletion case. However, looking at the compositional results, an interesting spectacle occurs. The gas cycling development scenarios show run-times which are roughly 2.2 times faster than the comparative natural depletion case. This would be because reservoir pressure does not fluctuate as much in these gas cycling cases (GOR and OGR curves for both above and below the dewpoint simulation runs are given in **Appendix E** and **F**, **Figures 7.16** through **7.19**), thus making the component exchange between oil and gas much easier to calculate. CPU running time curves for all gas cycling simulation runs are given in **Figure 7.20**, **Appendix F**.

5.5.2.1 Gas Cycling Below the Dewpoint

Delving deeper into the gas cycling development scenarios, **Figures 5.22** through **5.24** represent the results for the completed simulation runs done to reflect 'below the dewpoint gas-cycling'. It must be noted that, when talking about cycling below the dewpoint, GI1 is assigned a bottom hole pressure target of 3800 psia. This implies (as will be mentioned in the 6000 psia cases as well) that gas is injected in order to reach or get as close as possible to the target BHP. Contrary to the results and conclusions drawn by some of the authors mentioned in this study's literature review, the results of our study showed a moderate fit for recoveries between the MBO and compositional models. These cycling scenarios did in fact show to be much more complex in nature, and a lot of questions regarding the accuracy of these results arose since it was not clear whether the MBO model totally handled the voidage replacement control method due to the complexity of the component exchange during these cases. The results suggest that when gas cycling at lower pressures will be simulated, MBO results might be more problematic in nature, and thus further study must be done in order to fully understand if the MBO model would be able to simulate these scenarios.

Looking at deviation percentages between the MBO and compositional model, results show a deviation % of roughly 8.51 % for oil production, and a zero % deviation in the total volume of gas produced. This deviation in oil production volume is about 1 % greater than the comparative natural depletion deviation percentages.

As mentioned earlier, there is about a 22.4 % oil production volume difference for the MBO gas cycling model compared to its equivalent natural depletion scenario. This gain percentage (compared to the 4.6 % for the compositional model) could be attributed to the fact that with the addition of injection gas, reservoir pressure is kept much higher, completely inhibiting water production and thus the chance of any oil getting trapped by water encroachment or coning (this phenomenon is largely seen in the MBO natural depletion cases). Also, as will be explained later, in the MBO scenario injection gas travels much further into the reservoir implying re-vaporization of oil from a greater area. It could also be so large in comparison because of the fact that the compositional simulation simply handles the component exchange in a more realistic manner and it is felt that the MBO model does have a tendency to over predict/estimate production volumes.

Field pressure comparison throughout the entire 10 year interval of the simulation is given by **Figure 5.22**. The results show that pressure drop is consistently the same for the first 6 months of simulation. Thereafter, however, pressure decline is different, reflecting a 60 psia difference in reservoir pressure between the two models at the end of the 10 year simulation interval. The MBO model also shows consistently higher reservoir pressure compared to the results of the compositional run. To understand this discrepancy, one needs to look at the BHP and THP curves for both HW1 and GI1 given in **Figure 7.15**, **Appendix E**.

Firstly, these graphs are given in order to confirm that gas injection has been done correctly. The fact that the BHP and THP curves of GI1 appear to be similar throughout the entire duration of the simulation, confirms that. This also proves that, because of the difference in pressure between the MBO and compositional results for HW1, the gas injection's is much more effective in the MBO model. It proves that the injection gas travels much further into the reservoir compared to the compositional model (as will also be shown later in the 'cycling above the dewpoint' section), and that is why the BHP for HW1 is much higher for the MBO model. One can also see that even though the BHP of GI1 reflects that the target BHP set at the onset of the project was reached, this only raises the field reservoir pressure to approximately 3500 psia for the MBO and 3450 psia for the compositional model (thus reflecting gas cycling below the dewpoint).

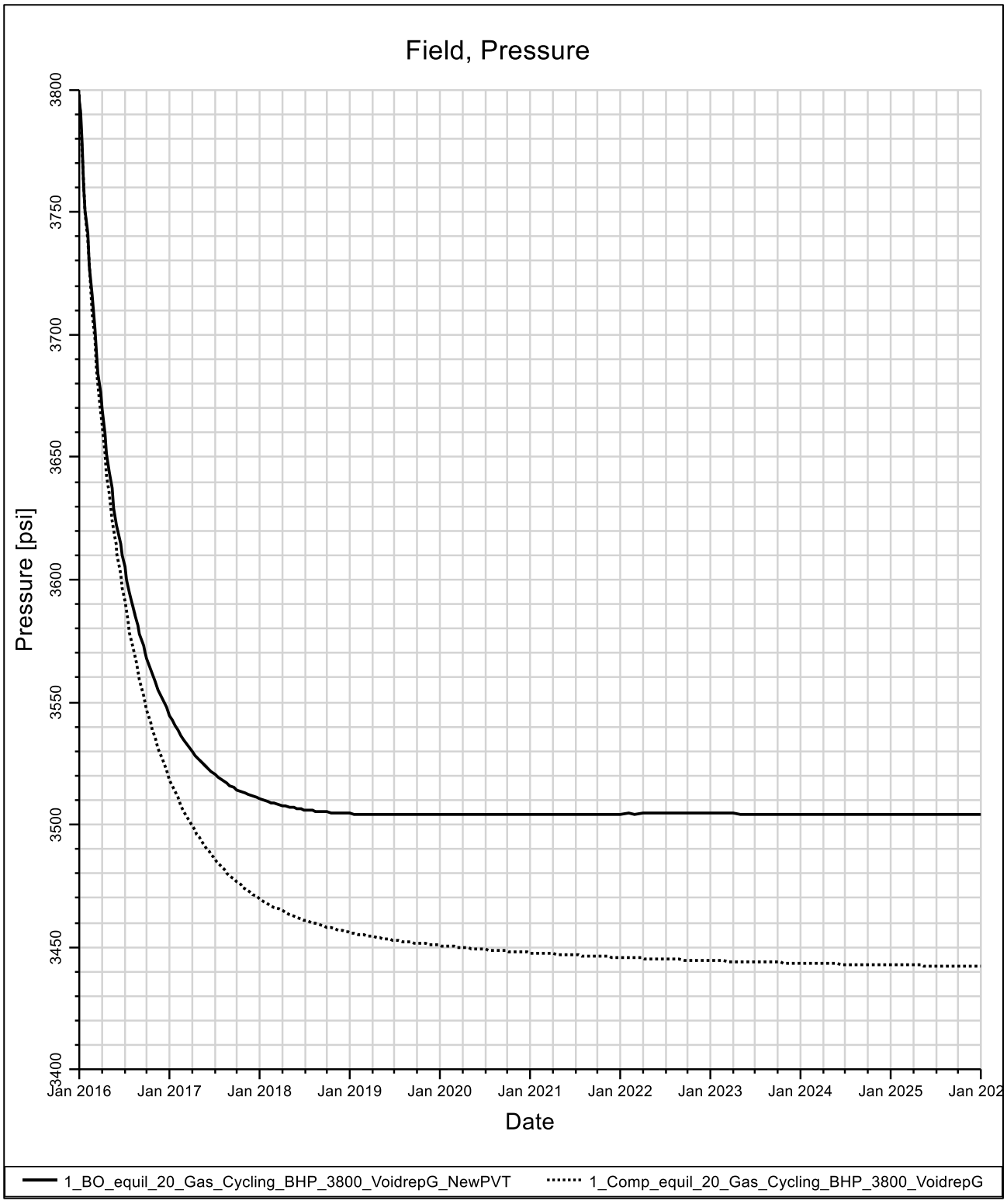

Figure 5.22: Pressure comparison for gas cycling below the dewpoint

Figure 5.23 gives the results regarding gas production and injection.

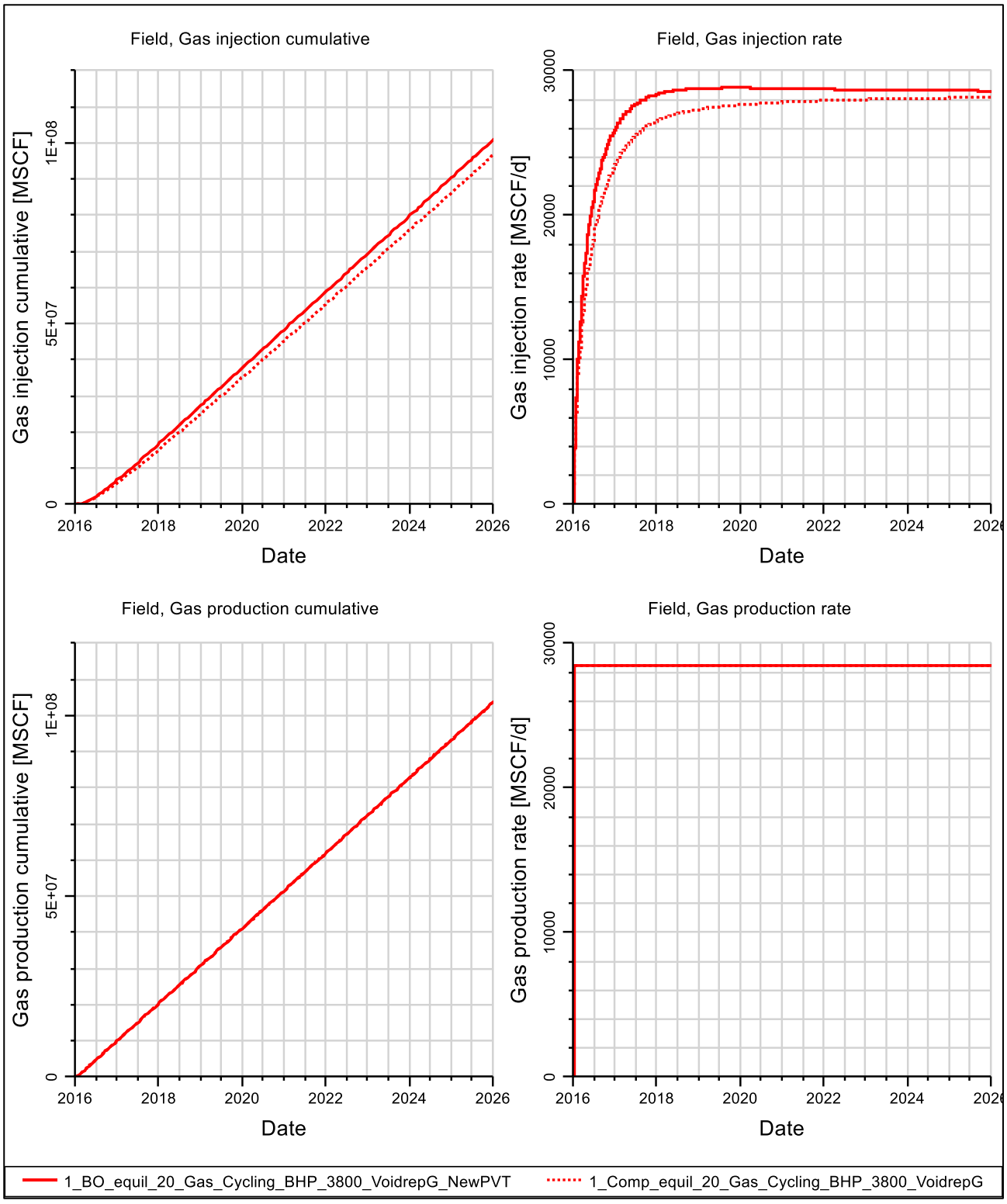

Figure 5.23: Gas production and injection volumes for gas cycling below the dewpoint

Figure 5.24 gives the subsequent oil produced from the gas-condensate reservoir fluid.

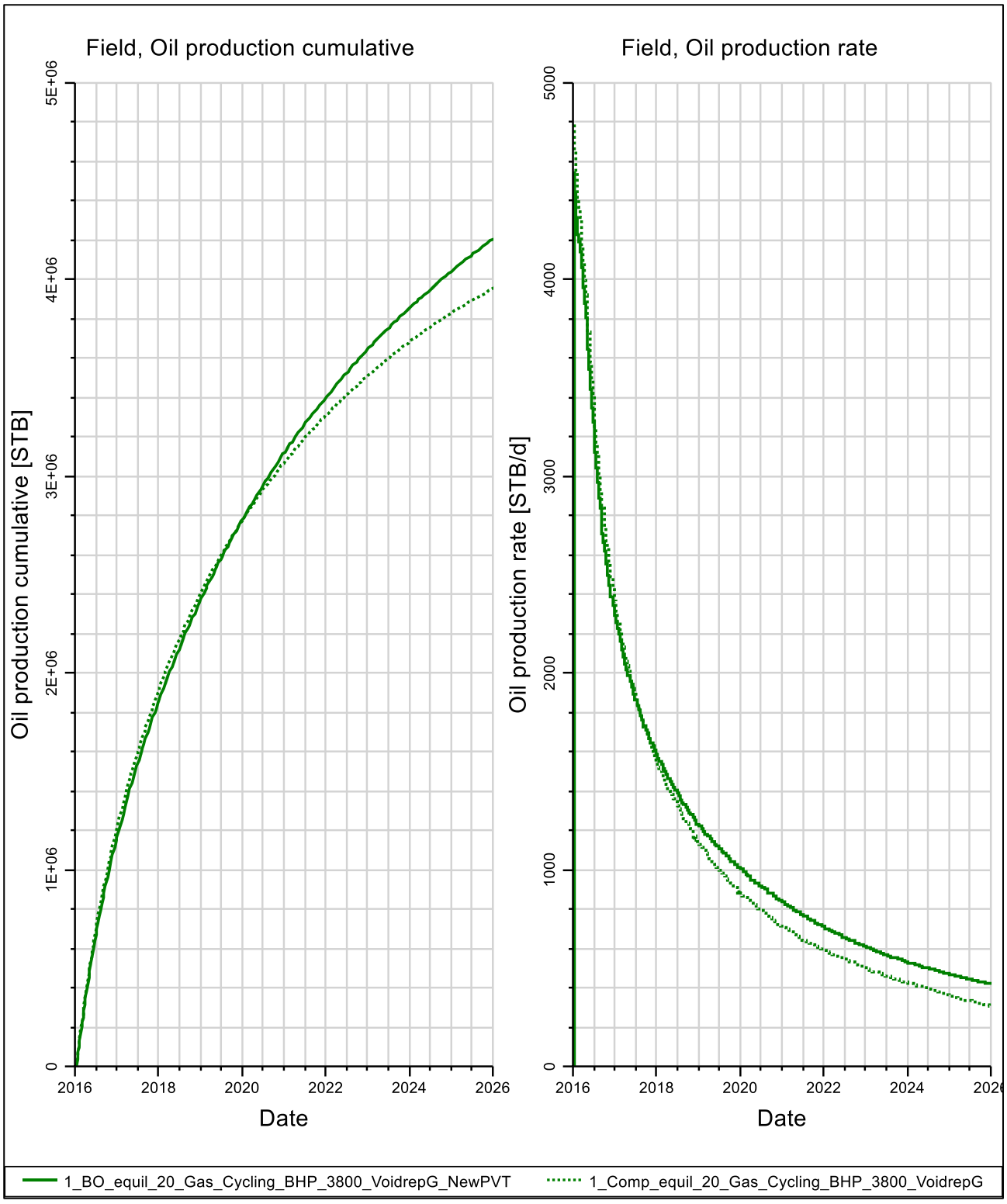

Figure 5.24: Oil production volumes for gas cycling below the dewpoint

Even though the pressure results show some discrepancy, the gas and oil production curves portray much closer similarity than anticipated. **Figure 5.23** does show that for injection gas volumes, the compositional model reflects smaller rates throughout the entire duration of the simulation. This is because, as was mentioned, the injected gas does not travel as fast into and affect the reservoir pressure to the extent of the MBO case. It takes the gas longer to affect the compositional model's reservoir (which would subsequently be the reason for less oil being produced since the injection gas does not travel as far into the reservoir, limiting oil vaporisation).

Looking at both the GOR and OGR (given in **Appendix E**, **Figure 7.16** and **7.17** respectively) for the gas cycling scenarios simulated with a BHP target of 3800 psia, we see that these graphs portray a much smoother contour line compared to the natural depletion GOR and OGR curves (**Appendix D**, **Figure 7.12** and **7.13** respectively). This is solely due to the reservoir pressure being kept up by the injection gas, thus making sure that these values are not as erratic. The match in results for the OGR (**Figure 7.16**) is excellent, showing minimal difference between the two models. Regarding the GOR (**Figure 7.15**) there seems to be a good match for about two years of simulation time. Thereafter, the MBO model begins to show a discrepancy in the calculated GOR compared to that of the compositional model. This is due to the MBO model being able to re-vaporise a lot more oil over a greater area compared to the compositional model, implying more oil is produced which in turn lowers the GOR calculated values.

In conclusion, from our results there is some evidence which would support the notion that a MBO model could in fact be able to model the component exchange between the gas and liquid phase when compared to a compositional model, looking at a gas cycling development scenario reflecting gas cycling below the dewpoint. These below the dewpoint cycling scenarios are however, much more complex than initially thought, and a word of caution must be issued. More research must be done in order to fully understand how the different modelling approaches account for production volumes during these cycling scenarios.

5.5.2.2 Gas Cycling Above the Dewpoint

For these 'above the dewpoint' injection scenarios, one must first assess the maximum pressure at which gas can be injected without affecting reservoir porosity in a negative way. The formation fracture pressure, which is the pressure above which injection of fluids will cause the rock formation to fracture hydraulically, must be clearly defined. To assist in answering this important question, one can use the formation fracture gradient in order to determine a safe target pressure for gas injection. From the engineering well completion report (leak-off tests conducted), it was calculated that the fracture pressure gradient of the reservoir formation where the gas injection well's perforations are situated (at a depth of 8500 ft), is 0.894 psia/ft. Thus, a simple calculation is required in order to determine the maximum target pressure for the injection gas.

Max Target Pressure (psia) = Fracture Gradient (psia/ft) x Perforation Depth (ft) (14)

The maximum pressure that the gas injection process can thus reach without introducing negative effects on porosity, is 7599.6 psia. To restrict further possible pitfalls, a 20% pressure safety deduction is added (1519.92 psia). All this imply that ultimately, injection pressures can safely reach a maximum of 6079.68 psia without affecting the reservoir negatively. Gas could thus be injected with a BHP target of 6000 psia, in order to reflect cycling above the reservoir fluid's dewpoint pressure. Subsequently, **Figure 5.25** represents the reservoir pressure over the entire duration of the simulation interval (BHP and THP for both wells are also given in **Appendix F**, **Figure 7.21** for the respective models). From these figures we see that even though a BHP target pressure of 6000 psia was introduced in the simulation models, the gas injector's (GI1) maximum BHP could only reach between 4080 and 4140 psia. This in turn, did have an effect on the surrounding reservoir, because the production well's (HW1) BHP was also raised to between 3720 and 3780 psia. This confirms that the injection process had an influence in the surrounding reservoir.

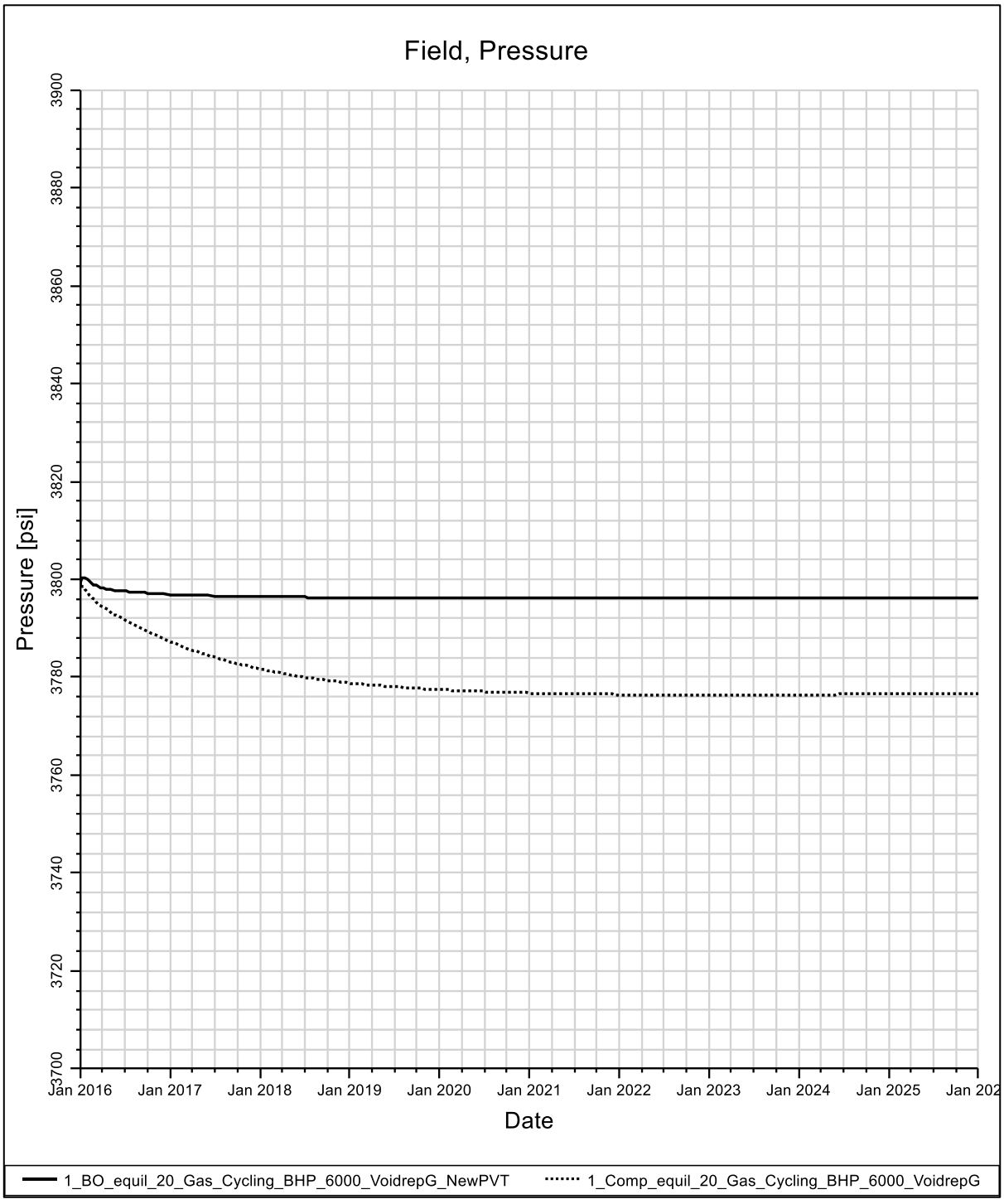

Figure 5.25: Pressure comparison for gas cycling above the dewpoint

As was mentioned for the cycling below the dewpoint scenario, pressure is kept much higher than in the equivalent natural depletion cases (also see **Figure 5.21**), ultimately producing more oil. We also see a discrepancy between the MBO and compositional reservoir pressure curves, as was seen with the below Dp cases; be it that the difference in pressure is much less (20 psia in comparison to about 60 psia for below the Dp cases). The pressure difference would be less, simply because more gas is injected in order to try and reach the 6000 psia BHP target (seen in **Table 5.18**). It also shows that the difference between injection gas volumes for the MBO and compositional model is less, which may be the main reason for a smaller reservoir pressure deviation (compared to the 'below the dewpoint' pressure comparison). In order to explain the discrepancy in reservoir pressure further, **Figures 5.26** and **5.27** were created to show gas saturation (Sg) at the end of the 10 year simulation interval for both MBO and compositional models.

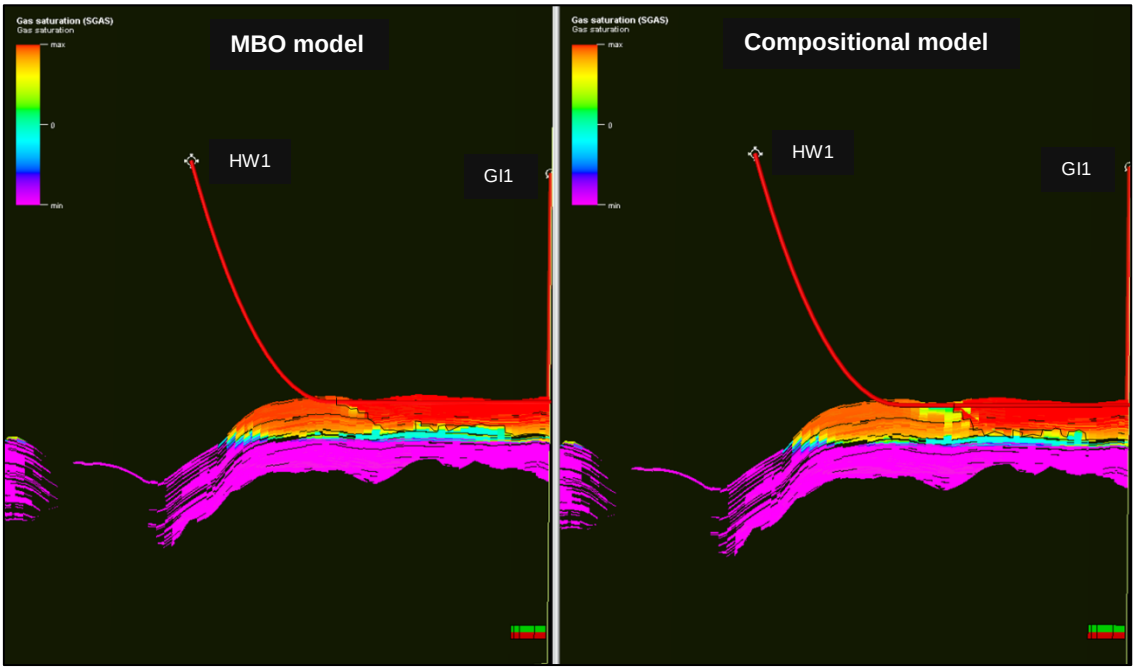

Figure 5.26: Cross-sectional view through HW1 showing Sg at the end of the 10 year simulation interval

As **Figure 5.26** clearly shows, after the allotted 10 year simulation interval, the injection gas front (depicted by the black line) has travelled much further into the MBO simulation reservoir, meaning that more oil could be re-vaporised and produced by HW1. To further emphasize this, **Figure 5.27** presents the same property, but from a different angle; a map view of the reservoir after the 10 year interval.

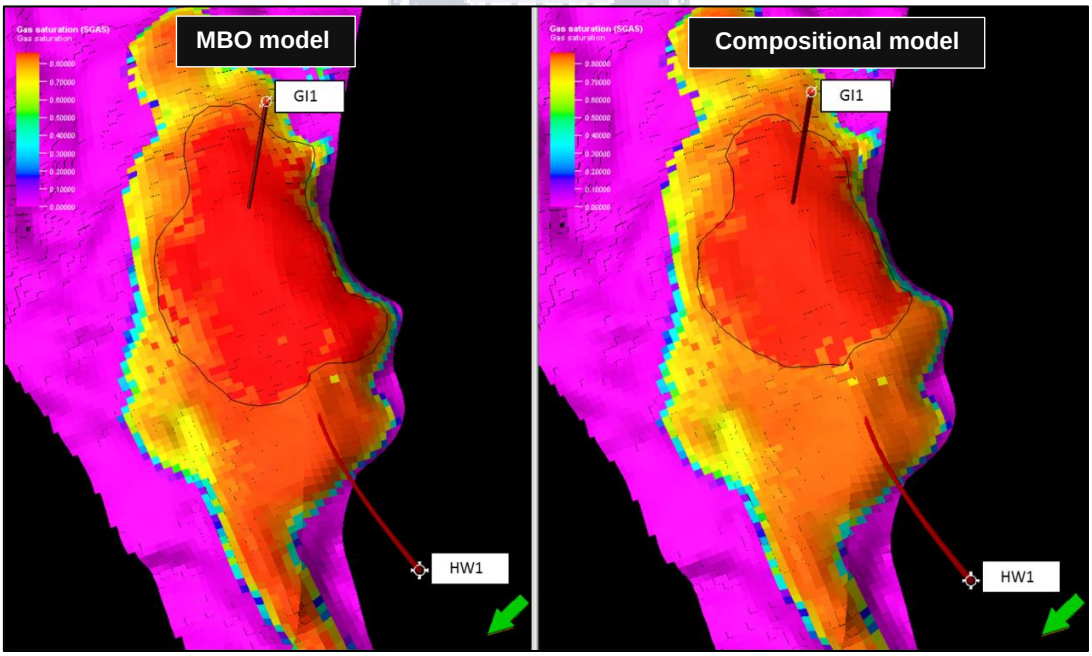

Figure 5.27: Top view showing the area covered by the injection gas at the end of the 10 year simulation interval

Again one can clearly see that the dark red area (emphasizing 100 % Sg, thus injection gas from GI1), covers a greater extent of the hydrocarbon zone in the MBO model compared to the compositional simulation results. This phenomenon is also evident with the 3800 psia gas injection cases, where the MBO model produces more oil in comparison to the compositional model (but not to the extent as is seen in the 6000 psia gas injection cases).

Figure 5.28 presents the results gathered for gas injection and production rates as well as cumulative volumes for the entire simulation interval.

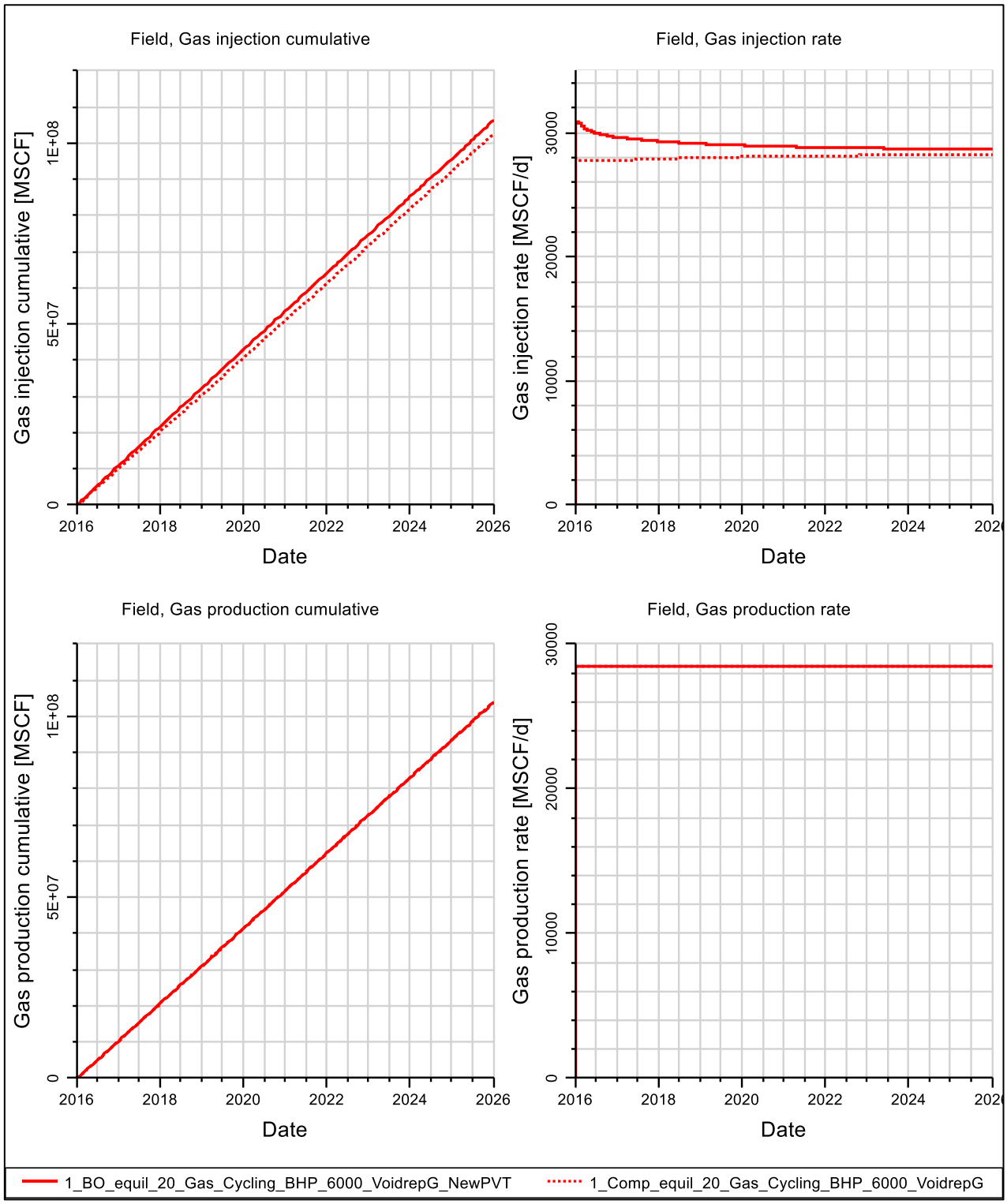

Figure 5.28: Gas production and injection volumes for gas cycling above the dewpoint

Finally, **Figure 5.29** depicts the subsequent oil production rates as well as the cumulative oil volume produced from the different simulation methods.

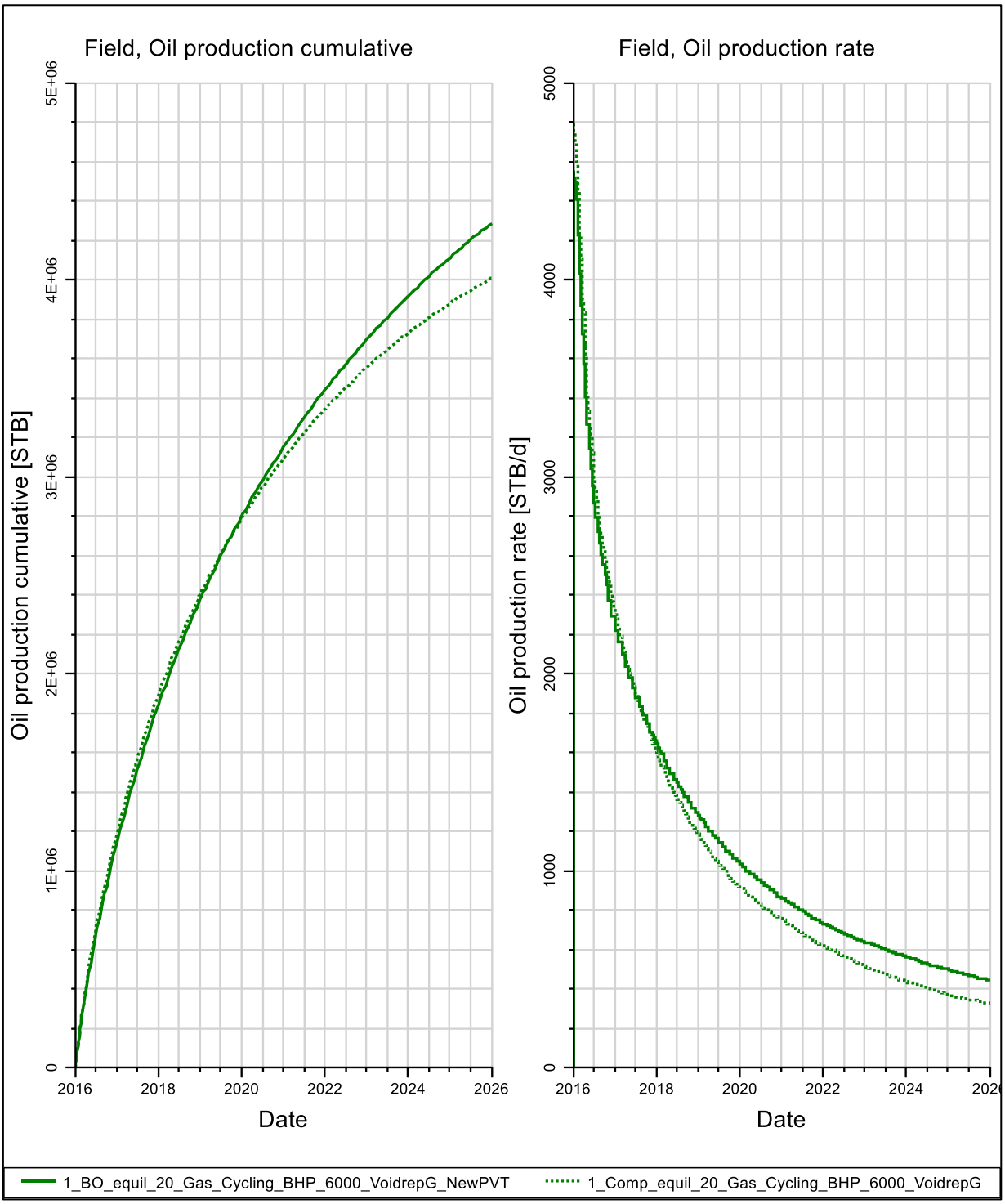

Figure 5.29: Oil production volumes for gas cycling above the dewpoint

From the results presented in **Table 5.18**, the deviation percentages between the MBO and compositional model for this scenario show a 9.69 % deviation for oil production, and a 0 % deviation in the total volume of gas produced. The MBO model also produces more oil than the compositional model as was evident from the 3800 psia gas injection cases, again due to the fact that injection gas re-vaporises more oil because of the greater extent of the reservoir which it covers.

In conclusion, we can see that as in the below the dewpoint cycling cases, recovery comparison results from the two modelling approaches do again compare favourably (within a 10 % accuracy range between the two modelling approaches). In our view, the accuracy of these results are much more reliable because reservoir pressure is kept above the dewpoint pressure, implying the reservoir fluid continues to exist outside the two phased liquid region (when looking at PVT diagrams), not adding the extra complexity of major component exchange and condensate formation to the simulation models (especially when looking at the MBO).

6 Chapter Six: Conclusion and Recommendations

When comparing the results of projects of a similar nature, correct fluid characterization is of paramount importance if accurate results are to be achieved. A personal opinion is that the use of the correct fluid model has to be considered the fundamental building block of reservoir engineering and simulation. The saying "garbage in, garbage out" comes to mind, since we encountered various problems with our first simulation attempts due to incorrect fluid characterization (especially in the case of the MBO lookup tables exported through using an incorrectly characterized fluid). The original results reflected major deviation percentages between MBO and compositional models, contrary to the results of the simulations performed later with more appropriate fluid models. Thus, the more correct the fluid characterization, the closer the results between the MBO and compositional simulation models and the more accurate the results of the study.

Regarding natural depletion simulation scenarios, this study demonstrated that the MBO approach could be used to model gas-condensate reservoirs above and below the dewpoint accurately, even for very rich (near critical) fluids. Multiple authors (e.g, Fevang *et al*. (2000:2) and Coats (1985:1822)) published results which reflected similar findings. Their comparisons, however, had been for single-well radial models.

Water production differences between the MBO and compositional models were an area of concern. Results showed that the MBO model produced about 10 times more water compared to the equivalent compositional model. Possible reasons for this discrepancy were given, chief among which were:

- The type of relative permeability model used, as well as how each model (MBO vs compositional) calculates the K_r.

Further research on this phenomenon was proposed to ascertain the causes of these water volume discrepancies. Even though these water production discrepancies were a cause of concern, no significant impact on hydrocarbon production rates and recoveries were evident. The results of this study thus confirm that a MBO model could be used as a supplement for a compositional model even when used on real-life field scale 3D-model development projects. The model still reflects accurate results with the bonus of some timesaving (up to six times faster than the equivalent compositional model).

The gas cycling scenarios of this study afforded some interesting results. The reservoir in question in this study had already been close to/ slightly below dewpoint pressure before development and production activities were initiated. The results of the gas cycling study showed that recovery volumes exhibited some promising matches between the two modelling approaches for oil and gas production rates. This was seen for both above and below the dewpoint cycling scenarios. Interestingly, the MBO model produced more oil than the compositional model in these cycling cases and not less, as was predicted by the natural depletion results. These results would suggest that the MBO model might be overestimating recovery volumes during the gas cycling scenarios because it is not as apt in simulating the complexity of the component exchange when gas cycling occurs.

The extent at which gas cycling influences reservoir pressure was established and given by **Figure 5.21**. Reservoir pressure comparisons were slightly different, reflecting a near 60 psia and 25 psia difference in HW1 BHP at the end of the 10-year simulation interval for the respective below and above the dewpoint cases. This discrepancy was attributed to the fact that in the case of the MBO model, injection gas affects a greater area of the reservoir thus increasing pressure more than in compositional simulations. When comparing the results of the two scenarios run, namely:

- gas injection with BHP target of 3800 psia (below Pd), and
- gas injected with BHP target of 6000 psia (above Pd),

it was found that even though gas was injected at a greater pressure, and thus travelled further into the reservoir, re-vaporising more oil, the gains achieved were not at all substantial as was expected. Only a small gain in oil production volume was noticeable upon the injection of gas with a BHP target of 6000 psia compared to the 3800 psia cases. Why then does the gas cycling recover so little oil? Is it because gas production, currently simulated at 30 000 MMscf/day because of comparison objectives between MBO and compositional models, could be way below the actual production capabilities of the reservoir? Could it have

to do with the fact that the injector is placed too close to the producing well? More study regarding this matter is thus also suggested since the scope of the study does not cover these questions.

Looking at below the dewpoint cycling cases, these scenarios showed to be much more complex than initially thought. Confidence in MBO model results were an issue, and thus it was felt that more research must be done in order to fully understand how the different modelling approaches account for production volumes during these cycling scenarios. A word of caution must be issued when using an MBO model for gas cycling scenarios below the dewpoint. The modelling approach did however show some promising comparison capabilities for the production recovery results, but is not recommended.

For above the dewpoint cycling scenarios, all recovery volume comparison results (oil, gas and water) between the MBO and compositional model compared favourably (within a 10 % accuracy range between the two modelling approaches). BHP and THP values also showed minimal differences. In our view, the accuracy of these results are much more reliable due to the fact that reservoir pressure is kept above the dewpoint pressure, implying the reservoir fluid continues to "exist" outside the two-phased liquid region (when looking at PVT diagrams), which in turn does not add-in the extra complexity of major component exchange and condensate formation to the simulation models (especially when looking at the MBO model). Thus, as was proposed by some authors (Fevang *et al*. (2000:2), Coats (1985:1822) and El-Banbi *et al.* (2000:14)), gas cycling above the dewpoint could in fact be modelled accurately with the MBO modelling approach.

Thus, from the above mentioned results the conclusion could be deduced that if the pressure difference between reservoir pressure and dewpoint pressure is small, or if it is higher than dewpoint pressure, the reliability of the MBO modelling approach's recovery results is sufficient and this method could be used for gas cycling scenarios. It is only when reservoir pressure falls far below dewpoint pressure that more study is required in order to have full confidence in MBO recovery results.

One final interesting aspect regarding the gas cycling scenarios, is that compositional model running times were only a maximum of two times longer than the equivalent MBO model runtime. This would suggest that regarding gas cycling the compositional model could be used. It could reflect more accurate and reliable results regarding the complex component exchange behaviour of the rich gas-condensate fluid without engendering too much extra time as was first surmised.

To conclude: in this thesis we presented the results of a simulation study for a gas-condensate reservoir with complex fluid behaviour. We also compared the MBO approach with the compositional simulation approach. Based on the results of the study, the following conclusions were drawn:

- Proper characterization of the reservoir fluid is of utmost importance to simulate production correctly and to acquire accurate results.
- The MBO simulation model can simulate all natural depletion cases for gas-condensate reservoirs adequately within 10% accuracy, compared to the compositional simulation model..
- Since the scope of this study does not cover the water production discrepancies, further research on the causes of these discrepancies are advised (relative permeability assessments).
- If the pressure difference is small between reservoir pressure and dewpoint pressure, or if it is higher than dewpoint pressure, the reliability of the MBO modelling approach's recovery results is sufficient and this method could be used for gas cycling scenarios. It is only at lower cycling pressures (when reservoir pressure falls far below dewpoint pressure) that more study is required in order to have full confidence in MBO recovery results.
- Why oil recovery volumes are so low for the gas cycling scenarios must be further assessed.
- Even though the MBO model produced comparable gas cycling production predictions, compositional model running times were only a maximum of two times longer.
- The MBO model tends to overestimate production and injection volumes (perhaps due to its inability to model the component exchange as accurately as the compositional model) although its findings are still within acceptable accuracy limits described in the study.

7 Appendixes

7.1 Appendix A

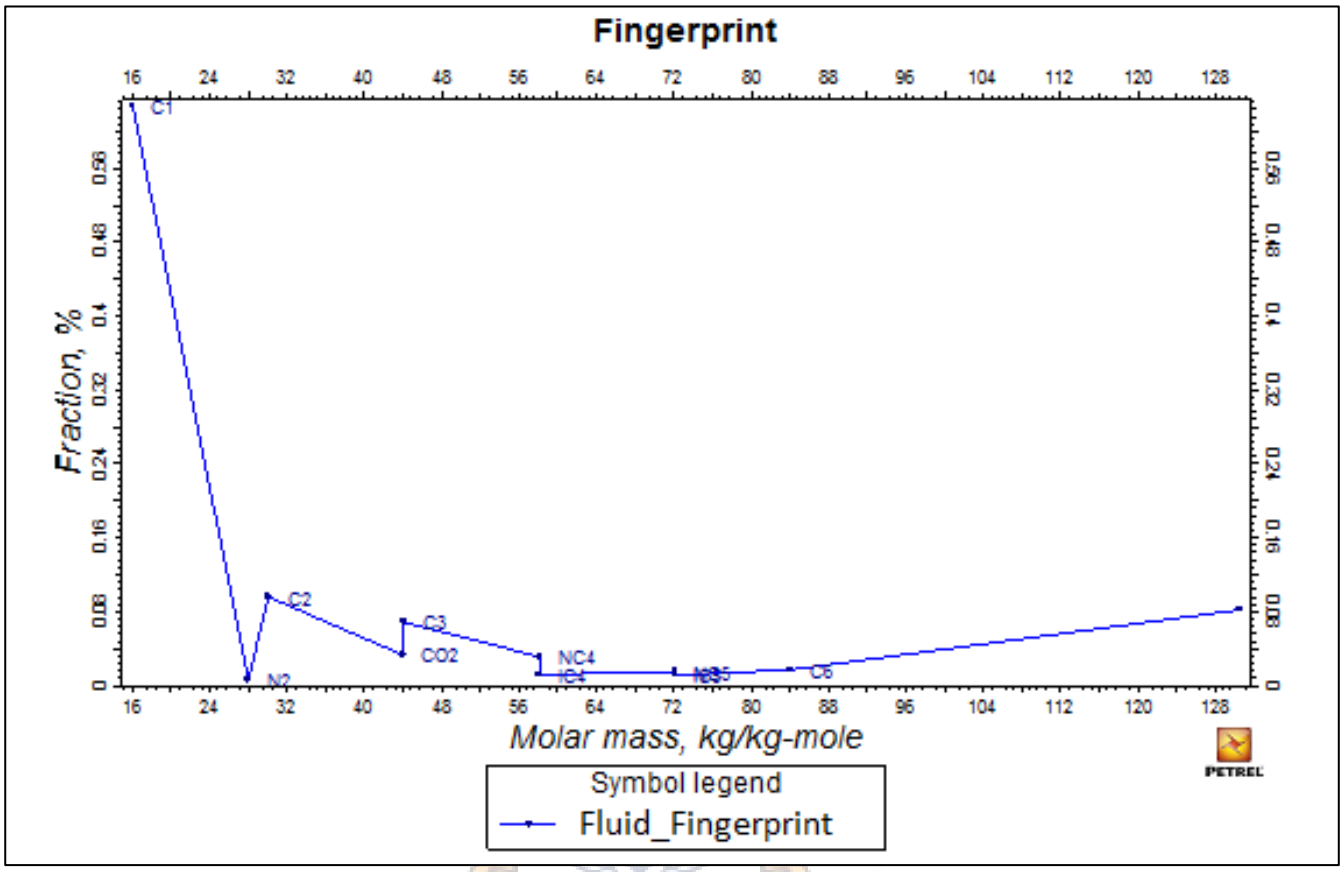

Figure 7.1: Molar composition of the recombined fluid

The Figure below (**Figure 7.2**) shows the fingerprinting analysis done from the Flopetrol-Johnston G.P.C system as well as shown by the Petrel software.

The method uses liquid chromatography with Gel Permeation columns. Each component is separated by size exclusion according to its molecular size. Ultraviolet (UV) and infrared (IR) detectors are used to determine the ratio of unsaturated to saturated bonds as a function of the molar mass. Unsaturated are generally aromatics and saturated are paraffinic components (Schlumberger; 1990:72).

A fingerprint can help:

- differentiate 2 liquids having similar molar masses and densities, but probably belonging to different hydrocarbon accumulations.
- to visualize the possible variations in the compositional distribution between zones of a given reservoir.
- to identify pollutants present in the sample (Schlumberger; 1990:72).

The abscissa is graduated on a Log scale in equivalent paraffin molar mass in order to obtain a constant reference scale; and the area is normalized by attributing 100% to the highest peak.

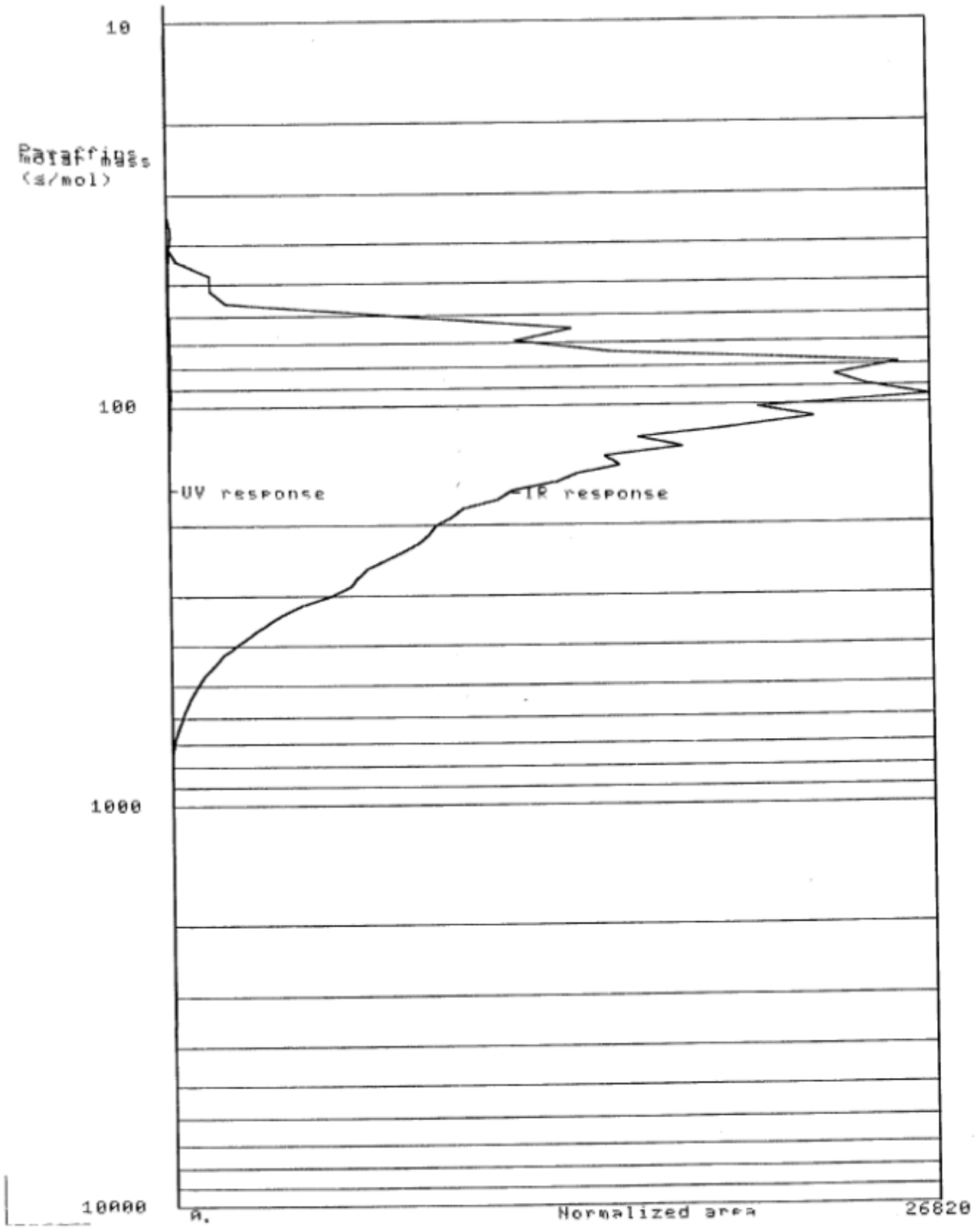

Figure 7.2: Fingerprinting analysis

7.2 Appendix B

Figures showing match between observed and calculated fluid properties for CCE, CVD and gas-oil ratio.

Constant Composition Expansion (CCE):

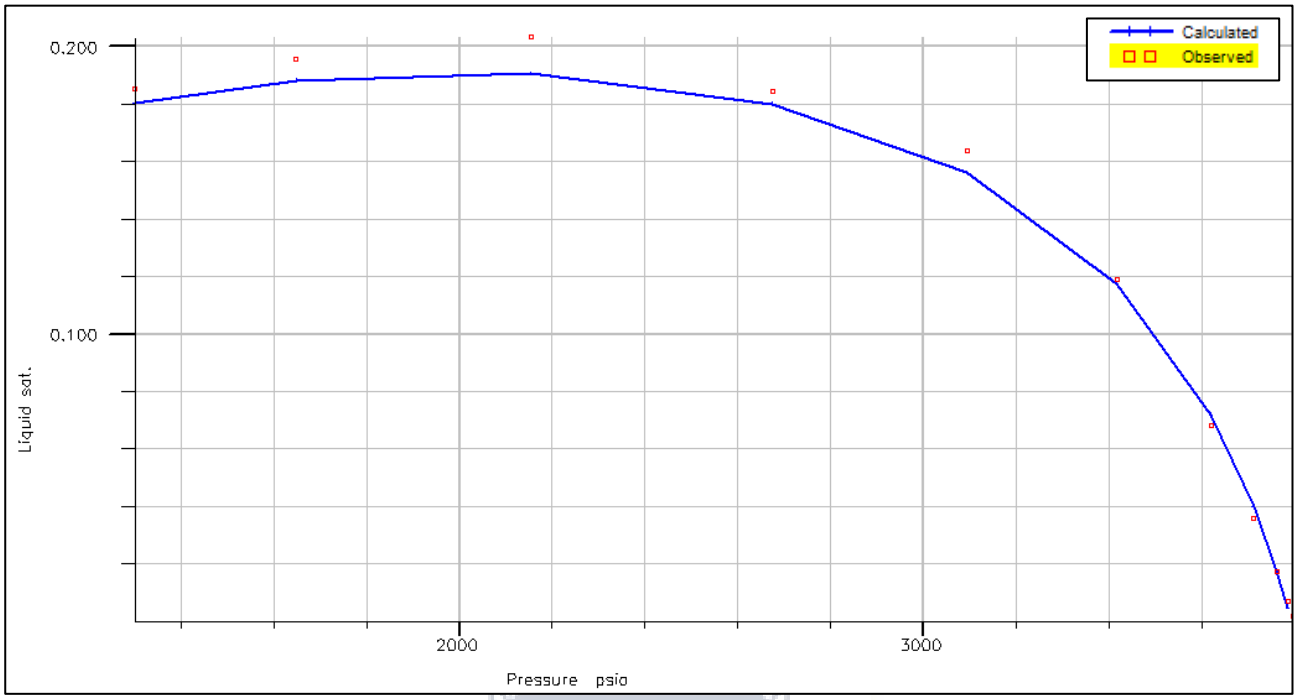

Figure 7.3: CCE - Liquid Saturation (liquid dropout)

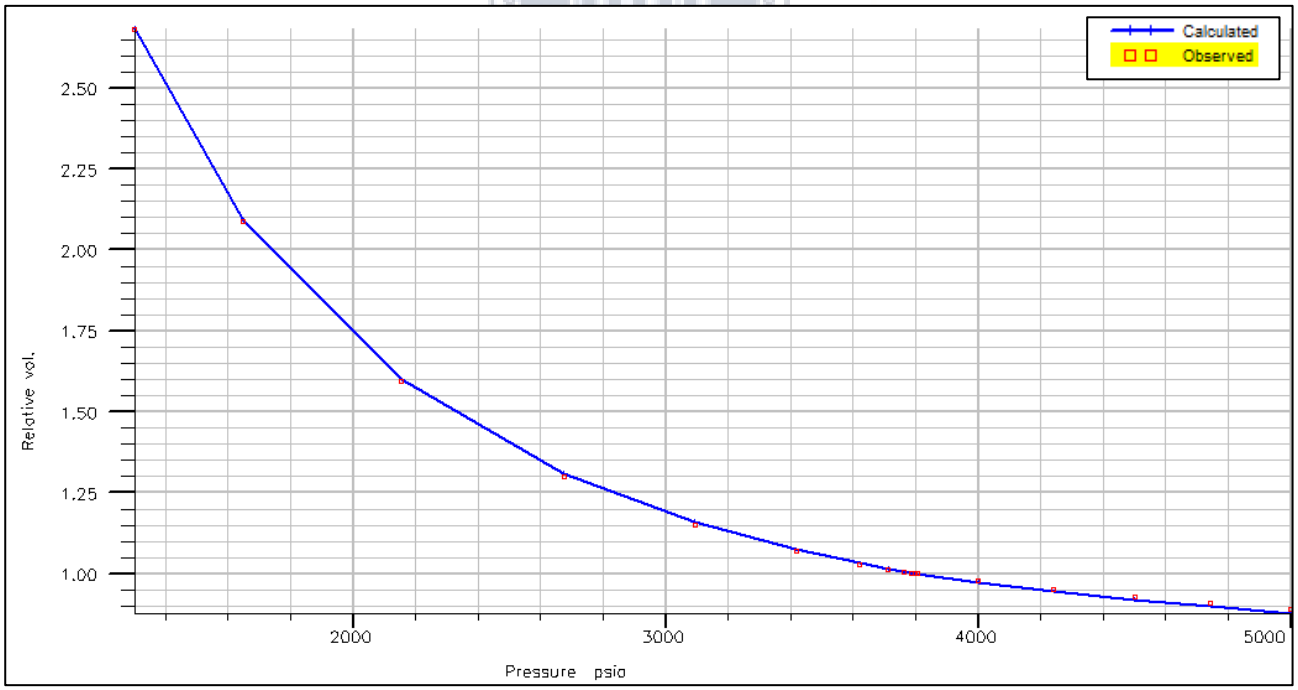

Figure 7.4: CCE - Relative Volume

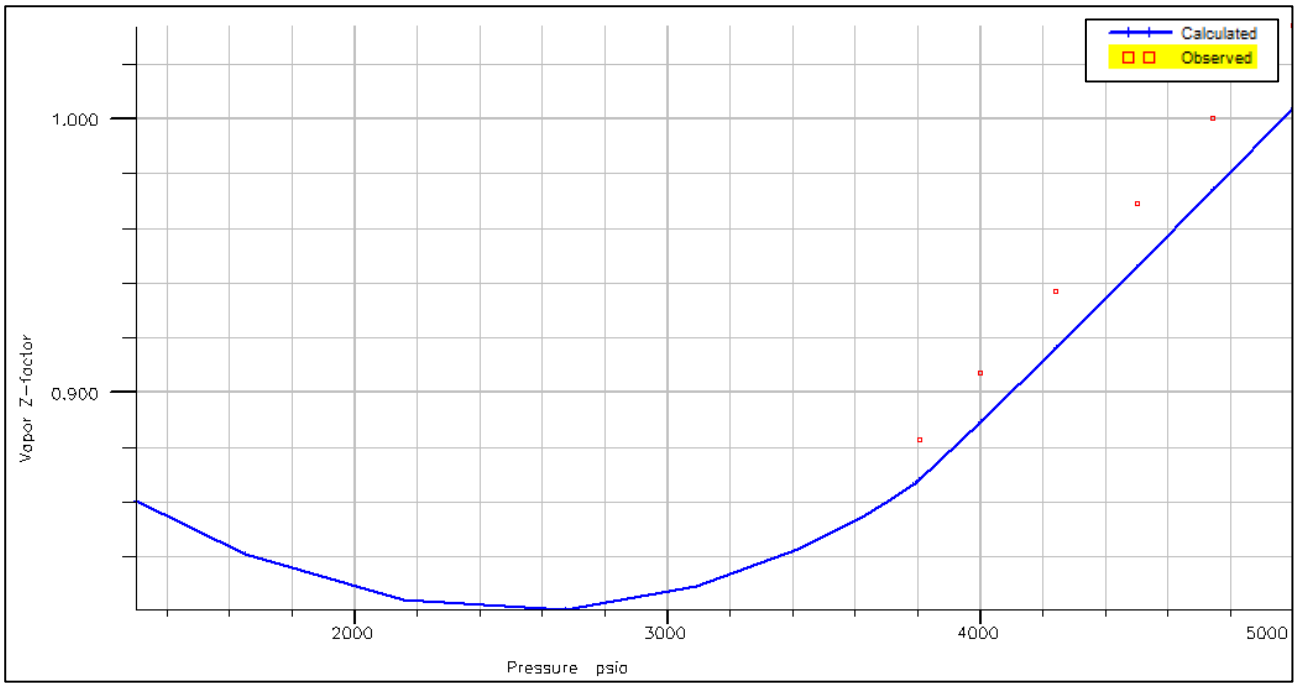

Figure 7.5: CCE - Vapour Z-factor

Constant Volume Depletion (CVD):

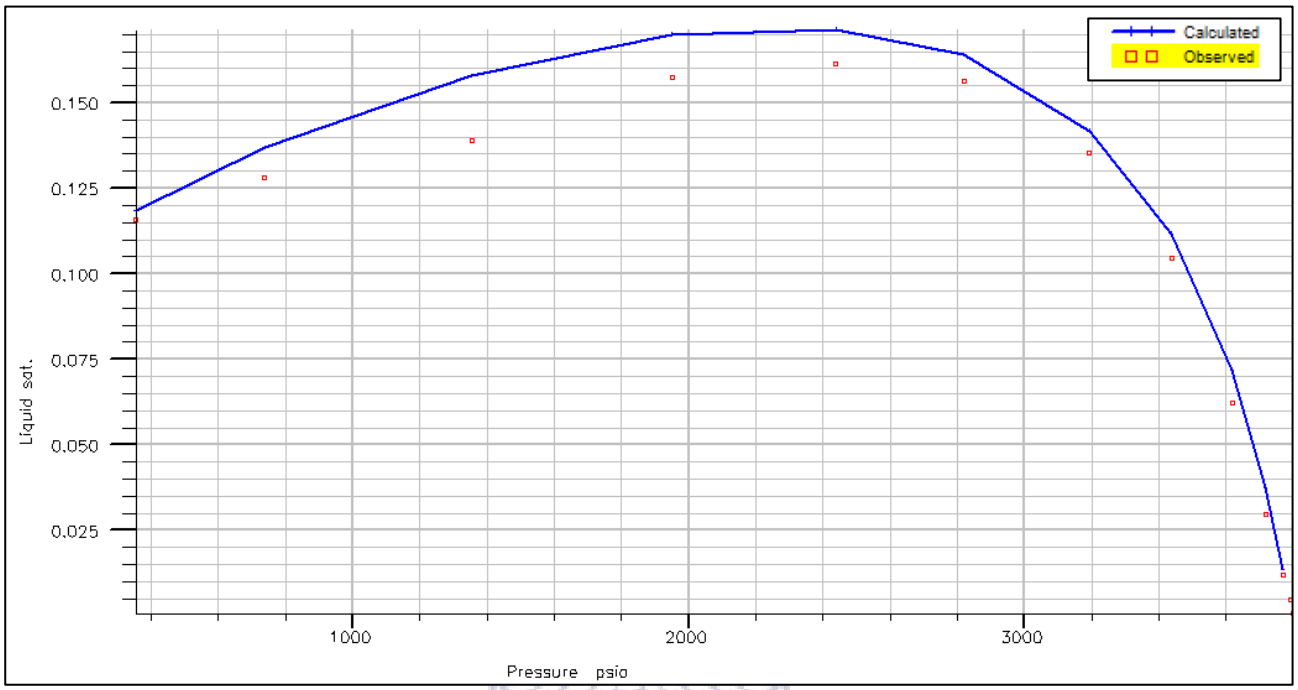

Figure 7.6: CVD - Liquid Saturation (liquid dropout)

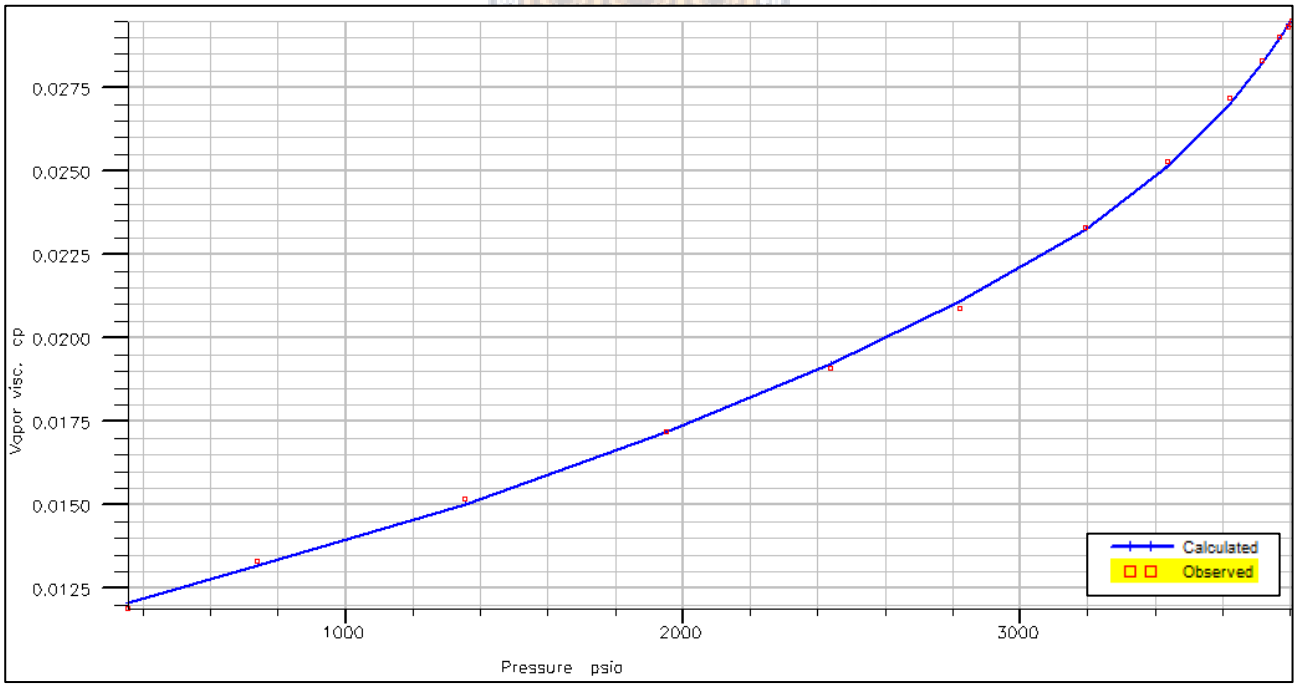

Figure 7.7: CVD - Vapour viscosity

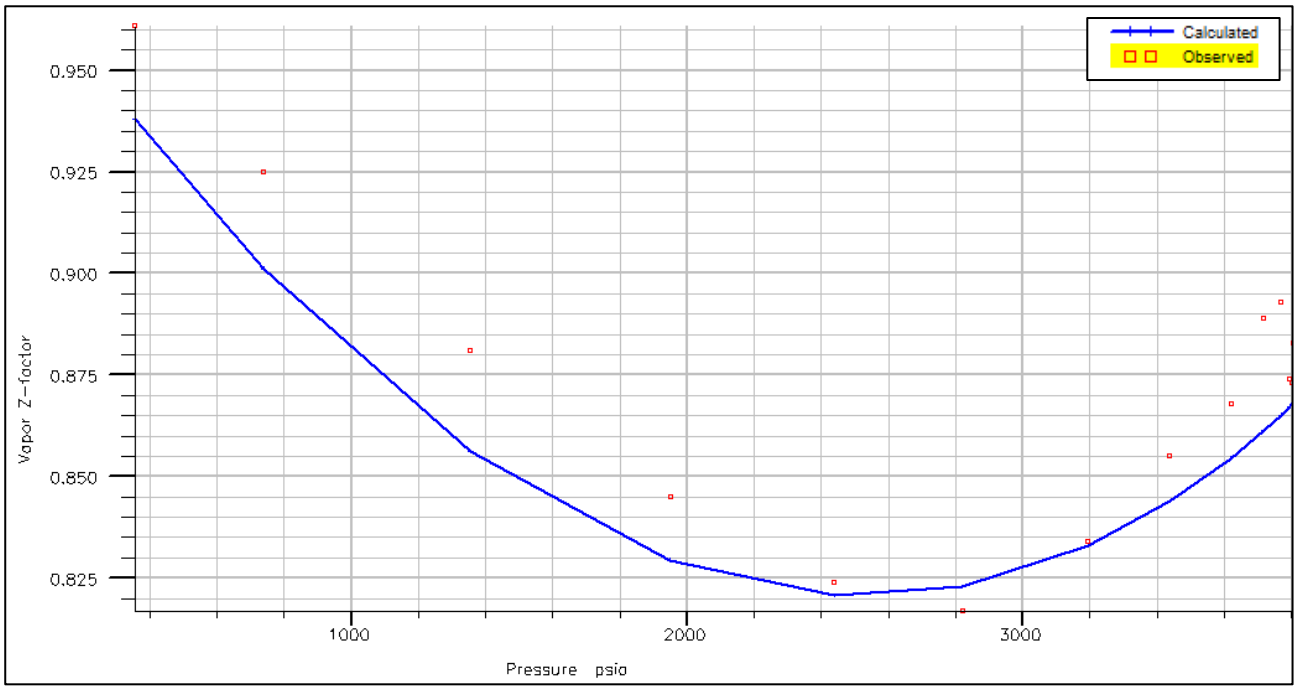

Figure 7.8: CVD - Vapour Z-factor

Separator Test (SEPS):

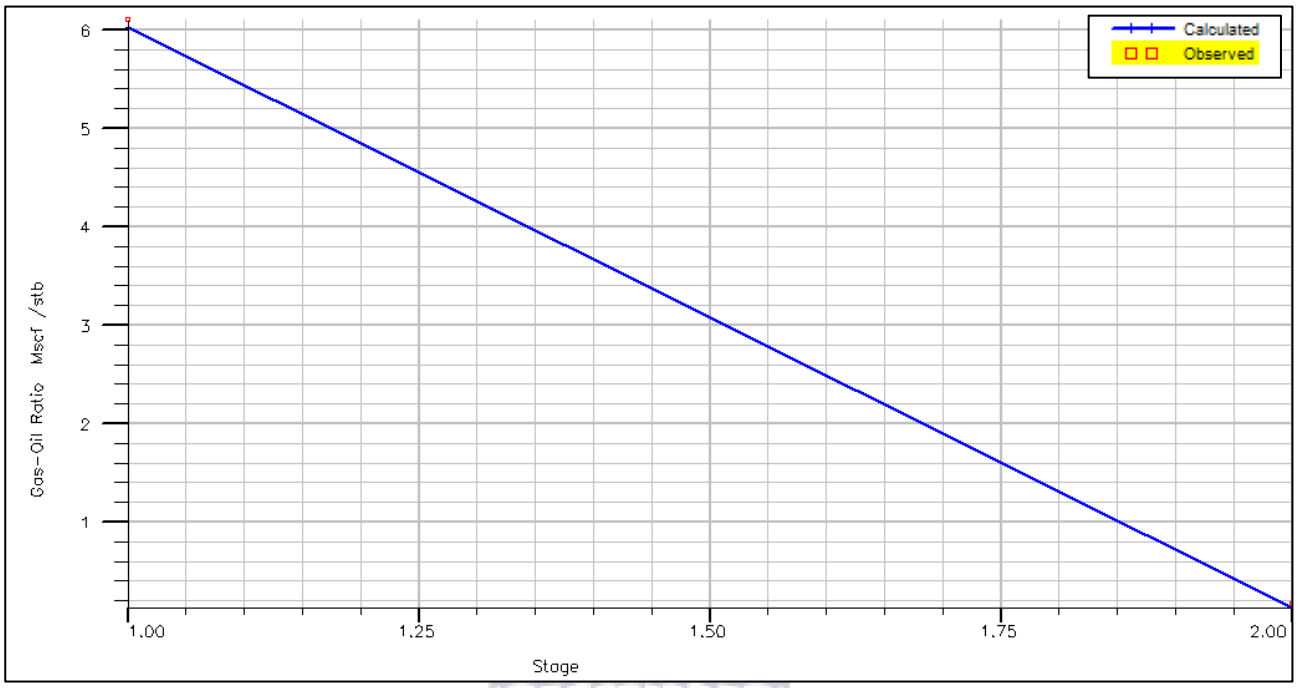

Figure 7.9: SEPS - Gas-oil Ratio

7.3 Appendix C

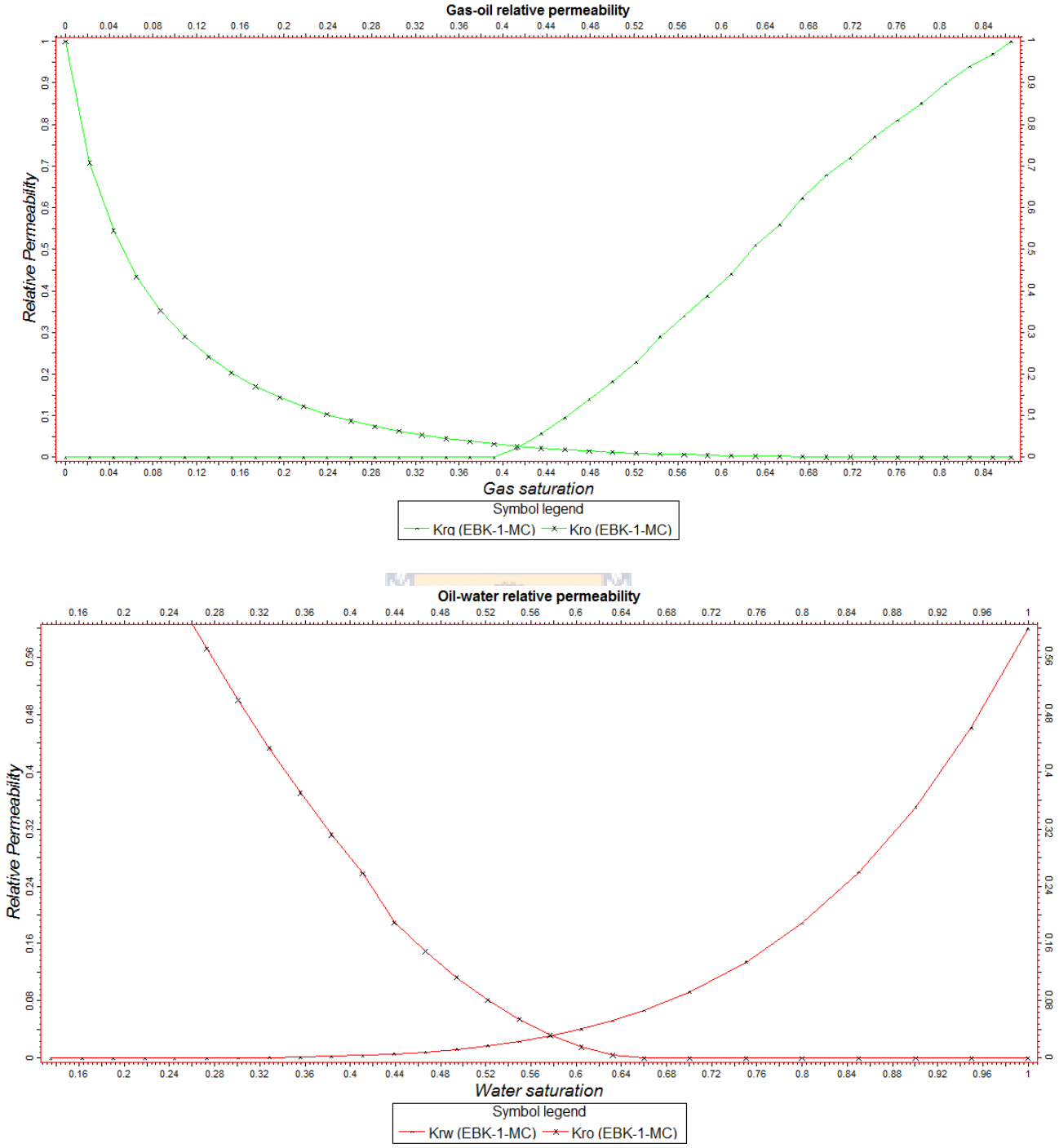

Figure 7.10: Rock relative permeability curves for AW1

7.4 Appendix D

Natural Depletion development scenario curves:

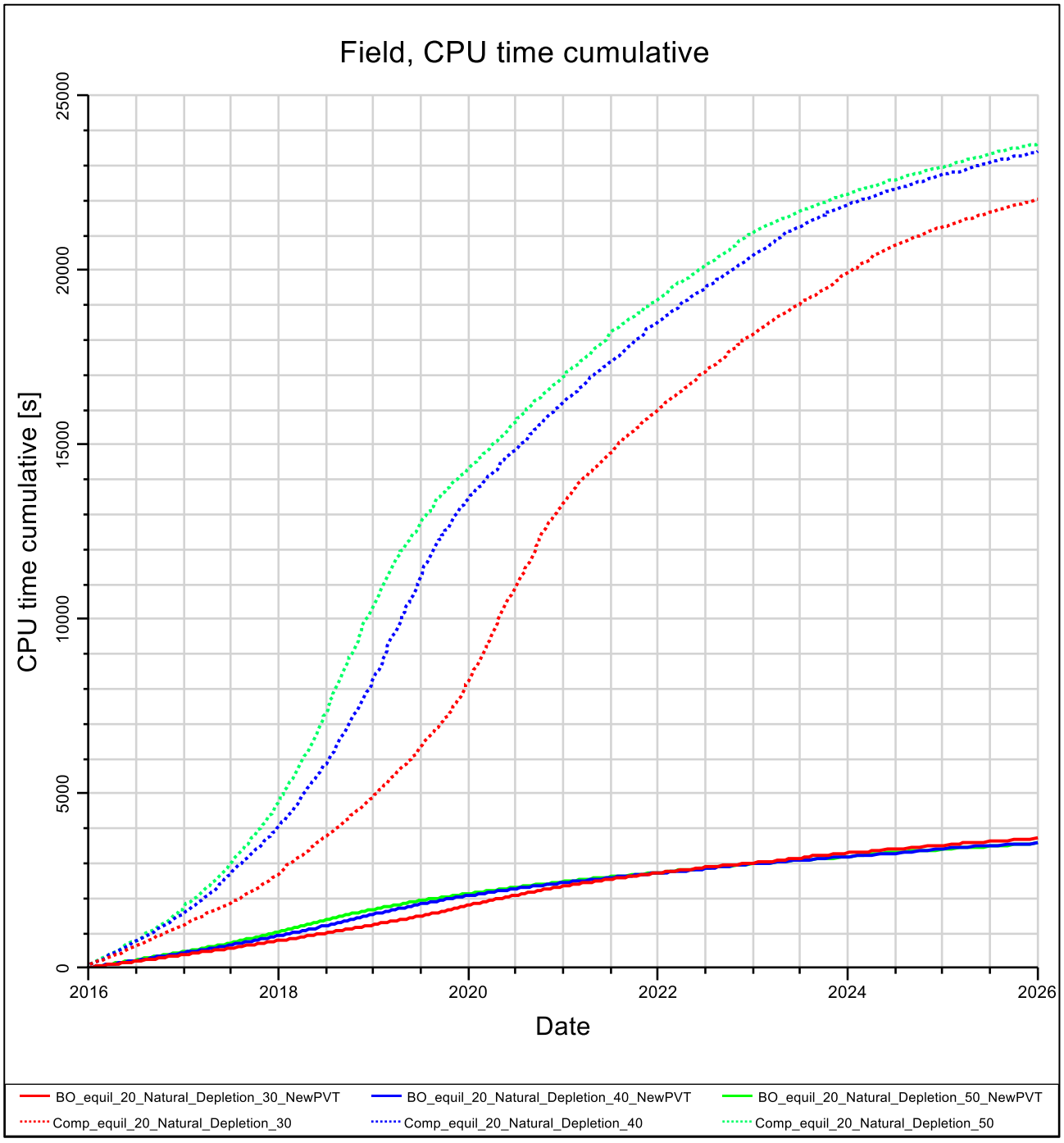

Figure 7.11: CPU running time for all natural depletion simulations run

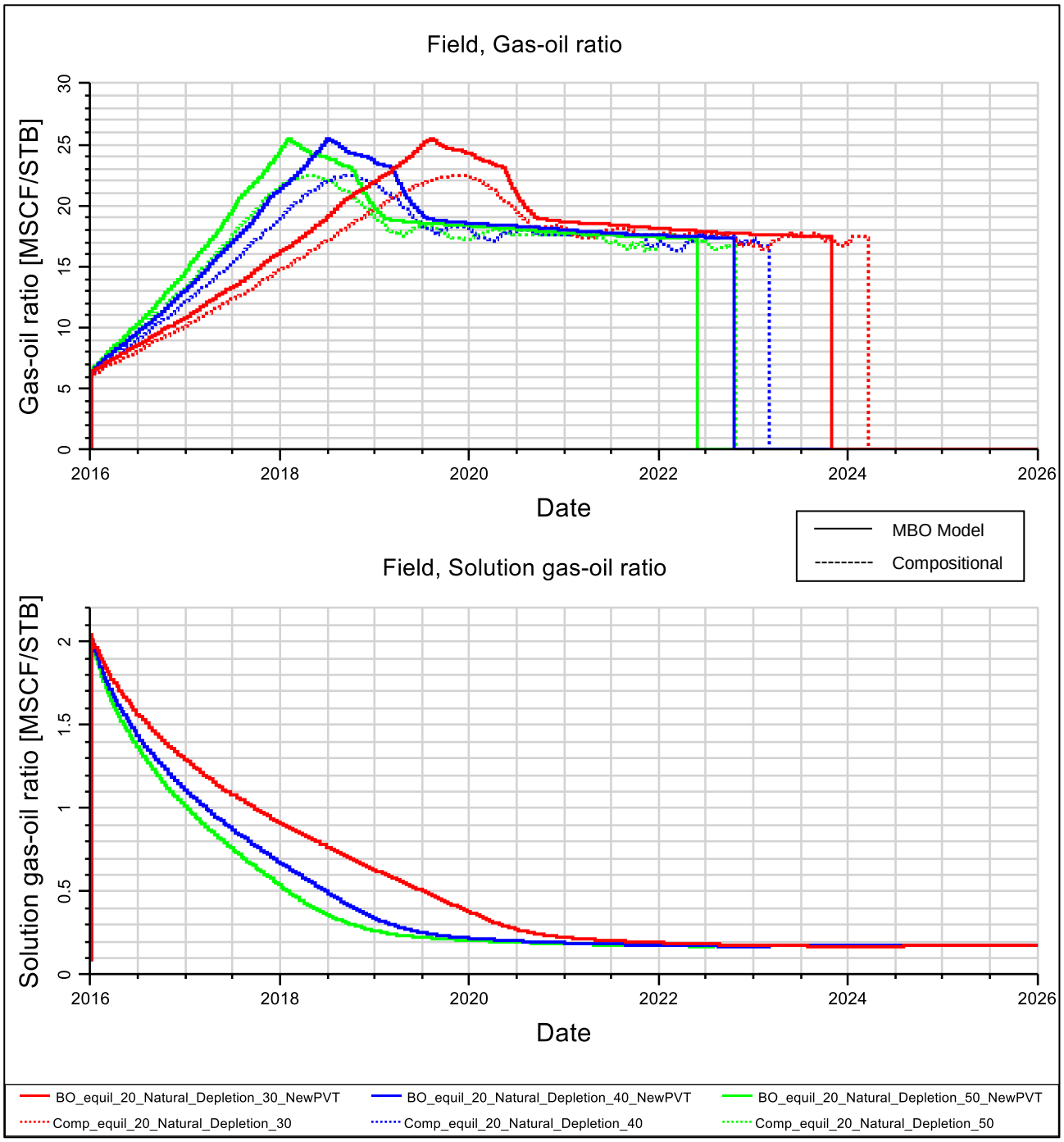

Figure 7.12: Producing gas-oil ratio and Solution gas-oil ratio (Rs)

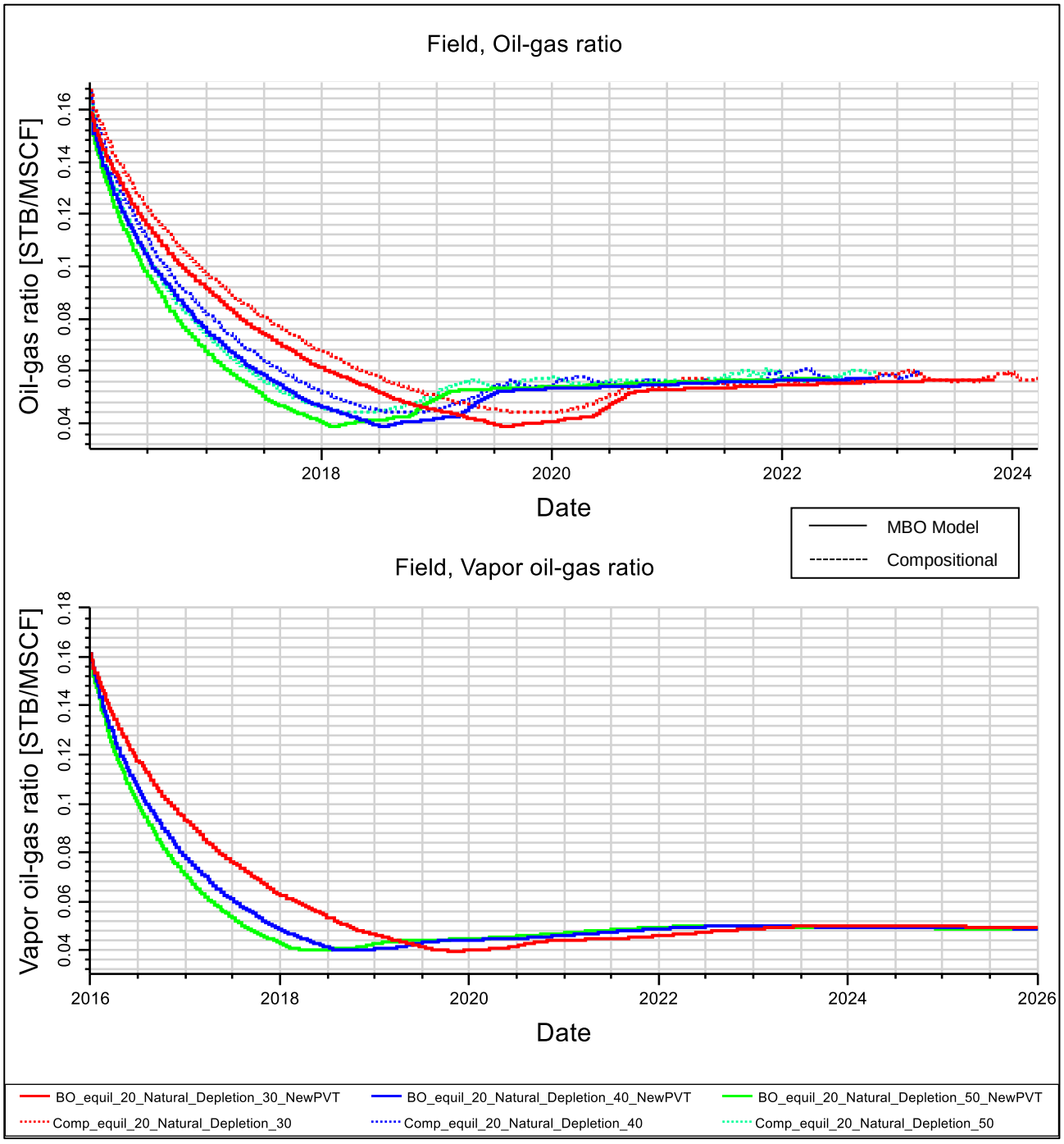

Figure 7.13: Producing oil-gas ratio and Vapour oil-gas ratio (r_v)

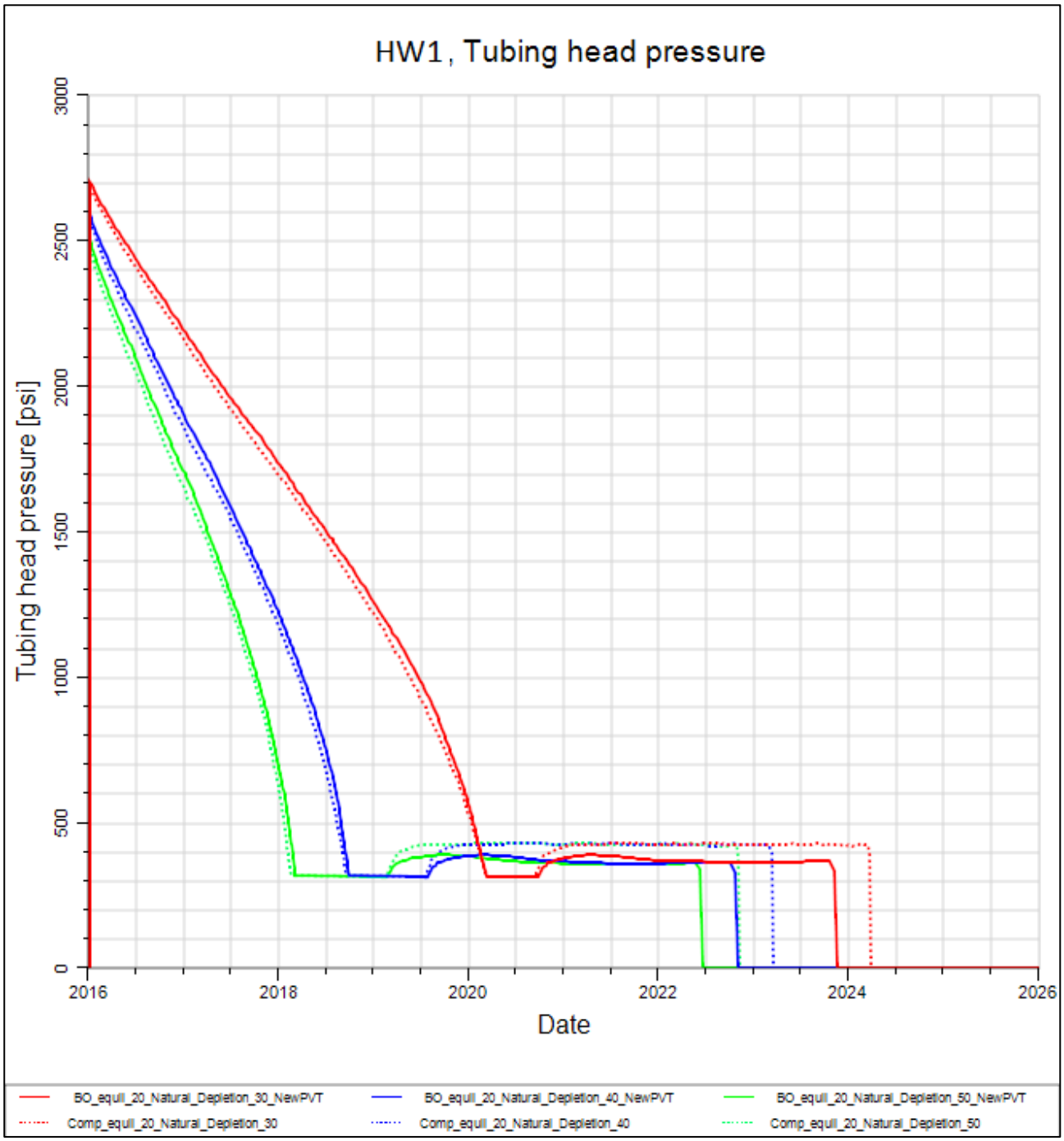

Figure 7.14: Tubing head pressure (THP) curves for HW1

7.5 Appendix E

Gas cycling below the dewpoint development scenario curves:

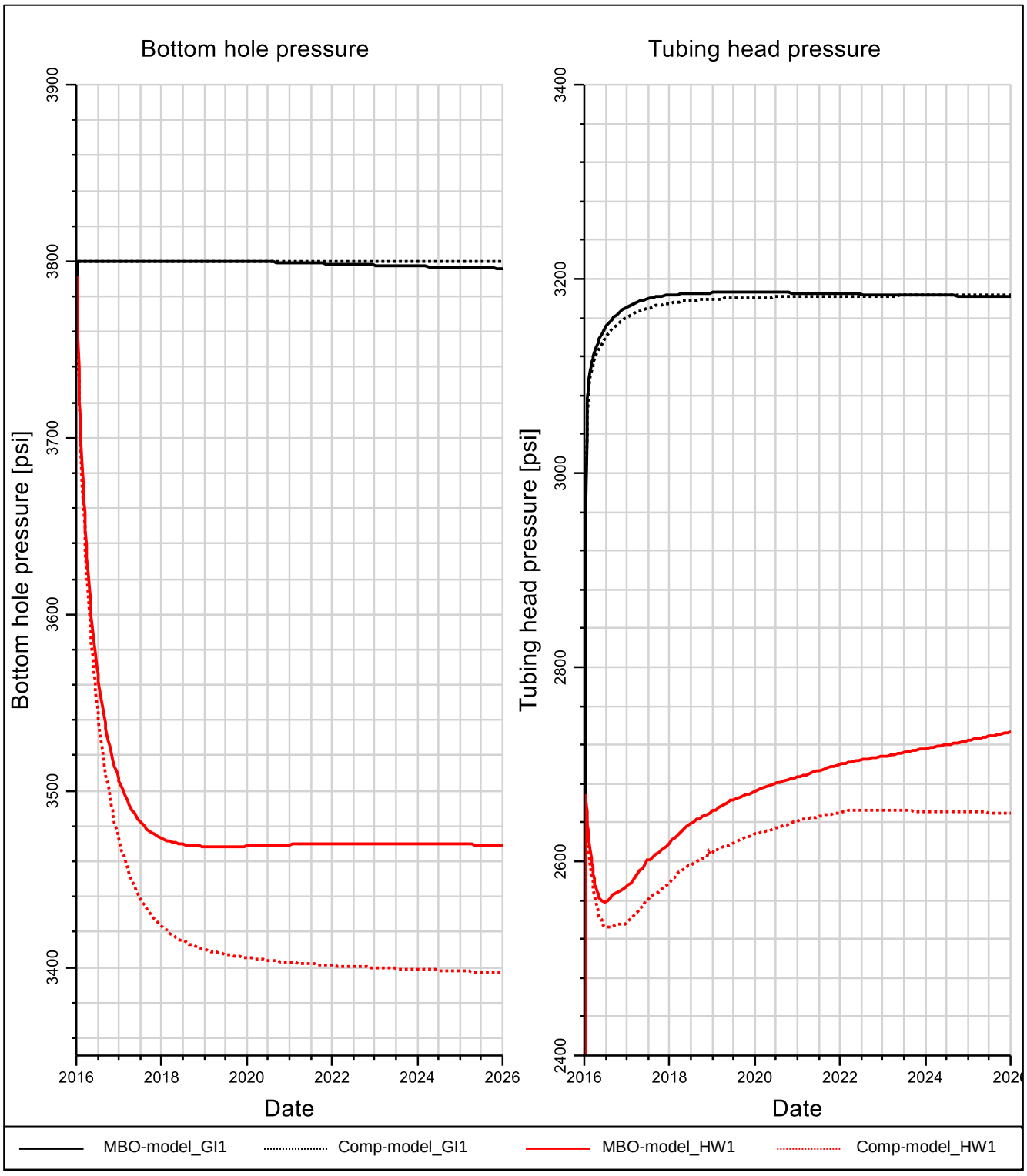

Figure 7.15: BHP and THP of HW1 and GI1 below the dewpoint cases

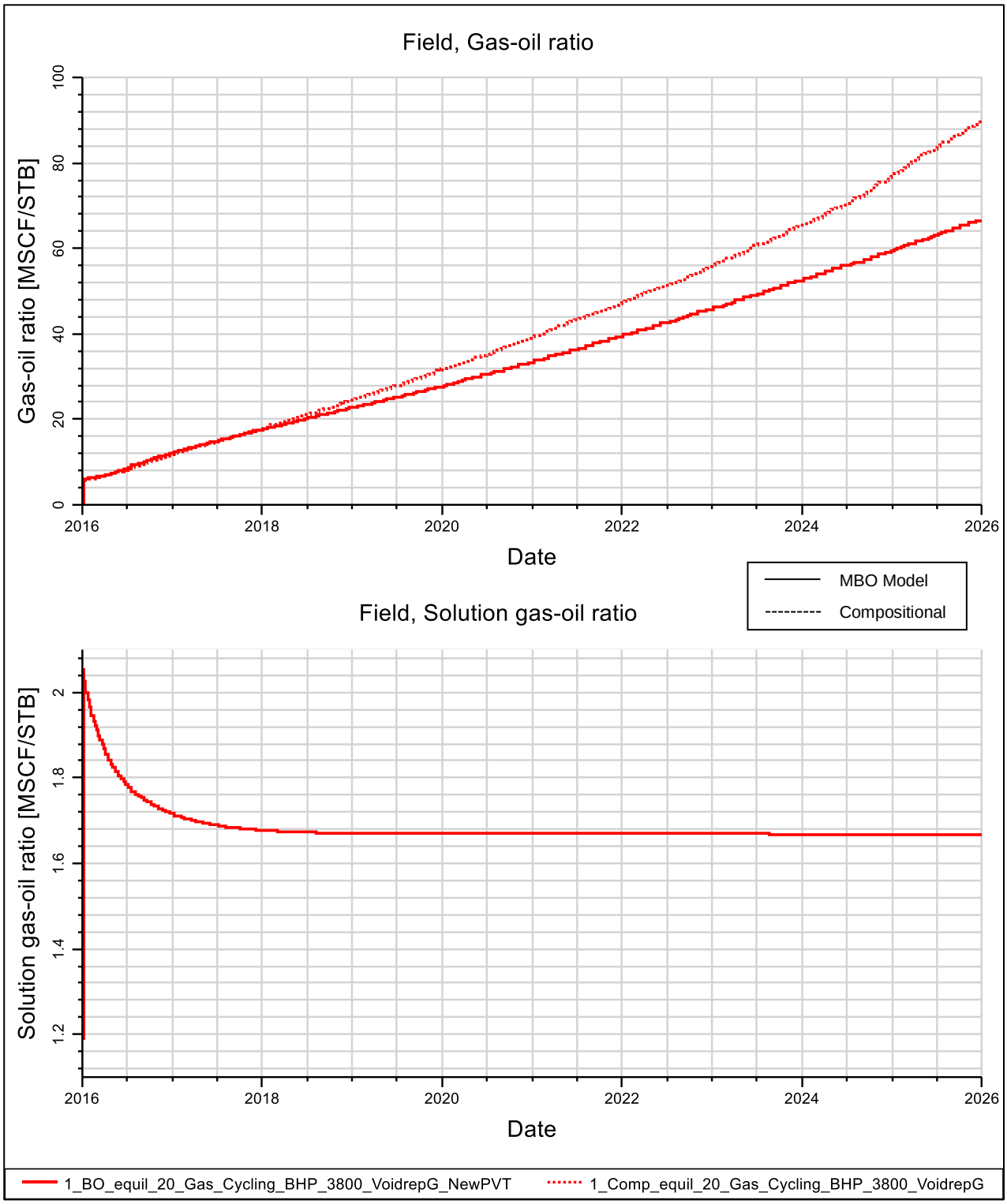

Figure 7.16: Producing gas-oil ratio and Solution gas-oil ratio (Rs) for gas cycling below the dewpoint

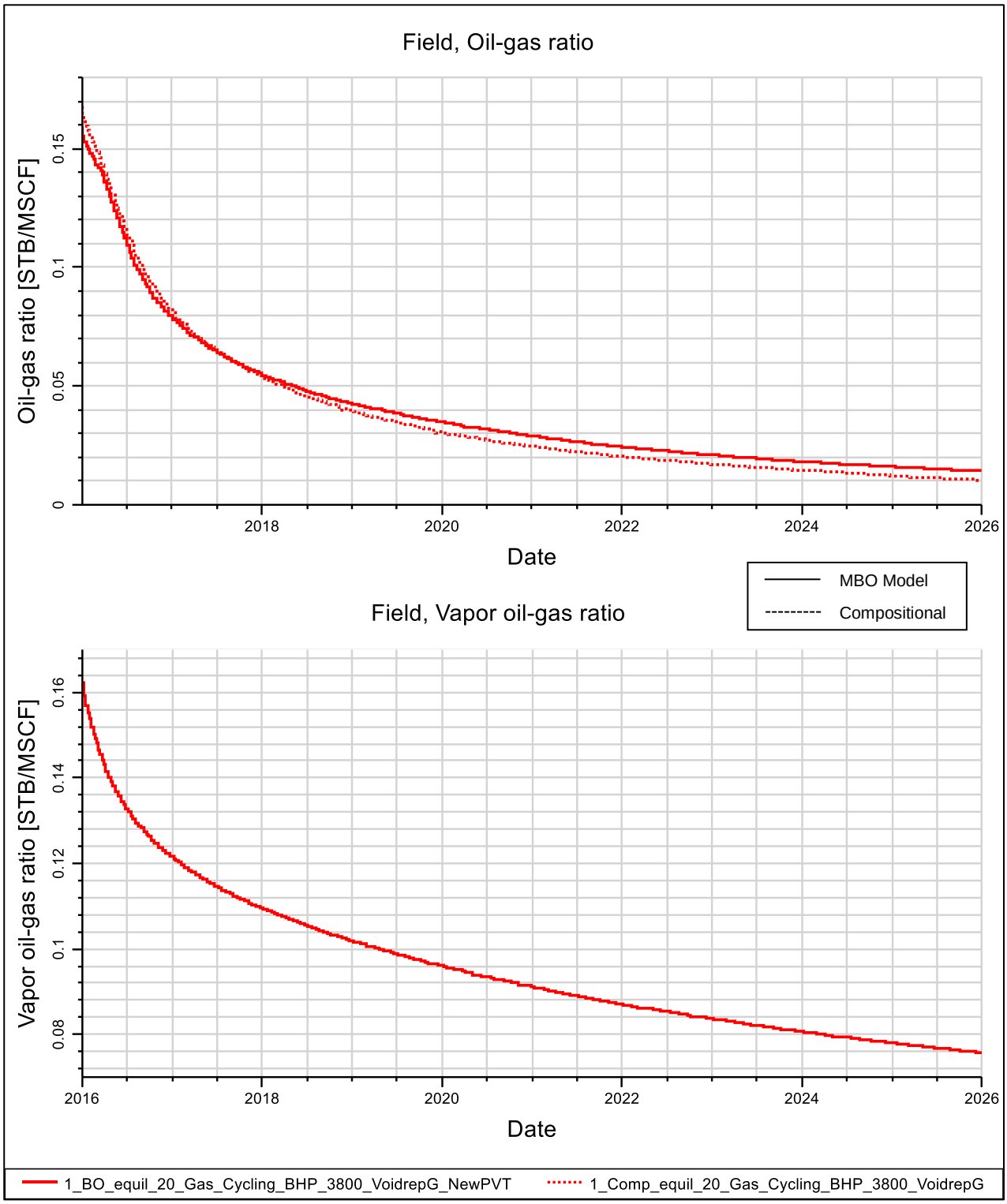

Figure 7.17: Producing oil-gas ratio and Vapour oil-gas ratio (r_v) for gas cycling below the dewpoint

7.6 Appendix F

Gas cycling above the dewpoint development scenario curves:

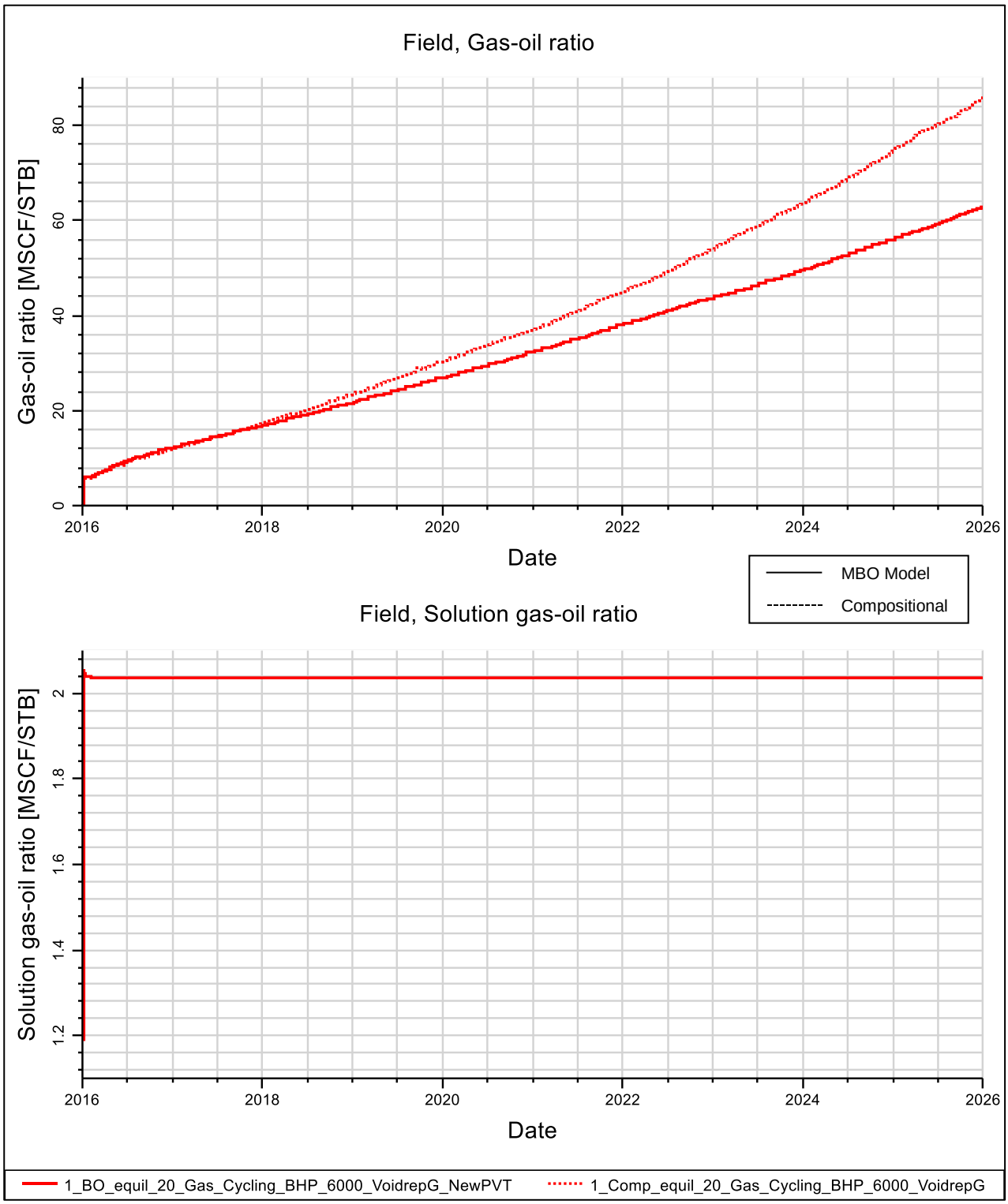

Figure 7.18: Producing gas-oil ratio and Solution gas-oil ratio (Rs) for gas cycling above the dewpoint

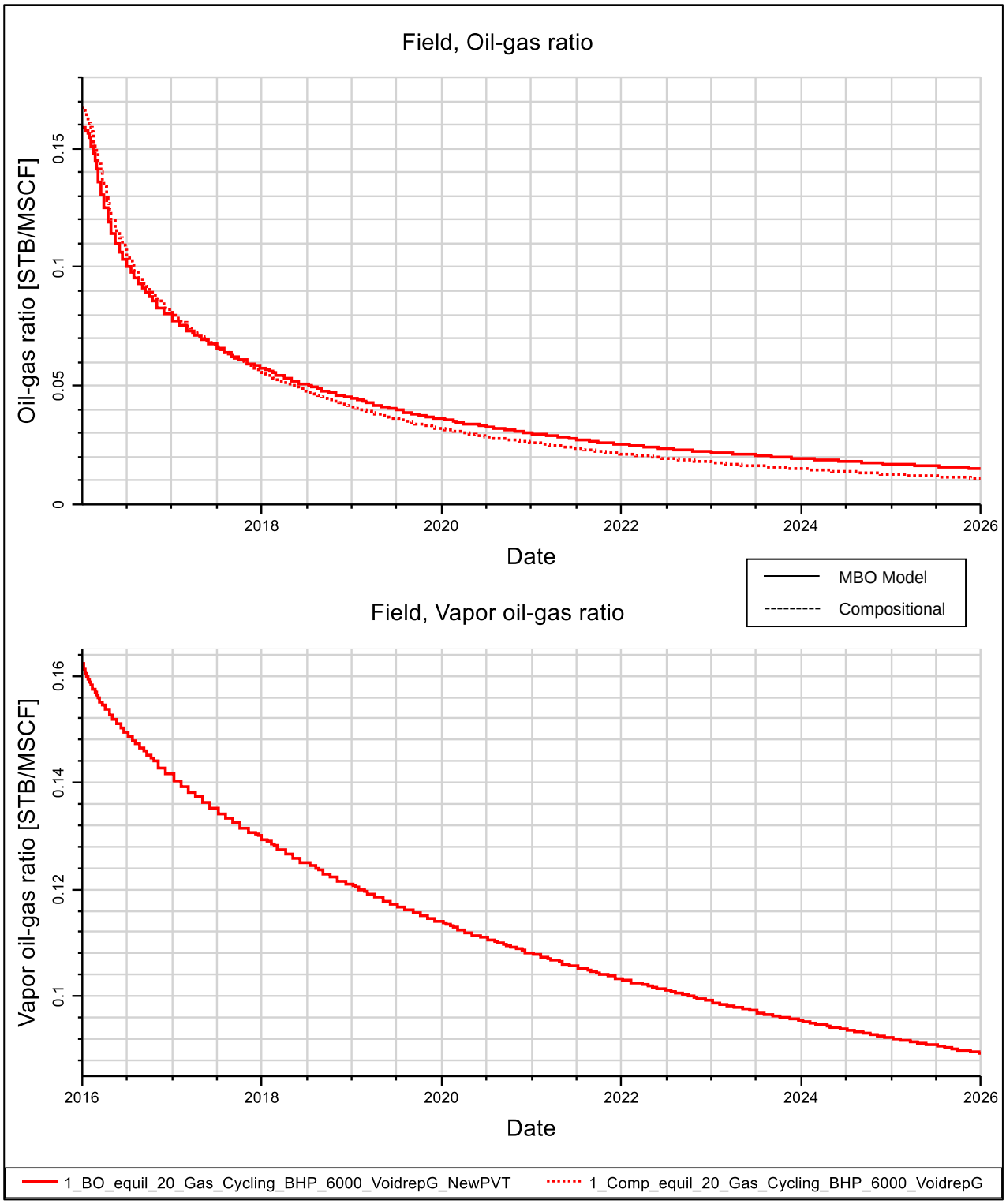

Figure 7.19: Producing oil-gas ratio and Vapour oil-gas ratio (r_v) for gas cycling above the dewpoint

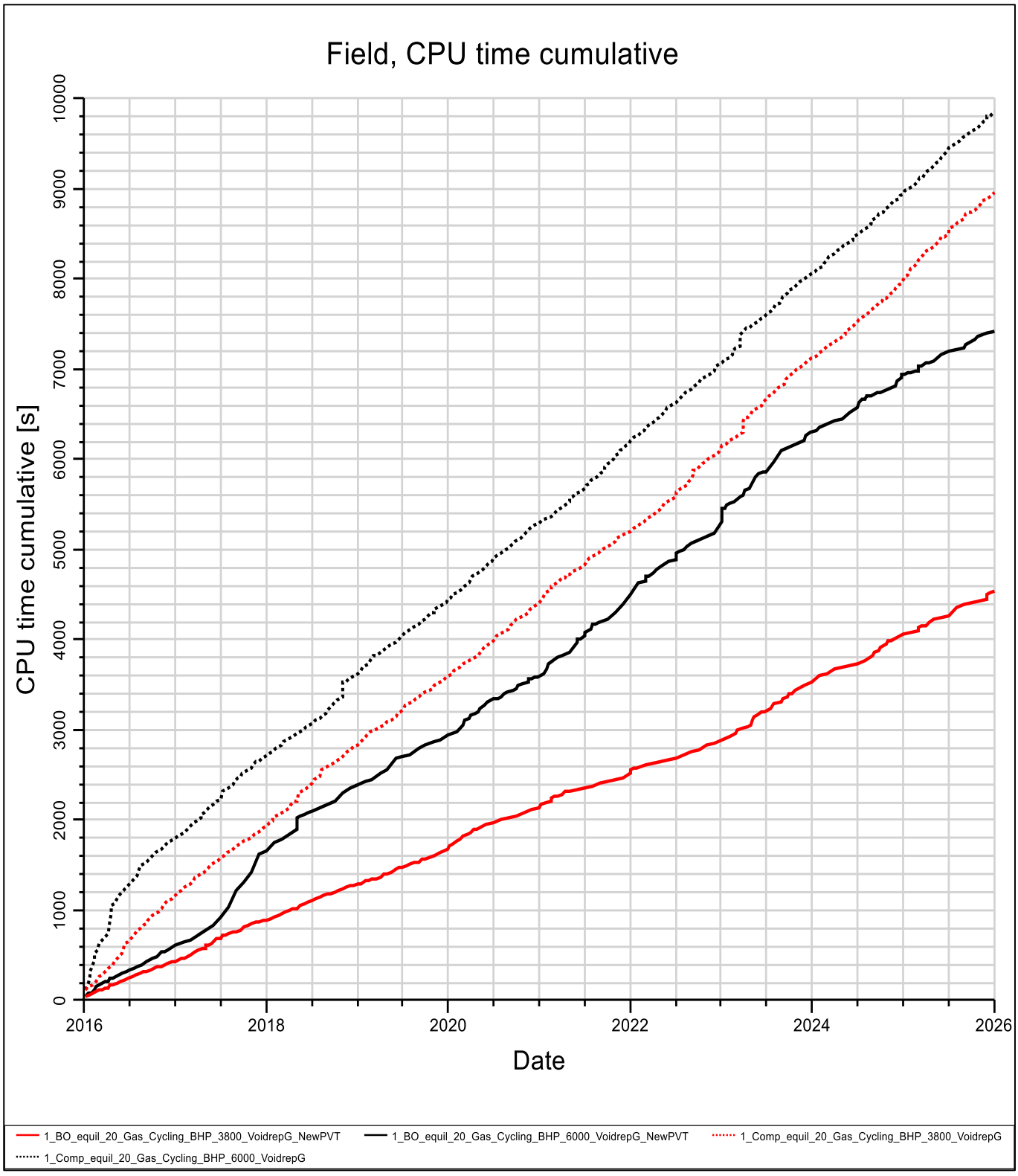

Figure 7.20: Comparative CPU running times for all gas cycling simulation cases

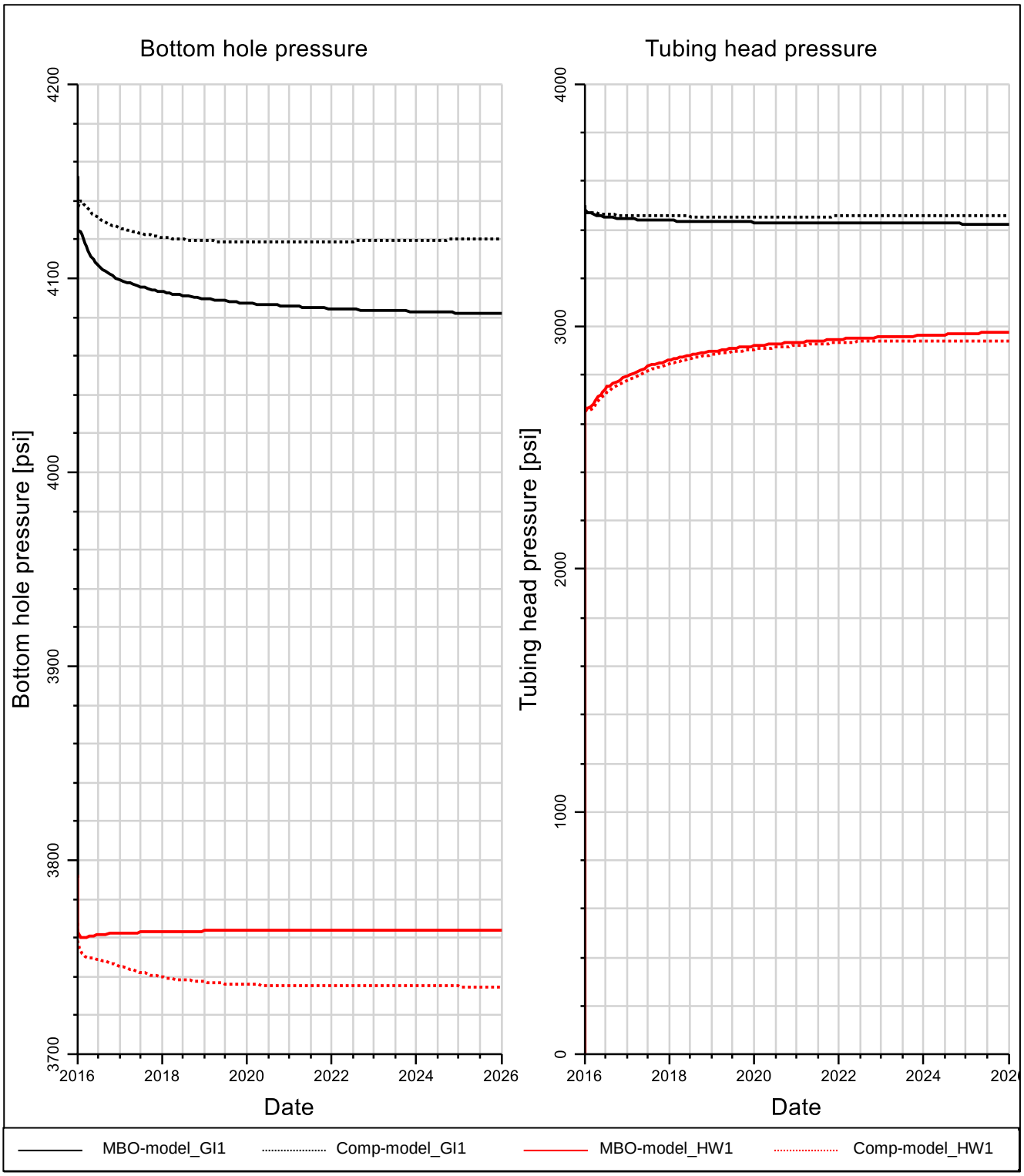

Figure 7.21: BHP and THP of HW1 and GI1 above the dewpoint cases

7.7 Appendix G – Project Simulation Data

EQUIL and PROPS section for MBO model

```
EQUIL                                   -- Generated : Petrel
        8591.5         3803       8591.5            0       8591.5
0 1 1 20 /

RSVD                                    -- Generated : Petrel
           -0            0
        13123            0
  /

RVVD                                    -- Generated : Petrel
           -0      0.16252
        13123      0.16252
  /

RPTRST                                  -- Generated : Petrel
  BASIC=3 FLOWS FLORES FREQ=2 BG BO /

RPTSOL                                  -- Generated : Petrel
  RESTART=2 FIP=2 /

PVTW                                    -- Generated : Petrel
        3855.1        1.036  3.0902E-006        0.272  5.0297E-006 /

ECHO
-- DENSITY created by PVTi
-- Units: lb /ft^3     lb /ft^3     lb /ft^3

DENSITY
--
-- Fluid Densities at Surface Conditions
--
         42.5456     62.4280      0.0617
/

PVTO
--
-- Live Oil PVT Properties (Dissolved Gas)
--
          0.0846    354.0000      1.1879      0.4096
                    738.0000      1.1789      0.4431
                   1355.0000      1.1665      0.4959
                   1950.0000      1.1562      0.5457
                   2438.0000      1.1488      0.5858
                   2820.0000      1.1435      0.6167
                   3194.0000      1.1387      0.6467
                   3438.0000      1.1357      0.6660
                   3619.0000      1.1336      0.6803
                   3718.0000      1.1325      0.6881
                   3769.0000      1.1319      0.6921
                   3800.0334      1.1316      0.6945
                   4000.0000      1.1294      0.7100
                   4089.6673      1.1284      0.7170
                   5000.0000      1.1195      0.7865
                   6000.0000      1.1109      0.8607 /
```

```
0.2132    738.0000      1.2708      0.3374
         1355.0000      1.2528      0.3891
         1950.0000      1.2384      0.4383
         2438.0000      1.2282      0.4783
         2820.0000      1.2210      0.5093
         3194.0000      1.2145      0.5395
         3438.0000      1.2106      0.5591
         3619.0000      1.2078      0.5735
         3718.0000      1.2063      0.5814
         3769.0000      1.2055      0.5855
         3800.0334      1.2051      0.5879
         4000.0000      1.2022      0.6038
         4089.6673      1.2009      0.6109
         5000.0000      1.1892      0.6823
         6000.0000      1.1782      0.7592 /
0.4385   1355.0000      1.4099      0.2501
         1950.0000      1.3859      0.2932
         2438.0000      1.3695      0.3288
         2820.0000      1.3582      0.3566
         3194.0000      1.3483      0.3840
         3438.0000      1.3423      0.4018
         3619.0000      1.3380      0.4151
         3718.0000      1.3358      0.4224
         3769.0000      1.3347      0.4261
         3800.0334      1.3340      0.4284
         4000.0000      1.3297      0.4430
         4089.6673      1.3278      0.4496
         5000.0000      1.3107      0.5163
         6000.0000      1.2950      0.5894 /
0.6806   1950.0000      1.5547      0.1900
         2438.0000      1.5287      0.2192
         2820.0000      1.5114      0.2424
         3194.0000      1.4964      0.2654
         3438.0000      1.4875      0.2805
         3619.0000      1.4813      0.2918
         3718.0000      1.4780      0.2980
         3769.0000      1.4764      0.3012
         3800.0334      1.4754      0.3031
         4000.0000      1.4692      0.3157
         4089.6673      1.4665      0.3214
         5000.0000      1.4422      0.3794
         6000.0000      1.4203      0.4441 /
0.9114   2438.0000      1.6909      0.1525
         2820.0000      1.6658      0.1714
         3194.0000      1.6445      0.1904
         3438.0000      1.6320      0.2030
         3619.0000      1.6233      0.2124
         3718.0000      1.6188      0.2176
         3769.0000      1.6165      0.2203
         3800.0334      1.6152      0.2219
         4000.0000      1.6066      0.2325
         4089.6673      1.6030      0.2373
         5000.0000      1.5702      0.2869
         6000.0000      1.5415      0.3431 /
1.1265   2820.0000      1.8181      0.1280
         3194.0000      1.7893      0.1438
         3438.0000      1.7727      0.1543
         3619.0000      1.7613      0.1623
         3718.0000      1.7553      0.1666
```

```
                3769.0000      1.7523      0.1689
                3800.0334      1.7505      0.1703
                4000.0000      1.7394      0.1793
                4089.6673      1.7347      0.1833
                5000.0000      1.6927      0.2259
                6000.0000      1.6565      0.2748 /
          1.3874   3194.0000      1.9742      0.1067
                3438.0000      1.9514      0.1152
                3619.0000      1.9360      0.1217
                3718.0000      1.9279      0.1253
                3769.0000      1.9239      0.1271
                3800.0334      1.9215      0.1283
                4000.0000      1.9067      0.1356
                4089.6673      1.9003      0.1390
                5000.0000      1.8454      0.1744
                6000.0000      1.7991      0.2159 /
          1.6038   3438.0000      2.1062      0.0936
                3619.0000      2.0867      0.0990
                3718.0000      2.0767      0.1021
                3769.0000      2.0717      0.1037
                3800.0334      2.0687      0.1046
                4000.0000      2.0502      0.1109
                4089.6673      2.0424      0.1138
                5000.0000      1.9752      0.1444
                6000.0000      1.9196      0.1808 /
          1.8053   3619.0000      2.2315      0.0838
                3718.0000      2.2194      0.0865
                3769.0000      2.2134      0.0878
                3800.0334      2.2097      0.0887
                4000.0000      2.1876      0.0942
                4089.6673      2.1782      0.0967
                5000.0000      2.0985      0.1236
                6000.0000      2.0335      0.1559 /
          1.9392   3718.0000      2.3163      0.0784
                3769.0000      2.3095      0.0796
                3800.0334      2.3054      0.0804
                4000.0000      2.2806      0.0854
                4089.6673      2.2701      0.0877
                5000.0000      2.1816      0.1125
                6000.0000      2.1100      0.1425 /
          2.0177   3769.0000      2.3665      0.0755
                3800.0334      2.3622      0.0762
                4000.0000      2.3357      0.0810
                4089.6673      2.3245      0.0832
                5000.0000      2.2306      0.1068
                6000.0000      2.1551      0.1357 /
          2.0695   3800.0334      2.3999      0.0737
                4000.0000      2.3723      0.0783
                4089.6673      2.3607      0.0804
                5000.0000      2.2632      0.1034
                6000.0000      2.1850      0.1314 /
          2.5335   4000.0000      2.7078      0.0608
                4089.6673      2.6918      0.0624
                5000.0000      2.5594      0.0803
                6000.0000      2.4560      0.1027 /
          2.9507   4089.6673      2.9986      0.0527
                5000.0000      2.8317      0.0675
                6000.0000      2.7038      0.0863 /
/
```

```
PVTG
--
-- Wet Gas PVT Properties (Vapourised Oil)
--
        354.0000     0.07256      9.9789     0.01201
                     0.06279      9.9132     0.01209
                      0.0483      9.8159     0.01216
                     0.04253      9.7771      0.0122
                     0.03894      9.7530     0.01222
                           0      9.4915     0.01246 /
        738.0000     0.04253      4.4722     0.01319
                     0.03894      4.4654     0.01321
                           0      4.3922     0.01336 /
       1355.0000     0.03894      2.3100     0.01504
                           0      2.3011     0.01489 /
       1950.0000      0.0483      1.5705      0.0172
                     0.04253      1.5708     0.01708
                     0.03894      1.5709     0.01703
                           0      1.5729     0.01655 /
       2438.0000     0.06279      1.2597     0.01924
                      0.0483      1.2597     0.01885
                     0.04253      1.2596     0.01874
                     0.03894      1.2596     0.01867
                           0      1.2593     0.01796 /
       2820.0000     0.07924      1.1076     0.02106
                     0.07256      1.1068     0.02073
                     0.06279      1.1056     0.02048
                      0.0483      1.1039     0.02012
                     0.04253      1.1032     0.01998
                     0.03894      1.1028     0.01989
                           0      1.0982     0.01903 /
       3194.0000      0.1014      1.0082     0.02324
                     0.07924      1.0027     0.02221
                     0.07256      1.0010     0.02201
                     0.06279      0.9986     0.02172
                      0.0483      0.9950     0.02131
                     0.04253      0.9935     0.02115
                     0.03894      0.9926     0.02105
                           0      0.9830     0.02006 /
       3438.0000      0.1206      0.9638     0.02511
                      0.1014      0.9574     0.02384
                     0.07924      0.9500     0.02307
                     0.07256      0.9477     0.02284
                     0.06279      0.9445     0.02253
                      0.0483      0.9396     0.02208
                     0.04253      0.9377     0.02191
                     0.03894      0.9365      0.0218
                           0      0.9234     0.02072 /
       3619.0000      0.1389      0.9406     0.02694
                      0.1206      0.9334     0.02532
                      0.1014      0.9257     0.02454
                     0.07924      0.9168     0.02371
                     0.07256      0.9142     0.02347
                     0.06279      0.9103     0.02313
                      0.0483      0.9045     0.02266
                     0.04253      0.9022     0.02247
                     0.03894      0.9007     0.02236
                           0      0.8852     0.02122 /
```

```
3718.0000       0.151      0.9317     0.02821
               0.1389      0.9264     0.02656
               0.1206      0.9185     0.02573
               0.1014      0.9101     0.02492
              0.07924      0.9005     0.02407
              0.07256      0.8976     0.02382
              0.06279      0.8934     0.02347
               0.0483      0.8871     0.02298
              0.04253      0.8846     0.02279
              0.03894      0.8830     0.02267
                    0      0.8661      0.0215 /
3769.0000      0.1582      0.9282     0.02897
                0.151      0.9250     0.02739
               0.1389      0.9195     0.02679
               0.1206      0.9112     0.02595
               0.1014      0.9025     0.02513
              0.07924      0.8925     0.02425
              0.07256      0.8895       0.024
              0.06279      0.8851     0.02365
               0.0483      0.8785     0.02315
              0.04253      0.8759     0.02295
              0.03894      0.8743     0.02283
                    0      0.8567     0.02164 /
3800.0334      0.1628      0.9265     0.02949
               0.1582      0.9244      0.0279
                0.151      0.9211     0.02753
               0.1389      0.9154     0.02693
               0.1206      0.9070     0.02608
               0.1014      0.8981     0.02525
              0.07924      0.8878     0.02437
              0.07256      0.8847     0.02411
              0.06279      0.8802     0.02376
               0.0483      0.8735     0.02325
              0.04253      0.8708     0.02305
              0.03894      0.8691     0.02294
                    0      0.8511     0.02173 /
4000.0000      0.2043      0.9272     0.03433
               0.1628      0.9048     0.02915
               0.1582      0.9023     0.02889
                0.151      0.8985      0.0285
               0.1389      0.8919     0.02786
               0.1206      0.8821     0.02696
               0.1014      0.8717     0.02607
              0.07924      0.8598     0.02513
              0.07256      0.8562     0.02486
              0.06279      0.8509     0.02448
               0.0483      0.8431     0.02394
              0.04253      0.8400     0.02374
              0.03894      0.8381     0.02361
                    0      0.8171     0.02234 /
4089.6673      0.2409      0.9426       0.039
               0.2043      0.9213     0.03215
               0.1628      0.8972      0.0296
               0.1582      0.8945     0.02933
                0.151      0.8903     0.02894
               0.1389      0.8832     0.02829
               0.1206      0.8726     0.02737
               0.1014      0.8614     0.02647
              0.07924      0.8485     0.02551
```

```
                    0.07256      0.8446     0.02524
                    0.06279      0.8389     0.02485
                     0.0483      0.8305      0.0243
                    0.04253      0.8271     0.02409
                    0.03894      0.8250     0.02396
                          0      0.8023     0.02267 /
       5000.0000     0.2409      0.8759     0.04875
                     0.2043      0.8493     0.03896
                     0.1628      0.8190     0.03522
                     0.1582      0.8156     0.03483
                      0.151      0.8104     0.03425
                     0.1389      0.8016      0.0333
                     0.1206      0.7883     0.03194
                     0.1014      0.7743     0.03061
                    0.07924      0.7581     0.02921
                    0.07256      0.7533     0.02881
                    0.06279      0.7462     0.02825
                     0.0483      0.7356     0.02746
                    0.04253      0.7314     0.02715
                    0.03894      0.7288     0.02697
                          0      0.7004     0.02514 /
       6000.0000     0.2409      0.8266     0.06149
                     0.2043      0.7966     0.04799
                     0.1628      0.7626     0.04271
                     0.1582      0.7588     0.04215
                      0.151      0.7530     0.04132
                     0.1389      0.7430     0.03996
                     0.1206      0.7280     0.03801
                     0.1014      0.7123      0.0361
                    0.07924      0.6941     0.03407
                    0.07256      0.6887     0.03349
                    0.06279      0.6806     0.03267
                     0.0483      0.6688     0.03152
                    0.04253      0.6640     0.03109
                    0.03894      0.6611     0.03082
                          0      0.6292     0.02819 /
/

ROCKOPTS                                -- Generated : Petrel
  1* 1* ROCKNUM /

ROCK                                    -- Generated : Petrel
     3618.0000     3.9E-006 /

INCLUDE                                 -- Generated : Petrel
'BO_EQUIL_20_NATURAL_DEPLETION_30_NEWPVT_PROP_PROPS.GRDECL' /

FILLEPS                                 -- Generated : Petrel

SWOF
         0.135            0           1       1.1322
        0.1626            0      0.9526      0.58694
        0.1903            0      0.9004      0.33674
        0.2179       0.0001      0.8073      0.20871
        0.2455       0.0003      0.7188      0.13696
        0.2732       0.0008      0.6348      0.09389
        0.3008       0.0017      0.5556     0.066833
        0.3284       0.0031       0.481     0.049016
        0.3561       0.0052      0.4113     0.036823
```

```
        0.3837       0.0084       0.3464     0.028289
        0.4113       0.0128       0.2866     0.022134
        0.4389       0.0188       0.2108     0.017597
        0.4666       0.0266       0.1657     0.014176
        0.4942       0.0366       0.1256     0.011572
        0.5218       0.0492       0.0904     0.009551
        0.5495       0.0649       0.0605    0.0079562
        0.5771        0.084       0.0361    0.0066916
        0.6047        0.107       0.0174    0.0056738
        0.6324       0.1345        0.005    0.0048436
          0.66        0.167    0.0046246    0.0041653
             1            1            0      0.00096
  /

SGOF
             0            0            1            0
         0.022            0      0.70809            0
         0.044            0      0.54497            0
         0.065            0      0.43389            0
         0.087            0      0.35264            0
         0.109            0      0.29058            0
         0.131            0      0.24178            0
         0.152            0      0.20258            0
         0.174            0      0.17059            0
         0.196            0      0.14416            0
         0.218            0      0.12211            0
         0.239            0      0.10357            0
         0.261            0       0.0879            0
         0.283            0      0.07459            0
         0.305            0      0.06323            0
         0.326            0      0.05353            0
         0.348            0      0.04522            0
          0.37       0.0099      0.03809            0
         0.392       0.0179      0.03198            0
         0.413       0.0414      0.02674            0
         0.435       0.0569      0.02225            0
         0.457       0.0953      0.01841            0
         0.479        0.139      0.01514            0
           0.5       0.1815      0.01235            0
         0.522        0.229         0.01            0
         0.544         0.29      0.00801            0
         0.566       0.3396      0.00634            0
         0.587       0.3878      0.00495            0
         0.609       0.4405      0.00381            0
         0.631         0.51      0.00287            0
         0.653       0.5587      0.00212            0
         0.674       0.6231      0.00152            0
         0.696        0.679      0.00105            0
         0.718         0.72       0.0007            0
          0.74         0.77      0.00044            0
         0.761         0.81      0.00025            0
         0.783       0.8509      0.00013            0
         0.805       0.8991       6E-005            0
         0.827        0.939       2E-005            0
         0.848       0.9696            0            0
         0.865            1            0            0
  /
```

```
FIELDSEP                                -- Generated : Petrel
  1 80.0000000000001 320 /
  2 60.0000000000001 14.7 /
  /

FIPSEP                                  -- Generated : Petrel
  1 1 80.0000000000001 320 /
  1 2 60.0000000000001 14.7 /
  2 1 80.0000000000001 320 /
  2 2 60.0000000000001 14.7 /
  /

EQUIL                                   -- Generated : Petrel
        8591.5         3803       8591.5            0       8591.5
0 0 0 20 1 /

RPTRST                                  -- Generated : Petrel
  BASIC=3 FLORES FLOC FREQ=2 RS RV SGAS SOIL SWAT VGAS VOIL BG BO /

RPTSOL                                  -- Generated : Petrel
  FIP=2 /


EOS                                     -- Generated : Petrel
  PR /

PRCORR                                  -- Generated : Petrel

CNAMES                                  -- Generated : Petrel
  N2 CO2 C1 C2 C3 IC4 NC4 IC5 NC5 C6 C7+ /

TCRIT                                   -- Generated : Petrel
  227.16 548.46 343.08 549.77 665.64 734.58 765.36 828.72 845.28 913.50
1119.02 /

PCRIT                                   -- Generated : Petrel
  492.3126 1071.3311 667.7817 708.3424 615.7582 529.0524 550.6554
491.5779 488.7856 436.6152 420.3029 /

VCRIT                                   -- Generated : Petrel
  1.44166 1.50574 1.56981 2.37073 3.20369 4.21285 4.08471 4.93369 4.98174
5.62248 7.64924 /

ZCRIT                                   -- Generated : Petrel
  0.29115 0.27408 0.28473 0.28463 0.27616 0.28274 0.27386 0.27271 0.26844
0.25042 0.26772 /

VCRITVIS                                -- Generated : Petrel
  1.44166 1.50574 1.56981 2.37073 3.20369 4.21285 4.08471 4.93369 4.98174
5.62248 7.64924 /

ZCRITVIS                                -- Generated : Petrel
  0.29115 0.27408 0.28473 0.28463 0.27616 0.28274 0.27386 0.27271 0.26844
0.25042 0.26772 /

MW                                      -- Generated : Petrel
```

```
  28.01 44.01 16.04 30.07 44.10 58.12 58.12 72.15 72.15 84.00 130.60 /

ACF                                     -- Generated : Petrel
  0.04 0.225 0.013 0.0986 0.1524 0.1848 0.201 0.227 0.251 0.299
0.3935010577 /

OMEGAA                                  -- Generated : Petrel
  10*0.457236 0.353321 /

OMEGAB                                  -- Generated : Petrel
  10*0.077796 0.064219 /

SSHIFT                                  -- Generated : Petrel
  -0.190672298124672 0.0256437075682212 -0.169406998828849 -
0.125557121062116 -0.0927986360349883 0.134135690827561
  0.0542137804420174 -0.00893350376060605 -0.00884858850406579 -
0.0164578564898799 -0.43512721823972 /

BIC                                     -- Generated : Petrel
  47*0.0 0.186 7*0.0 /

PARACHOR                                -- Generated : Petrel
  41 78 77 108 150.3 181.5 189.9 225 231.5 271 384.49064 /

TEMPVD                                  -- Generated : Petrel
  8591.54 242.01
  /

ZMFVD                                   -- Generated : Petrel
  8591.54
  0.0063 0.0331 0.6281 0.0959 0.0686 0.0117 0.0311 0.011 0.015 0.0171
0.0821
  /

PVTW                                    -- Generated : Petrel
        1692.2        1.036  3.0902E-006        0.272  5.0297E-006 /

DENSITY                                 -- Generated : Petrel
  1*       72.345 /

ROCKOPTS                                -- Generated : Petrel
  1* 1* ROCKNUM /

ROCK                                    -- Generated : Petrel
     3618.0000     3.9E-006 /

INCLUDE                                 -- Generated : Petrel
'COMP_EQUIL_20_NATURAL_DEPLETION_30_PROP_PROPS.GRDECL' /

FILLEPS                                 -- Generated : Petrel

SWOF                                    -- Generated : Petrel
         0.135            0          0.9       1.1322
        0.1627  1.5949E-007       0.8573      0.58694
        0.1904  3.3671E-006       0.8104      0.33674
        0.2181  2.0047E-005       0.7266      0.20871
        0.2445  6.7501E-005       0.6469      0.13696
        0.2731   0.00018717       0.5713      0.09389
        0.3008   0.00041843          0.5     0.066833
```

```
        0.3285   0.00082585       0.4329     0.049016
        0.3562     0.001488       0.3702     0.036823
        0.3835    0.0024817       0.3118     0.028289
        0.4112    0.0039513       0.2579     0.022134
        0.4389    0.0060175       0.1897     0.017597
        0.4666    0.0088336       0.1491     0.014176
        0.4943     0.012574        0.113     0.011572
        0.5216     0.017349       0.0814     0.009551
        0.5497     0.023634       0.0545    0.0079562
         0.577     0.031279       0.0325    0.0066916
        0.6047     0.040872       0.0157    0.0056738
        0.6324     0.052595       0.0045    0.0048436
        0.6601     0.066761            0    0.0041653
        0.7004     0.092402            0    0.0037852
        0.7506      0.13437            0    0.0033118
           0.8      0.18865            0     0.002846
        0.8502      0.25988            0    0.0023726
        0.9004      0.35031            0    0.0018992
        0.9498      0.46117            0    0.0014334
             1          0.6            0      0.00096
  /

SGOF                                        -- Generated : Petrel
             0            0       0.9997            0
         0.022            0       0.7081            0
         0.044            0        0.545            0
         0.065            0       0.4339            0
         0.087            0       0.3526            0
         0.109            0       0.2906            0
         0.131            0       0.2418            0
         0.152            0       0.2026            0
         0.174            0       0.1706            0
         0.196            0       0.1442            0
         0.218            0       0.1221            0
         0.239            0       0.1036            0
         0.261            0       0.0879            0
         0.283            0       0.0746            0
         0.305            0       0.0632            0
         0.326            0       0.0535            0
         0.348            0       0.0452            0
          0.37            0       0.0381            0
         0.392            0        0.032            0
         0.413       0.0214       0.0267            0
         0.435       0.0569       0.0223            0
         0.457       0.0953       0.0184            0
         0.479        0.139       0.0151            0
           0.5       0.1815       0.0124            0
         0.522        0.229         0.01            0
         0.544         0.29        0.008            0
         0.566       0.3396       0.0063            0
         0.587       0.3878        0.005            0
         0.609       0.4405       0.0038            0
         0.631         0.51       0.0029            0
         0.653       0.5587       0.0021            0
         0.674       0.6231       0.0015            0
         0.696        0.679       0.0011            0
         0.718         0.72       0.0007            0
          0.74         0.77       0.0004            0
         0.761         0.81       0.0003            0
```

```
         0.783       0.8509       0.0001            0
         0.805       0.8991       0.0001            0
         0.827        0.939            0            0
         0.848       0.9696            0            0
         0.865            1            0            0
  /
```

Natural Depletion simulation production and injection schedule (Eclipse SCHEDULE section) for both MBO and Compositional models

```
RPTSCHED                                  -- Generated : Petrel
'FIP=3' 'WELLS=5' 'RESTART=2' 'SUMMARY=2'/

WELSPECS                                  -- Generated : Petrel
--'EBK_H1_M' is the simulation well name used to describe flow from
'EBK_H1_M'
--
  EBK_H1_M EBK 108 59 1* GAS /
  /

WLIST                                     -- Generated : Petrel
  '*WELLS F' NEW
  EBK_H1_M /
  /

COMPDAT                                   -- Generated : Petrel
  EBK_H1_M 108 59 6 6 OPEN 1* 7.1526E+000 0.62500 13936.64 10.00 1* Z
13.95 /
  EBK_H1_M 108 59 5 5 OPEN 1* 3.5135E-001 0.62500 684.63 10.00 1* Z 13.96
/
  EBK_H1_M 109 59 5 5 OPEN 1* 2.5017E+000 0.62500 4883.76 10.00 1* X
14.32 /
  EBK_H1_M 110 59 5 5 OPEN 1* 2.2913E+000 0.62500 4480.73 10.00 1* X
14.67 /
  EBK_H1_M 111 59 5 5 OPEN 1* 1.8894E+000 0.62500 3686.68 10.00 1* X
14.23 /
  EBK_H1_M 111 59 6 6 OPEN 1* 2.9767E+000 0.62500 5808.05 10.00 1* X
14.22 /
  EBK_H1_M 112 59 6 6 OPEN 1* 3.5180E+000 0.62500 6848.26 10.00 1* Z
13.77 /
  EBK_H1_M 112 60 6 6 OPEN 1* 1.1548E+000 0.62500 2248.97 10.00 1* Z
13.86 /
  EBK_H1_M 112 60 7 7 OPEN 1* 2.7950E+000 0.62500 5442.91 10.00 1* Z
13.85 /
  EBK_H1_M 113 60 7 7 OPEN 1* 1.3529E+000 0.62500 2634.11 10.00 1* Z
13.81 /
  EBK_H1_M 113 60 8 8 OPEN 1* 1.0883E+000 0.62500 2118.86 10.00 1* Z
13.80 /
  EBK_H1_M 113 60 9 9 OPEN 1* 1.6391E-001 0.62500 319.11 10.00 1* Z 13.79
/
  EBK_H1_M 114 60 9 9 OPEN 1* 2.0901E+000 0.62500 4068.64 10.00 1* Z
13.77 /
  EBK_H1_M 114 60 10 10 OPEN 1* 9.6921E-001 0.62500 1886.62 10.00 1* Z
13.76 /
  EBK_H1_M 115 60 10 10 OPEN 1* 4.6690E+000 0.62500 9086.34 10.00 1* X
13.72 /
  EBK_H1_M 116 60 10 10 OPEN 1* 3.5695E+000 0.62500 6944.17 10.00 1* X
13.65 /
```

```
  EBK_H1_M 117 60 10 10 OPEN 1* 2.9158E+000 0.62500 5670.39 10.00 1* X
13.59 /
  EBK_H1_M 117 60 9 9 OPEN 1* 2.2551E-001 0.62500 438.58 10.00 1* X 13.60
/
  EBK_H1_M 118 60 9 9 OPEN 1* 2.5111E+000 0.62500 4882.75 10.00 1* X
13.56 /
  EBK_H1_M 119 60 9 9 OPEN 1* 5.4735E-001 0.62500 1064.30 10.00 1* X
13.56 /
  EBK_H1_M 119 60 8 8 OPEN 1* 2.0904E+000 0.62500 4064.87 10.00 1* X
13.57 /
  EBK_H1_M 120 60 8 8 OPEN 1* 2.1907E+000 0.62500 4260.76 10.00 1* X
13.61 /
  EBK_H1_M 121 60 8 8 OPEN 1* 7.1270E-002 0.62500 138.65 10.00 1* X 13.65
/
  EBK_H1_M 121 60 7 7 OPEN 1* 3.2068E+000 0.62500 6238.71 10.00 1* X
13.66 /
  EBK_H1_M 122 60 7 7 OPEN 1* 7.5751E-001 0.62500 1473.74 10.00 1* X
13.66 /
  EBK_H1_M 122 60 6 6 OPEN 1* 1.9226E+000 0.62500 3740.56 10.00 1* X
13.67 /
  EBK_H1_M 123 60 6 6 OPEN 1* 2.9672E+000 0.62500 5771.78 10.00 1* X
13.63 /
  EBK_H1_M 124 60 6 6 OPEN 1* 5.9616E-001 0.62500 1159.18 10.00 1* X
13.56 /
  EBK_H1_M 124 60 5 5 OPEN 1* 1.4901E+000 0.62500 2897.54 10.00 1* X
13.57 /
  EBK_H1_M 124 59 5 5 OPEN 1* 2.9082E+000 0.62500 5667.21 10.00 1* X
13.98 /
  EBK_H1_M 125 59 5 5 OPEN 1* 1.0960E+000 0.62500 2132.89 10.00 1* X
13.72 /
  EBK_H1_M 125 59 4 4 OPEN 1* 4.6900E+000 0.62500 9127.20 10.00 1* X
13.72 /
  EBK_H1_M 126 59 4 4 OPEN 1* 2.9371E+000 0.62500 5715.51 10.00 1* X
13.71 /
  EBK_H1_M 126 59 3 3 OPEN 1* 4.8916E+000 0.62500 9518.86 10.00 1* X
13.71 /
  EBK_H1_M 127 59 3 3 OPEN 1* 7.9965E+000 0.62500 15561.14 10.00 1* X
13.71 /
  EBK_H1_M 128 59 3 3 OPEN 1* 3.2996E+000 0.62500 6420.93 10.00 1* X
13.71 /
  /

GRUPTREE                                -- Generated : Petrel
  GROUP1 FIELD /
  EBK FIELD /
  /

WCONPROD
  EBK_H1_M 1* GRUP 1* 1* 30000.00 1* 1* 580.1510 319.0830 1 /
  /

GCONPROD                                -- Generated : Petrel
  FIELD GRAT 1* 1* 30000.00 6* RATE /
  /

GEFAC                                   -- Generated : Petrel
  EBK 0.9500 YES /
  /
```

```
WECON
 EBK_H1_M 1* 1000  /
/

WPIMULT                                  -- Generated : Petrel
  EBK_H1_M 1.00E+000 108 59 6 /
  EBK_H1_M 1.00E+000 108 59 5 /
  EBK_H1_M 1.00E+000 109 59 5 /
  EBK_H1_M 1.00E+000 110 59 5 /
  EBK_H1_M 1.00E+000 111 59 5 /
  EBK_H1_M 1.00E+000 111 59 6 /
  EBK_H1_M 1.00E+000 112 59 6 /
  EBK_H1_M 1.00E+000 112 60 6 /
  EBK_H1_M 1.00E+000 112 60 7 /
  EBK_H1_M 1.00E+000 113 60 7 /
  EBK_H1_M 1.00E+000 113 60 8 /
  EBK_H1_M 1.00E+000 113 60 9 /
  EBK_H1_M 1.00E+000 114 60 9 /
  EBK_H1_M 1.00E+000 114 60 10 /
  EBK_H1_M 1.00E+000 115 60 10 /
  EBK_H1_M 1.00E+000 116 60 10 /
  EBK_H1_M 1.00E+000 117 60 10 /
  EBK_H1_M 1.00E+000 117 60 9 /
  EBK_H1_M 1.00E+000 118 60 9 /
  EBK_H1_M 1.00E+000 119 60 9 /
  EBK_H1_M 1.00E+000 119 60 8 /
  EBK_H1_M 1.00E+000 120 60 8 /
  EBK_H1_M 1.00E+000 121 60 8 /
  EBK_H1_M 1.00E+000 121 60 7 /
  EBK_H1_M 1.00E+000 122 60 7 /
  EBK_H1_M 1.00E+000 122 60 6 /
  EBK_H1_M 1.00E+000 123 60 6 /
  EBK_H1_M 1.00E+000 124 60 6 /
  EBK_H1_M 1.00E+000 124 60 5 /
  EBK_H1_M 1.00E+000 124 59 5 /
  EBK_H1_M 1.00E+000 125 59 5 /
  EBK_H1_M 1.00E+000 125 59 4 /
  EBK_H1_M 1.00E+000 126 59 4 /
  EBK_H1_M 1.00E+000 126 59 3 /
  EBK_H1_M 1.00E+000 127 59 3 /
  EBK_H1_M 1.00E+000 128 59 3 /
  /

WDFAC                                    -- Generated : Petrel
EBK_H1_M 2.0E-4 /
/

TUNING                                   -- Generated : Petrel
/
/
2* 100/

VFPCHK                                   -- Generated : Petrel
 0.1000000E+11 /

DATES                                    -- Generated : Petrel
  1 FEB 2016 /
--One measurement every month/
```

```
DATES                                    -- Generated : Petrel
  1 JAN 2026 /
  /
```

Gas Cycling below the Dp simulation production and injection schedule (Eclipse SCHEDULE section) for both MBO and Compositional models

```
RPTSCHED                                 -- Generated : Petrel
'FIP=3' 'WELLS=5' 'RESTART=2' 'SUMMARY=2'/

WELSPECS                                 -- Generated : Petrel
--'EBK_H1_M' is the simulation well name used to describe flow from
'EBK_H1_M'
--'EBK_VGI' is the simulation well name used to describe flow from
'EBK_VGI'
--
  EBK_H1_M EBK 108 59 1* GAS /
  EBK_VGI EBK 134 57 8463.25 GAS /
  /

WELTARG
EBK_VGI BHP 3600 /
/

WLIST                                    -- Generated : Petrel
  '*WELLS F' NEW
  EBK_H1_M EBK_VGI /
  /

COMPDAT                                  -- Generated : Petrel
  EBK_H1_M 108 59 6 6 OPEN 1* 7.1526E+000 0.62500 13936.64 10.00 1* Z
13.95 /
  EBK_H1_M 108 59 5 5 OPEN 1* 3.5135E-001 0.62500 684.63 10.00 1* Z 13.96
/
  EBK_H1_M 109 59 5 5 OPEN 1* 2.5017E+000 0.62500 4883.76 10.00 1* X
14.32 /
  EBK_H1_M 110 59 5 5 OPEN 1* 2.2913E+000 0.62500 4480.73 10.00 1* X
14.67 /
  EBK_H1_M 111 59 5 5 OPEN 1* 1.8894E+000 0.62500 3686.68 10.00 1* X
14.23 /
  EBK_H1_M 111 59 6 6 OPEN 1* 2.9767E+000 0.62500 5808.05 10.00 1* X
14.22 /
  EBK_H1_M 112 59 6 6 OPEN 1* 3.5180E+000 0.62500 6848.26 10.00 1* Z
13.77 /
  EBK_H1_M 112 60 6 6 OPEN 1* 1.1548E+000 0.62500 2248.97 10.00 1* Z
13.86 /
  EBK_H1_M 112 60 7 7 OPEN 1* 2.7950E+000 0.62500 5442.91 10.00 1* Z
13.85 /
  EBK_H1_M 113 60 7 7 OPEN 1* 1.3529E+000 0.62500 2634.11 10.00 1* Z
13.81 /
  EBK_H1_M 113 60 8 8 OPEN 1* 1.0883E+000 0.62500 2118.86 10.00 1* Z
13.80 /
  EBK_H1_M 113 60 9 9 OPEN 1* 1.6391E-001 0.62500 319.11 10.00 1* Z 13.79
/
  EBK_H1_M 114 60 9 9 OPEN 1* 2.0901E+000 0.62500 4068.64 10.00 1* Z
13.77 /
  EBK_H1_M 114 60 10 10 OPEN 1* 9.6921E-001 0.62500 1886.62 10.00 1* Z
13.76 /
```

```
  EBK_H1_M 115 60 10 10 OPEN 1* 4.6690E+000 0.62500 9086.34 10.00 1* X
13.72 /
  EBK_H1_M 116 60 10 10 OPEN 1* 3.5695E+000 0.62500 6944.17 10.00 1* X
13.65 /
  EBK_H1_M 117 60 10 10 OPEN 1* 2.9158E+000 0.62500 5670.39 10.00 1* X
13.59 /
  EBK_H1_M 117 60 9 9 OPEN 1* 2.2551E-001 0.62500 438.58 10.00 1* X 13.60
/
  EBK_H1_M 118 60 9 9 OPEN 1* 2.5111E+000 0.62500 4882.75 10.00 1* X
13.56 /
  EBK_H1_M 119 60 9 9 OPEN 1* 5.4735E-001 0.62500 1064.30 10.00 1* X
13.56 /
  EBK_H1_M 119 60 8 8 OPEN 1* 2.0904E+000 0.62500 4064.87 10.00 1* X
13.57 /
  EBK_H1_M 120 60 8 8 OPEN 1* 2.1907E+000 0.62500 4260.76 10.00 1* X
13.61 /
  EBK_H1_M 121 60 8 8 OPEN 1* 7.1270E-002 0.62500 138.65 10.00 1* X 13.65
/
  EBK_H1_M 121 60 7 7 OPEN 1* 3.2068E+000 0.62500 6238.71 10.00 1* X
13.66 /
  EBK_H1_M 122 60 7 7 OPEN 1* 7.5751E-001 0.62500 1473.74 10.00 1* X
13.66 /
  EBK_H1_M 122 60 6 6 OPEN 1* 1.9226E+000 0.62500 3740.56 10.00 1* X
13.67 /
  EBK_H1_M 123 60 6 6 OPEN 1* 2.9672E+000 0.62500 5771.78 10.00 1* X
13.63 /
  EBK_H1_M 124 60 6 6 OPEN 1* 5.9616E-001 0.62500 1159.18 10.00 1* X
13.56 /
  EBK_H1_M 124 60 5 5 OPEN 1* 1.4901E+000 0.62500 2897.54 10.00 1* X
13.57 /
  EBK_H1_M 124 59 5 5 OPEN 1* 2.9082E+000 0.62500 5667.21 10.00 1* X
13.98 /
  EBK_H1_M 125 59 5 5 OPEN 1* 1.0960E+000 0.62500 2132.89 10.00 1* X
13.72 /
  EBK_H1_M 125 59 4 4 OPEN 1* 4.6900E+000 0.62500 9127.20 10.00 1* X
13.72 /
  EBK_H1_M 126 59 4 4 OPEN 1* 2.9371E+000 0.62500 5715.51 10.00 1* X
13.71 /
  EBK_H1_M 126 59 3 3 OPEN 1* 4.8916E+000 0.62500 9518.86 10.00 1* X
13.71 /
  EBK_H1_M 127 59 3 3 OPEN 1* 7.9965E+000 0.62500 15561.14 10.00 1* X
13.71 /
  EBK_H1_M 128 59 3 3 OPEN 1* 3.2996E+000 0.62500 6420.93 10.00 1* X
13.71 /
  EBK_VGI 134 57 1 1 OPEN 1* 1.6427E-001 0.62500 158.64 2.00 1* Z 39.50 /
  EBK_VGI 134 57 2 2 OPEN 1* 3.2270E-001 0.62500 311.61 2.00 1* Z 39.46 /
  EBK_VGI 134 57 3 3 OPEN 1* 6.6388E-001 0.62500 640.95 2.00 1* Z 39.42 /
  EBK_VGI 134 57 4 4 OPEN 1* 4.3177E-001 0.62500 416.80 2.00 1* Z 39.37 /
  EBK_VGI 134 57 5 5 OPEN 1* 1.6956E-001 0.62500 163.65 2.00 1* Z 39.33 /
  EBK_VGI 134 57 6 6 OPEN 1* 1.3331E-001 0.62500 128.64 2.00 1* Z 39.29 /
  EBK_VGI 134 57 7 7 OPEN 1* 4.5240E-001 0.62500 436.50 2.00 1* Z 39.25 /
  EBK_VGI 134 57 8 8 OPEN 1* 2.0936E-001 0.62500 201.97 2.00 1* Z 39.21 /
  EBK_VGI 134 57 9 9 OPEN 1* 1.4159E-001 0.62500 136.57 2.00 1* Z 39.16 /
  EBK_VGI 134 57 10 10 OPEN 1* 1.5944E-001 0.62500 153.76 2.00 1* Z 39.12
/
  EBK_VGI 134 57 11 11 OPEN 1* 2.4837E-001 0.62500 239.49 2.00 1* Z 39.08
/
  EBK_VGI 134 57 12 12 OPEN 1* 3.2085E-001 0.62500 309.33 2.00 1* Z 39.04
/
```

```
  EBK_VGI 134 57 13 13 OPEN 1* 1.4740E-001 0.62500 142.08 2.00 1* Z 39.00
/
  EBK_VGI 134 57 14 14 OPEN 1* 1.9802E-001 0.62500 190.85 2.00 1* Z 38.95
/
  EBK_VGI 134 57 15 15 OPEN 1* 2.3520E-001 0.62500 226.65 2.00 1* Z 38.91
/
  EBK_VGI 134 57 16 16 OPEN 1* 3.7081E-001 0.62500 357.28 2.00 1* Z 38.87
/
  EBK_VGI 134 57 17 17 OPEN 1* 2.7575E-001 0.62500 265.64 2.00 1* Z 38.83
/
  /

GRUPTREE                                -- Generated : Petrel
  'GROUP 1' FIELD /
  EBK FIELD /
  /

WCONPROD
  EBK_H1_M 1* GRUP 1* 1* 30000.00 1* 1* 580.1510 319.0830 1 /
  /

GCONPROD                                -- Generated : Petrel
  EBK GRAT 1* 1* 50000.00 6* RATE /
  /

GEFAC                                   -- Generated : Petrel
  EBK 0.9500 YES /
  /

GCONINJE                                -- Generated : Petrel
  EBK GAS VREP 1* 1* 1* 1.0000 /
  /

WCONINJE
  EBK_VGI GAS 1* GRUP 1* 1* 3800 1* 1 /
  /

WPIMULT                                 -- Generated : Petrel
  EBK_H1_M 1.00E+000 108 59 6 /
  EBK_H1_M 1.00E+000 108 59 5 /
  EBK_H1_M 1.00E+000 109 59 5 /
  EBK_H1_M 1.00E+000 110 59 5 /
  EBK_H1_M 1.00E+000 111 59 5 /
  EBK_H1_M 1.00E+000 111 59 6 /
  EBK_H1_M 1.00E+000 112 59 6 /
  EBK_H1_M 1.00E+000 112 60 6 /
  EBK_H1_M 1.00E+000 112 60 7 /
  EBK_H1_M 1.00E+000 113 60 7 /
  EBK_H1_M 1.00E+000 113 60 8 /
  EBK_H1_M 1.00E+000 113 60 9 /
  EBK_H1_M 1.00E+000 114 60 9 /
  EBK_H1_M 1.00E+000 114 60 10 /
  EBK_H1_M 1.00E+000 115 60 10 /
  EBK_H1_M 1.00E+000 116 60 10 /
  EBK_H1_M 1.00E+000 117 60 10 /
  EBK_H1_M 1.00E+000 117 60 9 /
  EBK_H1_M 1.00E+000 118 60 9 /
  EBK_H1_M 1.00E+000 119 60 9 /
  EBK_H1_M 1.00E+000 119 60 8 /
```

```
  EBK_H1_M 1.00E+000 120 60 8 /
  EBK_H1_M 1.00E+000 121 60 8 /
  EBK_H1_M 1.00E+000 121 60 7 /
  EBK_H1_M 1.00E+000 122 60 7 /
  EBK_H1_M 1.00E+000 122 60 6 /
  EBK_H1_M 1.00E+000 123 60 6 /
  EBK_H1_M 1.00E+000 124 60 6 /
  EBK_H1_M 1.00E+000 124 60 5 /
  EBK_H1_M 1.00E+000 124 59 5 /
  EBK_H1_M 1.00E+000 125 59 5 /
  EBK_H1_M 1.00E+000 125 59 4 /
  EBK_H1_M 1.00E+000 126 59 4 /
  EBK_H1_M 1.00E+000 126 59 3 /
  EBK_H1_M 1.00E+000 127 59 3 /
  EBK_H1_M 1.00E+000 128 59 3 /
  /

WDFAC                                   -- Generated : Petrel
EBK_H1_M 2.0E-4 /
EBK_VGI 2.0E-4 /
/

TUNING                                  -- Generated : Petrel
/
/
2* 100/

VFPCHK                                  -- Generated : Petrel
 0.1000000E+11 /

DATES                                   -- Generated : Petrel
  1 FEB 2016 /
--One measurement every month/

DATES                                   -- Generated : Petrel
  1 JAN 2026 /
  /
```


Gas Cycling above the Dp simulation production and injection schedule (Eclipse SCHEDULE section) for both MBO and Compositional models

```
RPTSCHED                                -- Generated : Petrel
'FIP=3' 'WELLS=5' 'RESTART=2' 'SUMMARY=2'/

WELSPECS                                -- Generated : Petrel
--'EBK_H1_M' is the simulation well name used to describe flow from
'EBK_H1_M'
--'EBK_VGI' is the simulation well name used to describe flow from
'EBK_VGI'
--
  EBK_H1_M EBK 108 59 1* GAS /
  EBK_VGI EBK 134 57 8463.25 GAS /
  /

WLIST                                   -- Generated : Petrel
  '*WELLS F' NEW
  EBK_H1_M EBK_VGI /
  /
```

```
COMPDAT                                    -- Generated : Petrel
  EBK_H1_M 108 59 6 6 OPEN 1* 7.1526E+000 0.62500 13936.64 10.00 1* Z
13.95 /
  EBK_H1_M 108 59 5 5 OPEN 1* 3.5135E-001 0.62500 684.63 10.00 1* Z 13.96
/
  EBK_H1_M 109 59 5 5 OPEN 1* 2.5017E+000 0.62500 4883.76 10.00 1* X
14.32 /
  EBK_H1_M 110 59 5 5 OPEN 1* 2.2913E+000 0.62500 4480.73 10.00 1* X
14.67 /
  EBK_H1_M 111 59 5 5 OPEN 1* 1.8894E+000 0.62500 3686.68 10.00 1* X
14.23 /
  EBK_H1_M 111 59 6 6 OPEN 1* 2.9767E+000 0.62500 5808.05 10.00 1* X
14.22 /
  EBK_H1_M 112 59 6 6 OPEN 1* 3.5180E+000 0.62500 6848.26 10.00 1* Z
13.77 /
  EBK_H1_M 112 60 6 6 OPEN 1* 1.1548E+000 0.62500 2248.97 10.00 1* Z
13.86 /
  EBK_H1_M 112 60 7 7 OPEN 1* 2.7950E+000 0.62500 5442.91 10.00 1* Z
13.85 /
  EBK_H1_M 113 60 7 7 OPEN 1* 1.3529E+000 0.62500 2634.11 10.00 1* Z
13.81 /
  EBK_H1_M 113 60 8 8 OPEN 1* 1.0883E+000 0.62500 2118.86 10.00 1* Z
13.80 /
  EBK_H1_M 113 60 9 9 OPEN 1* 1.6391E-001 0.62500 319.11 10.00 1* Z 13.79
/
  EBK_H1_M 114 60 9 9 OPEN 1* 2.0901E+000 0.62500 4068.64 10.00 1* Z
13.77 /
  EBK_H1_M 114 60 10 10 OPEN 1* 9.6921E-001 0.62500 1886.62 10.00 1* Z
13.76 /
  EBK_H1_M 115 60 10 10 OPEN 1* 4.6690E+000 0.62500 9086.34 10.00 1* X
13.72 /
  EBK_H1_M 116 60 10 10 OPEN 1* 3.5695E+000 0.62500 6944.17 10.00 1* X
13.65 /
  EBK_H1_M 117 60 10 10 OPEN 1* 2.9158E+000 0.62500 5670.39 10.00 1* X
13.59 /
  EBK_H1_M 117 60 9 9 OPEN 1* 2.2551E-001 0.62500 438.58 10.00 1* X 13.60
/
  EBK_H1_M 118 60 9 9 OPEN 1* 2.5111E+000 0.62500 4882.75 10.00 1* X
13.56 /
  EBK_H1_M 119 60 9 9 OPEN 1* 5.4735E-001 0.62500 1064.30 10.00 1* X
13.56 /
  EBK_H1_M 119 60 8 8 OPEN 1* 2.0904E+000 0.62500 4064.87 10.00 1* X
13.57 /
  EBK_H1_M 120 60 8 8 OPEN 1* 2.1907E+000 0.62500 4260.76 10.00 1* X
13.61 /
  EBK_H1_M 121 60 8 8 OPEN 1* 7.1270E-002 0.62500 138.65 10.00 1* X 13.65
/
  EBK_H1_M 121 60 7 7 OPEN 1* 3.2068E+000 0.62500 6238.71 10.00 1* X
13.66 /
  EBK_H1_M 122 60 7 7 OPEN 1* 7.5751E-001 0.62500 1473.74 10.00 1* X
13.66 /
  EBK_H1_M 122 60 6 6 OPEN 1* 1.9226E+000 0.62500 3740.56 10.00 1* X
13.67 /
  EBK_H1_M 123 60 6 6 OPEN 1* 2.9672E+000 0.62500 5771.78 10.00 1* X
13.63 /
  EBK_H1_M 124 60 6 6 OPEN 1* 5.9616E-001 0.62500 1159.18 10.00 1* X
13.56 /
```

```
  EBK_H1_M 124 60 5 5 OPEN 1* 1.4901E+000 0.62500 2897.54 10.00 1* X
13.57 /
  EBK_H1_M 124 59 5 5 OPEN 1* 2.9082E+000 0.62500 5667.21 10.00 1* X
13.98 /
  EBK_H1_M 125 59 5 5 OPEN 1* 1.0960E+000 0.62500 2132.89 10.00 1* X
13.72 /
  EBK_H1_M 125 59 4 4 OPEN 1* 4.6900E+000 0.62500 9127.20 10.00 1* X
13.72 /
  EBK_H1_M 126 59 4 4 OPEN 1* 2.9371E+000 0.62500 5715.51 10.00 1* X
13.71 /
  EBK_H1_M 126 59 3 3 OPEN 1* 4.8916E+000 0.62500 9518.86 10.00 1* X
13.71 /
  EBK_H1_M 127 59 3 3 OPEN 1* 7.9965E+000 0.62500 15561.14 10.00 1* X
13.71 /
  EBK_H1_M 128 59 3 3 OPEN 1* 3.2996E+000 0.62500 6420.93 10.00 1* X
13.71 /
  EBK_VGI 134 57 1 1 OPEN 1* 1.6427E-001 0.62500 158.64 2.00 1* Z 39.50 /
  EBK_VGI 134 57 2 2 OPEN 1* 3.2270E-001 0.62500 311.61 2.00 1* Z 39.46 /
  EBK_VGI 134 57 3 3 OPEN 1* 6.6388E-001 0.62500 640.95 2.00 1* Z 39.42 /
  EBK_VGI 134 57 4 4 OPEN 1* 4.3177E-001 0.62500 416.80 2.00 1* Z 39.37 /
  EBK_VGI 134 57 5 5 OPEN 1* 1.6956E-001 0.62500 163.65 2.00 1* Z 39.33 /
  EBK_VGI 134 57 6 6 OPEN 1* 1.3331E-001 0.62500 128.64 2.00 1* Z 39.29 /
  EBK_VGI 134 57 7 7 OPEN 1* 4.5240E-001 0.62500 436.50 2.00 1* Z 39.25 /
  EBK_VGI 134 57 8 8 OPEN 1* 2.0936E-001 0.62500 201.97 2.00 1* Z 39.21 /
  EBK_VGI 134 57 9 9 OPEN 1* 1.4159E-001 0.62500 136.57 2.00 1* Z 39.16 /
  EBK_VGI 134 57 10 10 OPEN 1* 1.5944E-001 0.62500 153.76 2.00 1* Z 39.12
/
  EBK_VGI 134 57 11 11 OPEN 1* 2.4837E-001 0.62500 239.49 2.00 1* Z 39.08
/
  EBK_VGI 134 57 12 12 OPEN 1* 3.2085E-001 0.62500 309.33 2.00 1* Z 39.04
/
  EBK_VGI 134 57 13 13 OPEN 1* 1.4740E-001 0.62500 142.08 2.00 1* Z 39.00
/
  EBK_VGI 134 57 14 14 OPEN 1* 1.9802E-001 0.62500 190.85 2.00 1* Z 38.95
/
  EBK_VGI 134 57 15 15 OPEN 1* 2.3520E-001 0.62500 226.65 2.00 1* Z 38.91
/
  EBK_VGI 134 57 16 16 OPEN 1* 3.7081E-001 0.62500 357.28 2.00 1* Z 38.87
/
  EBK_VGI 134 57 17 17 OPEN 1* 2.7575E-001 0.62500 265.64 2.00 1* Z 38.83
/
  /

GRUPTREE                                -- Generated : Petrel
  'GROUP 1' FIELD /
  EBK FIELD /
  /

WCONPROD
  EBK_H1_M 1* GRUP 1* 1* 30000.00 1* 1* 580.1510 319.0830 1 /
  /

GCONPROD                                -- Generated : Petrel
  EBK GRAT 1* 1* 50000.00 6* RATE /
  /

GEFAC                                   -- Generated : Petrel
  EBK 0.9500 YES /
  /
```

```
GCONINJE                                -- Generated : Petrel
  EBK GAS VREP 1* 1* 1* 1.0000 /
  /

WCONINJE                                -- Generated : Petrel
  EBK_VGI GAS 1* GRUP 1* 1* 6000.0000 1* 1 /
  /

WPIMULT                                 -- Generated : Petrel
  EBK_H1_M 1.00E+000 108 59 6 /
  EBK_H1_M 1.00E+000 108 59 5 /
  EBK_H1_M 1.00E+000 109 59 5 /
  EBK_H1_M 1.00E+000 110 59 5 /
  EBK_H1_M 1.00E+000 111 59 5 /
  EBK_H1_M 1.00E+000 111 59 6 /
  EBK_H1_M 1.00E+000 112 59 6 /
  EBK_H1_M 1.00E+000 112 60 6 /
  EBK_H1_M 1.00E+000 112 60 7 /
  EBK_H1_M 1.00E+000 113 60 7 /
  EBK_H1_M 1.00E+000 113 60 8 /
  EBK_H1_M 1.00E+000 113 60 9 /
  EBK_H1_M 1.00E+000 114 60 9 /
  EBK_H1_M 1.00E+000 114 60 10 /
  EBK_H1_M 1.00E+000 115 60 10 /
  EBK_H1_M 1.00E+000 116 60 10 /
  EBK_H1_M 1.00E+000 117 60 10 /
  EBK_H1_M 1.00E+000 117 60 9 /
  EBK_H1_M 1.00E+000 118 60 9 /
  EBK_H1_M 1.00E+000 119 60 9 /
  EBK_H1_M 1.00E+000 119 60 8 /
  EBK_H1_M 1.00E+000 120 60 8 /
  EBK_H1_M 1.00E+000 121 60 8 /
  EBK_H1_M 1.00E+000 121 60 7 /
  EBK_H1_M 1.00E+000 122 60 7 /
  EBK_H1_M 1.00E+000 122 60 6 /
  EBK_H1_M 1.00E+000 123 60 6 /
  EBK_H1_M 1.00E+000 124 60 6 /
  EBK_H1_M 1.00E+000 124 60 5 /
  EBK_H1_M 1.00E+000 124 59 5 /
  EBK_H1_M 1.00E+000 125 59 5 /
  EBK_H1_M 1.00E+000 125 59 4 /
  EBK_H1_M 1.00E+000 126 59 4 /
  EBK_H1_M 1.00E+000 126 59 3 /
  EBK_H1_M 1.00E+000 127 59 3 /
  EBK_H1_M 1.00E+000 128 59 3 /
  /

WDFAC                                   -- Generated : Petrel
EBK_H1_M 2.0E-4 /
EBK_VGI 2.0E-4 /
/

TUNING                                  -- Generated : Petrel
/
/
2* 100/

VFPCHK                                  -- Generated : Petrel
```

```
 0.1000000E+11 /

DATES                                    -- Generated : Petrel
  1 FEB 2016 /
--One measurement every month/

DATES                                    -- Generated : Petrel
  1 JAN 2026 /
  /
```

8 References

Barker, J.W. 2005. Experience with Simulation of Condensate Banking Effects in Various Gas Condensate Reservoirs. Paper presented at the International Petroleum Technology Conference, 21-23 November, Doha, Qatar. Source: http://dx.doi.org/10.2523/IPTC-10382-MS.

Coats, K.H. 1985. Simulation of Gas Condensate Reservoir Performance. Journal of Petroleum Technology (October 1985), 5, page 1870-1886.

El-Banbi, A.H. and McCain, W.D. 2000. Investigation of Well Productivity in Gas-Condensate Reservoirs. Paper SPE 59773 presented at the 2000 SPE/CERI Gas Technology Symposium, Calgary, Alberta, Canada, 3-5 April.

Fan, Li. Harris, B.W. Jamaluddin, A.J. Kamath, J. Mott, R. Pope, G.A. Shandrygin, A. and Whitson, C.H. 2005. Understanding Gas-Condensate Reservoirs. Publication: Oilfield Review Volume: 17 Issue: 4 Publication Date: 12/01/2005.

Fevang, O. Singh, K. and Whitson, C.H. 2000. Guidelines for Choosing Compositional and Black-Oil Models for Volatile Oil and Gas-Condensate Reservoirs. Paper SPE 63087 presented at the 2000 SPE Annual Technical Conference and Exhibition held in Dallas, Texas, 1-4 October.

Gundersen, P.L. 2013. Compositional Simulations of Producing Oil-Gas Ratio Behaviour in Low Permeable Gas-condensate Reservoir. University of Stavanger, Faculty of Science and Technology: Master's Thesis.

Haukas, J. Aavatsmark, I and Espedal, M. 2004. A black-oil and compositional IMPSAT simulator with improved compositional convergence. Centre for Integrated Petroleum Research (CIPR), University of Bergen, Norway. Included in Proceedings of the 9th European Conference on the Mathematics of Oil Recovery, Cannes, France, 30 August – 2 September 2004.

IHS Energy. 2010. Basin Monitor – South Africa: Outeniqua Basin.

Izgec, B. 2003. Performance analysis of compositional and modified black-oil models for rich gas-condensate reservoirs with vertical and horizontal wells. Office of Graduate Studies, Texas A&M University. December 2003. 198 pages.

Lal, R. R. 2003. Well testing in gas-condensate reservoirs - A report submitted to the Department of Petroleum Engineering of Stanford University in partial fulfilment of the requirements for the degree of Master of Science. June 2003. 72 pages.

Mahmudi, M. and Taghi Sadeghi, M. 2013. Performance analysis of compositional and modified black-oil models for a gas lift process. Oil & Gas Science and Technology – Rev. IFP Energies nouvelles, Vol. 68, No. 2, pp. 319-330. Final manuscript received: October 2011. Published online: March 2013.

Petrowiki. 2015. Formation damage from condensate banking. Source: http://petrowiki.org/Formation_damage_from_condensate_banking

Schlumberger. 2014. ECLIPSE 2014 - Compositional Reservoir Simulation Module 1: Introduction to PVT. Schlumberger Next course notes.

Schlumberger. 2015. ECLIPSE Blackoil Reservoir Simulation, 14th Edition. Schlumberger. VitalBook file. 344 pages.

Schlumberger. 2015. ECLIPSE Reference Manual. Version 2015.1. 2831 pages.

Schlumberger. 2015. ECLIPSE Technical Description. Version 2015.1. 1156 pages.

Schlumberger. 1990. PVT Laboratory Study Report. Flopetrol-Johnston PVT Software VR 1.1. 75 pages.

Shi, C. 2009. Flow behaviour of gas-condensate wells - A dissertation submitted to the Department of Energy Resources Engineering and the committee on graduate studies of Stanford University in partial fulfilment of the requirements for the degree of Doctor of Philosophy. March 2009. 187 pages.

Wang, Y. 2007. Implementation of a two pseudo-component approach for variable bubble point problems in GPRS. A report submitted to the Department of Energy Resources Engineering. Stanford University. June 2007.

Whitson, C.H. Fevang, O. and Yang, T. 1999. Gas-condensate PVT – What's Really Important and Why? Paper presented at the IBC Conference: "Optimisation of Gas-condensate Fields", London, Jan. 28-29, 1999, Cumberland Hotel. IBC UK Conferences Ltd., Gilmoora House, 57-61 Mortimer Street, London W1N 81X, UK. http://www.ibc-uk.com.

Original details: Victor (3518573) E:\ A comparison of black-oil versus compositional simulation methods for evaluating a rich gas-condensate reservoir.docm
21 February 2017